SHROOM3 IN THE KIDNEY

SHROOM3 PLAYS A ROLE IN PODOCYTE

CYTOARCHITECTURE

By HADISEH KHALILI, M.Sc.

A Thesis Submitted to the School of Graduate Studies in Partial Fulfillment of the Requirements for the Degree Master of Science

TITLE: Shroom3 plays a role in podocyte architecture

AUTHOR: Hadiseh Khalili, M.Sc. (University of Birmingham)

SUPERVISOR: Dr. Darren Bridgewater

NUMBER OF PAGES: xvi-114

ABSTRACT

Chronic kidney disease (CKD), defined as an irreversible reduction in glomerular filtration rate, is a large public health concern. Dissecting the genetic components of CKD is required to improve our understanding of disease pathogenesis. Researchers have identified that *SHROOM3*, has very high associations with kidney disease and function. Shroom3 encodes an actin-binding protein important in regulating cell and tissue morphogenesis. However, there is a lack of evidence supporting a role for Shroom3 in kidney function or disease. Here, I investigated the developmental and functional role of Shroom3 in the mammalian kidney. For the first time, I described the expression pattern of Shroom3 in the embryonic and adult mouse kidneys. By performing in situ hybridization and immunohistochemistry, I demonstrated that Shroom3 is expressed in the condensing mesenchyme, podocytes, and collecting ducts. I further showed that Shroom3 protein is localized in the foot processes of podocytes, utilizing immunogold labeling and transmission electron microscopy. In order to uncover a potential role of Shroom3 in the kidney, we utilized *Shroom3* knockout mice. *Shroom3* mutants demonstrated marked glomerular abnormalities including cystic and degenerating glomeruli, and reduced glomerular number. Scanning and transmission electron microscopic analyses of *Shroom3* mutant glomeruli revealed disruptions in podocyte morphology characterized by disorganized foot processes with less interdigitation and segmental foot processes effacement. Furthermore, immunofluorescence analysis of mutant kidneys revealed aberrant distribution of podocyte actin-associated proteins. Elucidating the underlying molecular mechanism of this abnormal podocyte architecture;

we demonstrated that in the absence of Shroom3, Rho kinase is mislocalized in the apical membrane of podocytes. As a result, mislocalized Rho kinase failed to phosphorylate non-muscle myosin and induce actomyosin contraction resulting in a patchy granular distribution of actin in the podocytes of *Shroom3* mutants. Taken together, our findings established that Shroom3 is essential for proper actin organization in the podocytes through interaction with Rock. Furthermore, we took advantage of a haploinsufficiency phenotype of *Shroom3* heterozygote adult mice and demonstrated these mice develop glomerulosclerosis and proteinuria. In conclusion, our studies provided evidence to support a role for Shroom3 in kidney development and disease and support the GWAS studies that suggested a correlation between *SHROOM3* variants and kidney function in humans.

ACKNOWLEDGEMENTS

My special thanks go to my labmates, Felix Boivin and Sanjay Sarin for helping me at each and every stage of my work.

Finally, I am thankful that I have had the love and support of my husband, Sajad, through this journey and cannot wait to see what the future brings. Also thanks to my parents for helping to cheer me on to the finish line.

TABLE OF CONTENTS

LIST OF SUPPLEMENTARY FIGURES

LIST OF FIGURES

LIST OF ABBREVIATIONS

CKD	Chronic kidney disease
GFR	Glomerular filtration rate
ESRD	End stage renal disease
UB	Ureteric bud
FSGS	Focal segmental glomerulosclerosis
MET	Mesenchymal to epithelial transition
GWAS	Genome-wide association studies
GBM	Glomerular basement membrane
Wt-1	Wilms tumor-1
UMOD	Uromodulin
SNP	Single nucleotide polymorphism
FHH	Fawn hooded hypertensive
CAN	Chronic allograft nephropathy
Rock	Rho-associated coiled-coil kinase
MRLC	Myosin regulatory light chain
SBD	Shroom-binding domain
RBD	Rock-binding domain
SA	Splice acceptor
β-gal	*β-galactosidase*
pA	polyadenylation

WT	Wild-type
PBS	Phosphate-buffered saline
PFA	Paraformaldehyde
H&E	Haematoxylin and Eosin
PAS	Periodic acid-Schiff
JMS	Jone's Methamine Silver
TUNEL	Terminal deoxynucleotidyl transferase-mediated dUTP nick-end labeling
SDS	Sodium dodecyl sulfate
EM	Electron microscopy
TEM	Transmission electron microscopy
SEM	Scanning electron microscopy
cA	Constitutive active
ISH	In situ hybridization
SSB	S-Shaped body
CSB	Comma-shaped body
P	Podocyte
PE	Parietal epithelium
UE	Ureteric epithelium
CM	Condensing mesenchyme
FP	Foot process
MLC	Myosin light chain
pMLC	Phosphorylated myosin light chain

MYPT	Myosin phosphatase
CB	Cell body
CD	Collecting duct
G	Glomerulus
RV	Renal vesicle
C	Capillary
PFP	Primary foot process
SFP	Secondary foot process
TFP	Tertiary foot process
SD	Slit diaphragm
E	Endothelium
PAN	Puromycin aminucleoside nephrosis

DECLARATION OF ACADEMIC ACHIEVEMENT

I personally accomplished all the research and necessary tasks for Figure 1 through

Figure 25.

1. BACKGROUND:

1.1 Chronic Kidney Disease

Chronic kidney disease (CKD), defined as an irreversible reduction in glomerular filtration rate (GFR), affects at least 10% of the population (Price et al., 2010). An early sign of CKD is elevated levels of urinary albumin (albuminuria), even within the low normal range. The progression of CKD is divided into five stages based on the level of the patient's renal function (Schwartz et al., 2009). More advanced stages of CKD gradually progress to end-stage renal disease (ESRD), requiring renal dialysis and transplantation. There are a number of potential risk factors for the initiation and progression of CKD, including environmental and clinical factors such as diabetes and hypertension. Apart from the risk conferred by these traditional factors, a genetic component undoubtedly underlies CKD (Parsa et al., 2013, Devuyst et al., 2014). Although many candidate genes have been identified to contribute to CKD, it is not yet clear how disruption in these genes and their underlying molecular mechanism can lead to impaired kidney function.

1.2 Kidney Anatomy and Function

1.2.1 Normal Kidney Anatomy

The kidneys are a pair of bean shaped organs that are located at the rear of the abdominal cavity. The medial portion of the kidney is grooved and forms the renal hilum, where the renal artery and vein enter and exit, and ureter emerges (Supplementary 1). Kidneys receive about 20% of the total cardiac output via the renal arteries. Once the blood is received by the kidney, it is filtered and then exits via the renal veins (Stead et al., 1950). The filtered plasma (urine) then exits the kidney and passes down the ureter to the urinary bladder (Supplementary 1).
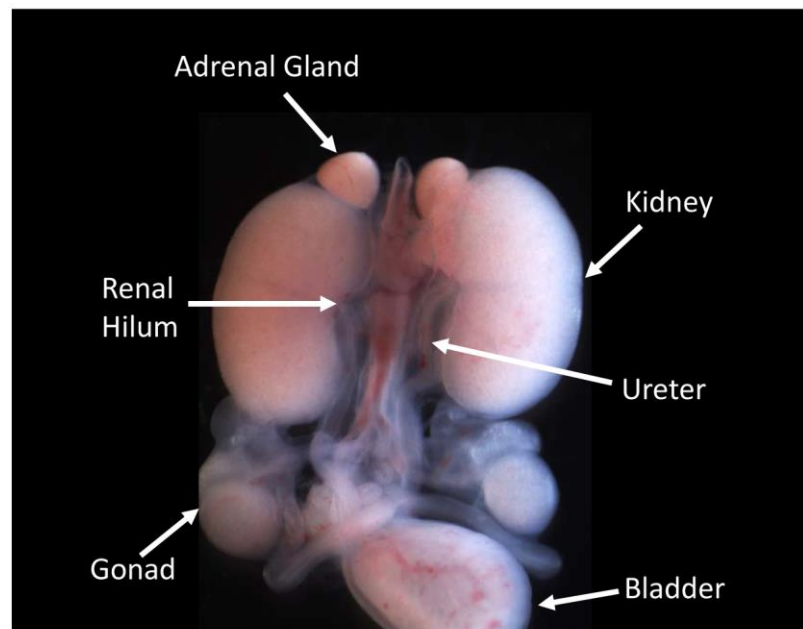
Supplementary 1. Gross Anatomy of Mouse Kidneys. Gross anatomy of a resected embryonic day 18.5 mouse kidneys with the ureters and bladder.

A coronal section of the kidney reveals three major regions: the cortical region, the medullary region and the renal pelvis, which connects the kidney to the ureter (Supplementary 2A). The cortex contains microscopic clusters of capillaries, called renal corpuscles, and convoluted tubules. The medulla is subdivided into a number of cone-shaped sections called renal pyramids. At the tips of each renal pyramid, known as the renal papillae, tubules called collecting ducts drain into common passageway called minor calyces. Several minor calyces merge to form major calyces, which drain into a funnel-shaped channel called the renal pelvis that connects to the ureter (Supplementary 2A).

The functional unit of the mammalian kidney, termed the nephron, is composed of the renal corpuscle and renal tubules. The renal tubule is segmented into three distinct regions: the proximal convoluted tubule, the loop of Henle, and the distal convoluted tubule (Supplementary 2B). These regions are essential for reabsorption of ions, glucose and water; and secretion of toxins and drugs. Of particular importance to CKD is the renal corpuscle, also termed glomerulus. The glomerulus is made up of a glomerular tuft, a network of convoluted capillaries surrounded by the Bowman's space and Bowman's capsule, which is a single layer of parietal epithelial cells (Supplementary 2B). Within the Bowman's capsule, the visceral epithelial cells (termed podocytes) sit on top of the capillaries. The structural integrity of the kidney is essential for maintaining normal kidney function. For instance, the integrity of the glomerular structure plays a critical role in normal glomerular filtration process.
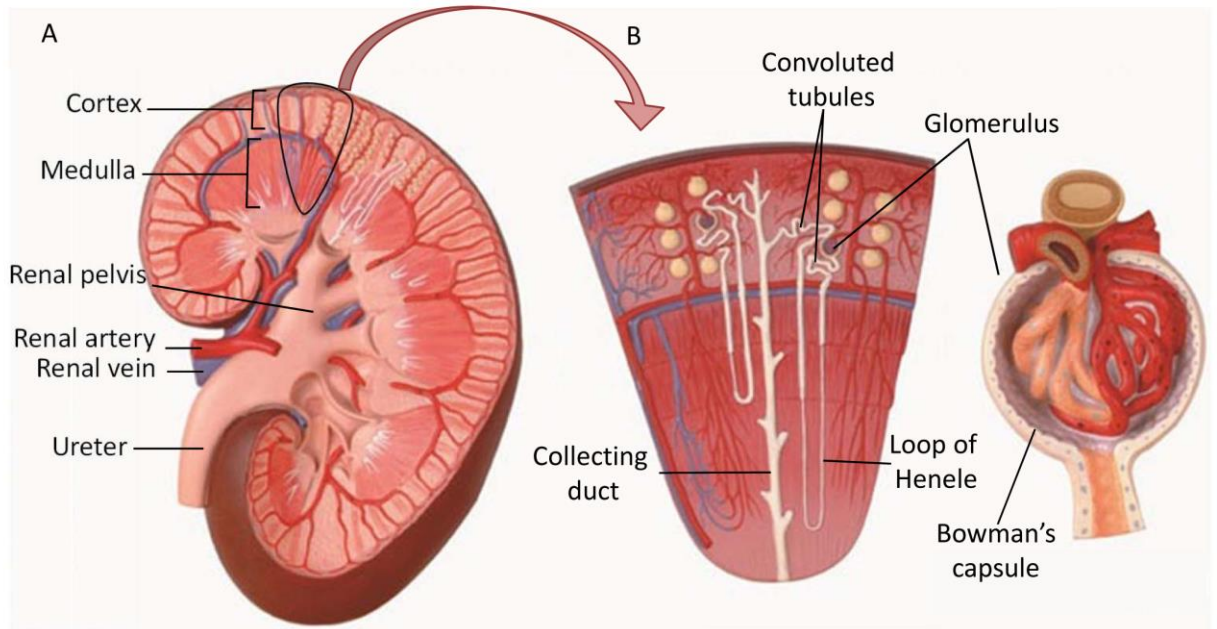
Supplementary 2. Basic Structure of The Kidney. (A) Coronal section through a cartoon diagram of the human kidney representing different regions. (B) Cartoon diagram outlines various regions of the mammalian nephron. Image adopted from http://yijiajx.com /product-1027.html

1.2.2 Normal Kidney Function

The main function of the kidney is to filter waste products and electrolytes from the blood. These waste products and any excessive electrolytes are excreted in the form of urine. Urine is formed through a series of processes in the nephron including filtration, reabsorption, and secretion. The glomerular capillaries perform the first step of blood filtration, forcing fluids, small solutes and other substances such as toxins and drugs out through the filtration barrier into the Bowman's space. The glomerular filtrate then moves to the proximal convoluted tubules. The composition and volume of glomerular filtrate are modified as it travels through the proximal tubule by the processes of reabsorption and secretion. From here, the filtrate becomes more concentrated by moving down into the medullary region and back to the cortical region through the descending and ascending loop of Henle. Reabsorption continues to occur once the filtrate enters the distal convoluted tubule. Distal convoluted tubules lead to the collecting ducts. From the collecting ducts, the urine drains into the renal pelvis via the renal papilla and enters the ureter.

1.3 Kidney and Nephron Development

Mammalian kidney development begins at E10.5 in the mouse and at 5 weeks gestation in humans. An outgrowth from the nephric duct forms, termed the ureteric bud (UB), and invades into the adjacent metanephric mesenchyme. The UB forms a T-shaped structure and undergoes about 10 cycles of branching morphogenesis and elongation in the mouse and 15 cycles in humans to generate the collecting duct system (Saxen and Sariola, 1987,

Cebrian et al., 2004). During the process of branching morphogenesis, the tips of the UB epithelium will become surrounded by metanephric mesenchymal cells, termed the 'cap mesenchyme'. A subset of these mesenchymal cells will undergo nephrogenesis to form the nephron (Cebrian et al., 2004).

Nephrogenesis begins when the ureteric epithelium induces a subset of surrounding mesenchymal cells to form mesenchymal aggregates. These mesenchymal cell aggregates will undergo a mesenchymal-to-epithelial transition (MET) to form the first distinct morphological nephrogenic structure called 'the renal vesicle' (Supplementary 3A) (Cebrian et al., 2004). The renal vesicles are polarized epithelial cells. A series of cleft formations (proximal and distal clefts) in this structure produces the comma- and S-shaped bodies (Supplementary 3B). The distal end of S-shaped body remains connected to the UB epithelium and fuses to form an epithelial tubule. The proximal end is infiltrated by endothelial and mesangial cells, forming the glomerular capillary (Supplementary 3C) (Dressler, 2006). A layer of cuboidal epithelial cells lines the medial aspect of the proximal cleft, which will differentiate into the podocyte (Kreidberg, 2003). At this stage, there is a double-layered basement membrane between the podocytes and endothelial cells of the developing glomeruli. The double layer basement membrane fuses, forming a single basement membrane, known as the glomerular basement membrane (GBM). Following this step, the glomerular filtration barrier, which is a specific structural organization, starts to develop. The glomerular filtration barrier consists of three layers: the fenestrated endothelial cells, the GBM, and the podocyte layer. All of these developmental processes occur in a region called the 'nephrogenic

zone', which is located in the cortex of the developing kidney. As glomerular development proceeds, the nephron begins to adopt a more complex structure by elongating the proximal tubule and forming the descending and ascending limbs of loop of Henle and distal tubule (Supplementary 3D).
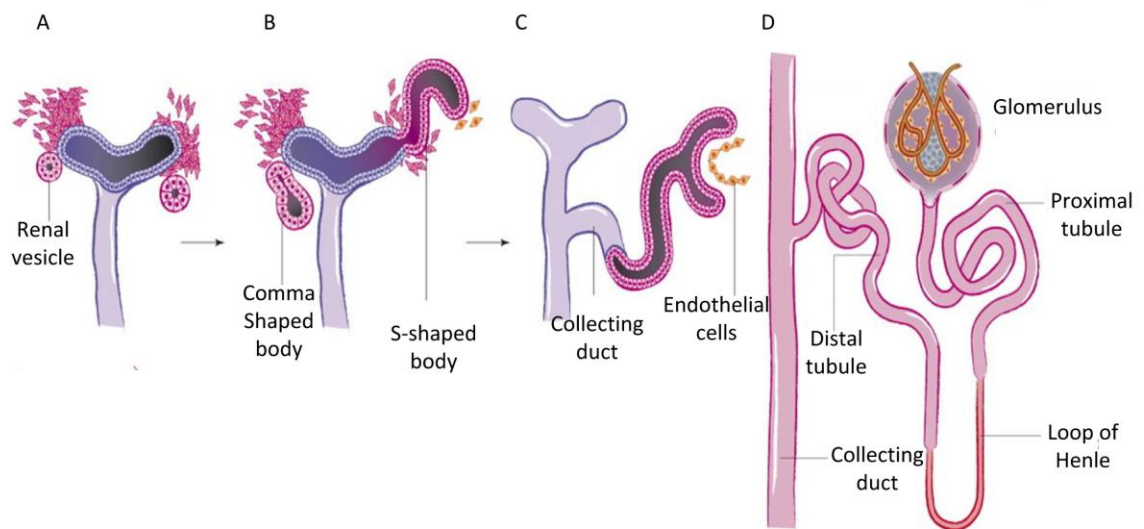
Supplementary 3. Schematic overview of nephrogenesis in the developing kidney. Reciprocal induction between ureteric bud tips and metanephric mesenchyme causes the metanephric mesenchymal cells to condense around the ureteric bud tips, and a subset of these cells undergo mesenchymal-to-epithelial transition to form renal vesicles that differentiate to Comma-shaped, S-shaped bodies and finally nephrons that join the collecting duct. Image adopted (Uhlenhaut and Treier, 2008).

1.3.1   The Podocyte

1.3.1.1   Podocyte Structure

Podocytes are terminally differentiated epithelial cells within the glomerulus with a complex cytoarchitecture. The podocyte is a highly polarized cell that consists of three compartments: a main cell body facing the urinary space, primary processes, and secondary and tertiary foot processes (Supplementary 4A). Morphologically, the primary processes extend out from the cell body and further branch into the secondary and tertiary foot processes (Supplementary 4A, B). The cytoskeleton of primary processes is composed of microtubules, which provides structural support for the cell body and primary processes. While the secondary and tertiary foot processes contain an actin-based cytoskeleton that is connected to the GBM via focal adhesion contacts (Faul et al., 2007). The function of podocytes largely depends on the integrity and maintenance of the actin cytoskeleton structure (Faul et al., 2007). The actin bundles of foot processes are associated with non-muscle myosin II, which runs along the longitudinal axis of the foot processes (Supplementary 5). The foot processes can change their actin cytoskeleton quickly to contract the expansive forces of the capillary wall. Numerous actin-associated proteins mediate the assembly and reorganization of the actin cytoskeleton, demonstrating that actin regulatory proteins are critical for sustained podocyte function and structure (Faul et al., 2007). Synaptopodin is the major cytoskeletal component of differentiated podocytes that associates with actin filaments. Synaptopodin regulates the dynamics of the actin cytoskeleton via modulation of RhoA signaling. Gene silencing of synaptopodin in the podocytes suppresses the formation of actin stress fibers, indicating a critical role

for synaptopodin in the development and maintenance of the podocyte contractile apparatus. Nephrin and podocin are structural components of the slit diaphragm, which are linked to the actin cytoskeleton of the podocyte (Shono et al., 2007). Interaction between the slit diaphragm components and the actin cytoskeleton of the podocyte is important for the regulation of slit diaphragm integrity and foot process structure (Shono et al., 2007). Alteration or disruption in the podocyte actin cytoskeleton arising from genetic or acquired diseases can lead to foot process effacement and impaired slit diaphragm filtration accompanied by urinary protein loss (Mundel and Shankland, 2002, He et al., 2013). The effacement of the podocyte foot processes is a common feature in most glomerular diseases, including focal segmental glomerulosclerosis (FSGS) (D'Agati et al., 2004, Deegens et al., 2008). FSGS is one of the most prevalent causes of chronic kidney disease (Kiffel et al., 2011).
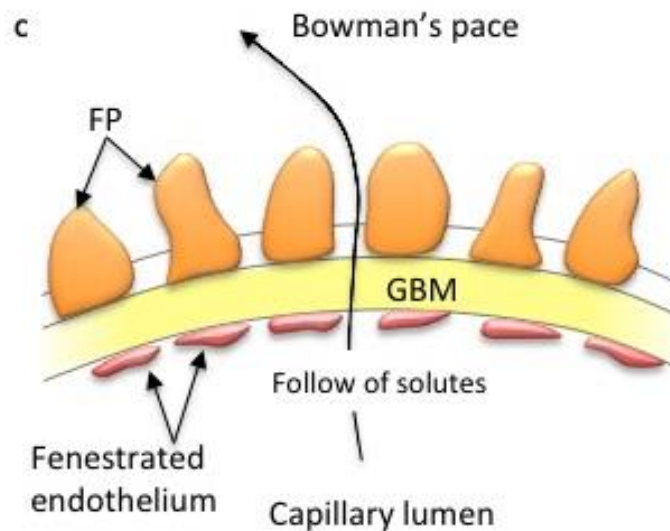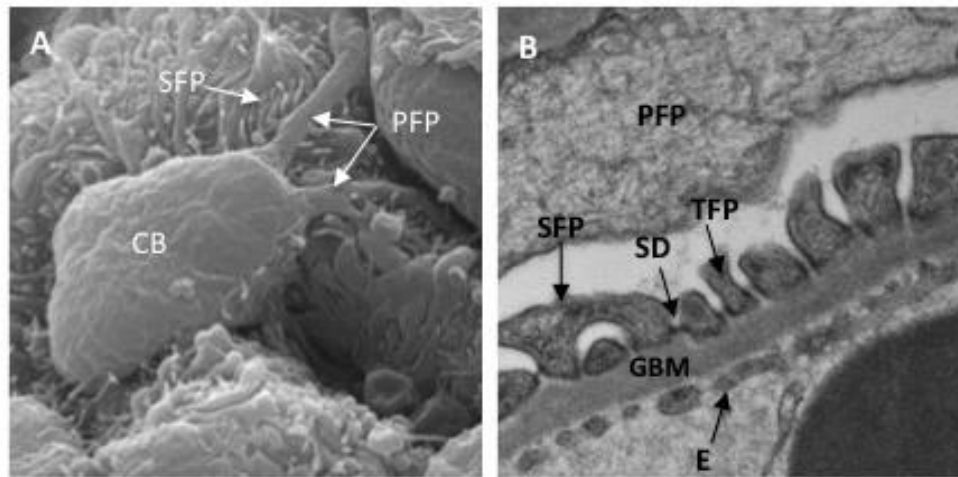
Supplementary 4. Podocyte with a complex cytoarchitecture. (A) Scanning electron microscopy demonstrates complexity of podocyte structure. A large cell body facing the urinary space sends out primary foot processes. Secondary and tertiary foot processes arising from the primary foot processes interdigitate with foot processes of neighboring podocytes. (B) Transmission electron micrograph of foot processes and a region of the glomerular filtration barrier consisting of fenestrated endothelium, GBM, and podocyte secondary and tertiary foot processes with filtration slits. (CB- cell body, PFP- primary foot process, SFP- secondary foot process, TFP- tertiary foot process, SD- slit diaphragm, E- endothelium, and GBM- glomerular basement membrane).
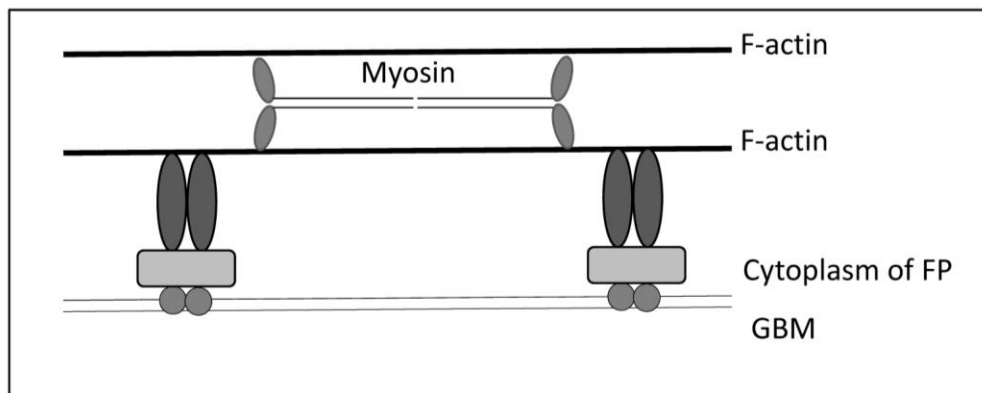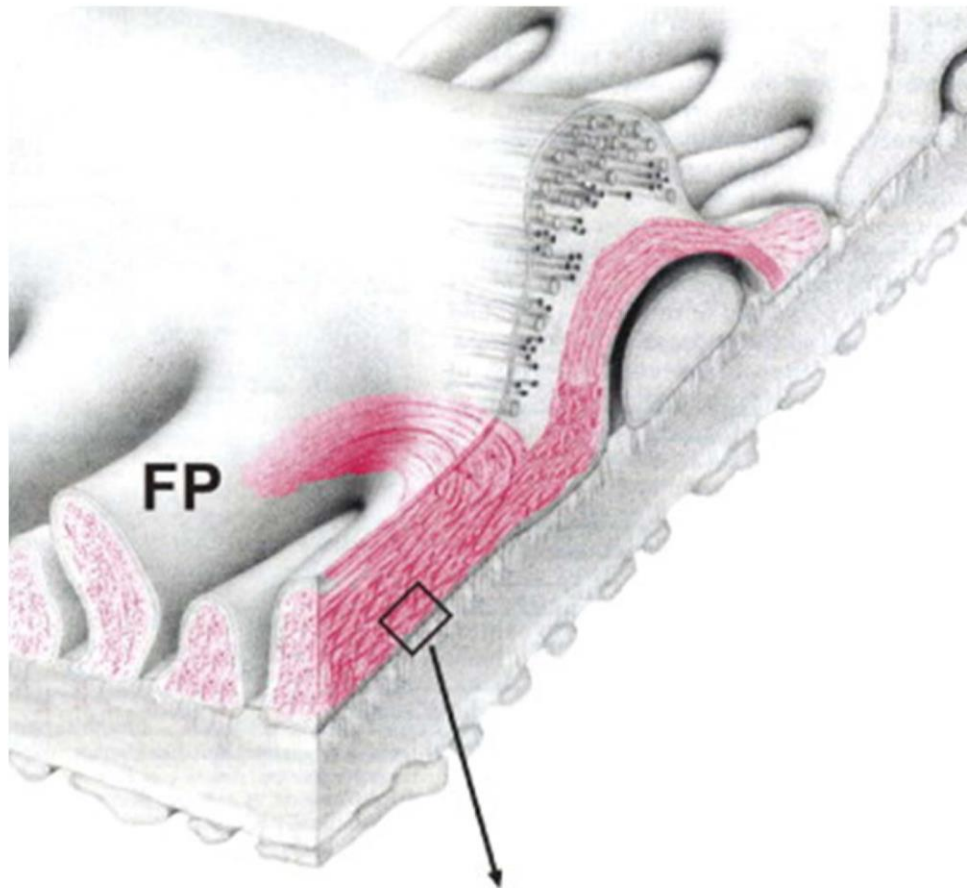
Supplementary 5. Schematic of cytoskeletal organization of foot process. The foot processes contain a microfilament-based contractile apparatus consisting of actin, myosin II, and other actin-associated proteins (Faul et al., 2007).

1.3.1.2 Podocyte Development

At the early stages of the glomerular development, the renal vesicle and comma-shaped, podocyte progenitors display a typical columnar epithelium with apical cell-cell contacts. During the S-shaped stage, podocytes expand their apical surface by shifting their apical cell-cell junctions toward the basal aspect (Hartleben et al., 2012). Throughout transition from the S-shaped to the glomerular capillary stage, podocytes lose their lateral cell-cell contacts, but remain attached to each other at a point adjacent to the basal membrane and the GBM (Kreidberg, 2003, Hartleben et al., 2012) (Supplementary 6). Podocytes then reorganize their actin cytoskeleton and extend numerous primary actin-based foot processes from their cell bodies to cover the underlying capillary loops. Primary foot processes further branch into the secondary and tertiary foot processes. These tertiary foot processes interdigitate with of adjacent podocytes to form specialized intercellular junctions known as the slit diaphragms (Kreidberg, 2003) (Supplementary 6).

This podocyte maturation coincides with the expression of podocyte-specific protein, Wilms' tumor-1 (Wt-1). Wt-1, which is a transcriptional factor, is the key to podocyte development and viability. During kidney development, Wt-1 expression is first detected at low levels in the condensing mesenchyme. The epithelial cells of the renal vesicle express Wt-1. As the renal vesicle differentiates into the comma- and S-shaped bodies, Wt-1 expression becomes restricted to the nuclei of the podocyte precursors (Armstrong et al., 1993).
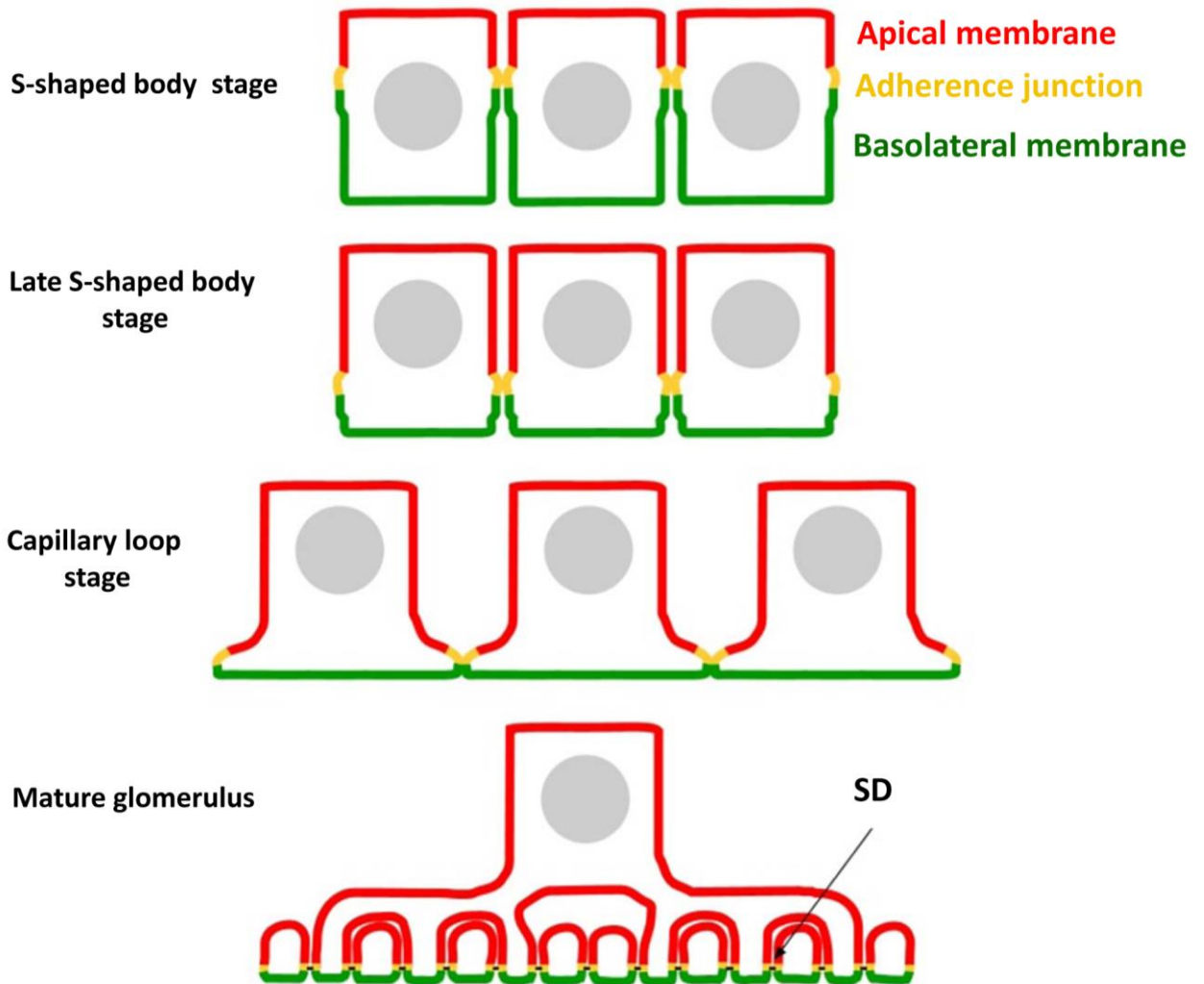
Supplementary 6. Schematic of the podocyte Differentiation. During early phase of podocyte differentiation, apical cell-cell contact translocate toward the basal side (Shown in yellow), where the foot processes and slit diaphragm form. This process is accompanied with expansion of the apical membrane area of the podocyte (Shown in red). In both immature and mature podocytes, the basolateral membrane (Shown in green) is located beneath the cell-cell junction. These alterations cause podocyte to lose their lateral junction and acquire a complex architecture with specialized cell interactions, slit diaphragm. Image adopted (Hartleben et al., 2012).

1.4   Shroom3 in Kidney

To understand the underlying genetic components of CKD, researchers have performed genome-wide association studies (GWAS). GWAS for index of renal function, the glomerular filtration rate (GFR), identified several loci including *uromodulin* (*UMOD*), which has specific mutations that lead to multiple types of kidney disease (Kottgen et al., 2009). Another locus strongly linked to reduced GFR and CKD is an intronic SNP (rs17319721) at the *SHROOM3* gene. It ranked as the second most significant locus associated with CKD and GFR, behind the *UMOD* (Boger et al., 2011b). More recent studies on the development of chronic allograft nephropathy (CAN) in a cohort of renal allograft recipients demonstrated that the risk allele of rs17319721 within the *SHROOM3* gene in the donor kidney is associated with a higher risk of CAN and renal fibrosis in the allograft at 12 months after transplantation (Menon et al., 2015).

Recent studies in Fawn-Hooded Hypertensive (FHH) rat, a model for renal disease, identified 13 variants in the FHH *Shroom3* gene compared to the wild type allele (Yeo et al., 2015). They discovered that one of these variants disrupts the actin-binding function of the Shroom3 in the FHH rats, resulting in defects in the glomerular filtration barrier. They also demonstrated that introgression of the wild type *Shroom3* gene onto the FHH rats improves glomerular structure and function (Yeo et al., 2015).

1.5   Shroom3

1.5.1   Shroom Proteins

The family of Shroom comprises a class of actin binding proteins. There are four Shroom proteins in vertebrates, which were previously named, Apx (Staub et al., 1992), Apxl (Schiaffino et al., 1995), Shroom (Hildebrand and Soriano, 1999), KIAA1202 (Hagens et al., 2006b) and recently renamed as Shroom1, Shroom2, Shroom3, and Shroom4; respectively (Hagens et al., 2006a). The Shroom family possesses at least two of three conserved domains that include an N-terminal PDZ domain, a centrally located ASD1 domain, and a C-terminal ASD2 domain (Supplementary 7) (Hildebrand and Soriano, 1999, Hagens et al., 2006b). The PDZ domain is a protein-protein interaction module that links membrane bound proteins to the cytoskeleton and facilitates the assembly of signaling complexes (Hildebrand and Soriano, 1999). The ASD1 domain is required to bind directly to actin filaments and regulates subcellular localization of Shroom3 (Dietz et al., 2006). The ASDietz et al., 2006). The ASD2 domain binds to Rho kinases (Rocks), and is essential for Shroom-mediated contractile activity (Hildebrand and Soriano, 1999, Plageman et al., 2010). The Shroom family of proteins also contains a proline-rich sequence (FPPPP or FPn) and PDZ binding sites. The Shroom3 protein contains all domains, while Shroom1 lacks the PDZ and FPn domains, Shroom2 lacks a PDZ binding site, and Shroom4 lacks the ASD1 domain (Supplementary 7). Differences seen in the activity of Shroom proteins is due to their distinct subcellular distributions and actin-binding properties (Dietz et al., 2006). Shroom2 localizes to cortical actin and Shroom4 binds to a punctate population of actin, whereas Shroom3 localizes to actin stress fibers

and bundles them (Dietz et al., 2006). Although the ASD2 domain is shared by all the members of the Shroom protein family, only Shroom3 can induce apical constriction in epithelial cells (Dietz et al., 2006).
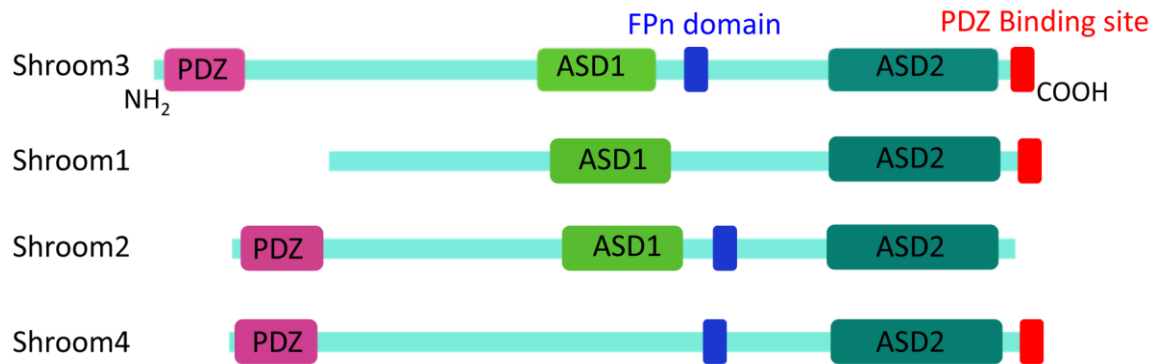
Supplementary 7. Domain Structure of Different Shroom Family Members. ASD2 domain is the most highly conserved domain shared by Shroom family proteins.

16

1.5.2 Shroom3 Expression and Function in Epithelial Cells

Shroom3 was originally identified using a gene trap mutagenesis approach. Mice carrying the gene trap mutation display neural folds that "mushroom" away from the dorsal midline, resulting in exencephaly and spina bifida (Hildebrand and Soriano, 1999). At the onset of neural tube closure, neural epithelial cells undergo robust apical constriction and form hinge point to ensure proper neural plate bending (Haigo et al., 2003). Knockout and dominant-negative mutant of *Shroom3* in mice and xenopus demonstrated failure of hinge point formation and subsequent defects in neural tube closure (Hildebrand and Soriano, 1999, Haigo et al., 2003). The Shroom3 protein, which is localized at the adherence junction of neural epithelial cells, is essential to induce apical constriction in these polarized epithelial cells (Hildebrand and Soriano, 1999). In addition to the neural tube, *Shroom3* is also expressed in the developing gut, eye, lungs and somites (Hildebrand and Soriano, 1999, Sevilla-Perez et al., 2008). Its expression is required for cell shape changes and morphogenesis in these tissues as evidenced by *Shroom3* mutant embryos that demonstrate defects in gut looping (Chung et al., 2010), and lens pit invagination (Plageman et al., 2010). In humans, a recessive missense mutation in *SHROOM3* is associated with heterotaxy syndrome, suggesting *SHROOM3* as a novel target for the control of left-right asymmetry (Tariq et al., 2011).

Shroom3 controls cell morphology and tissue architecture by interacting directly or indirectly with the components of the cytoskeletal machinery (Hildebrand, 2005, Nishimura and Takeichi, 2008, Mohan et al., 2012). The ASD1 domain controls subcellular localization of Shroom3 by directly binding to F-actin resulting in the

localization of Shroom3 to the apical junctional complex (Dietz et al., 2006). The ASD2 domain induces apical constriction by interacting with the Shroom-binding domain (SBD) of Rho kinases 1 and 2 (Rocks) at the adherence junction (Supplementary 8) (Nishimura and Takeichi, 2008). In vitro studies have shown that only expression of the ASD2 domain of Shroom3 causes its diffused localization in the cytoplasm and failing to induce apical constriction (Hildebrand, 2005). Although apical targeting of the ASD2 domain of Shroom3 alters the apical architecture of the cells (Hildebrand, 2005). It also has been shown that the mutant form of Shroom3, lacking ASD2, is localized to the adherence junction but does not induce apical constriction (Dietz et al., 2006). Thus, proper activity of Shroom3 protein is dependent on its ASD1 and ASD2 domains working in *cis*.
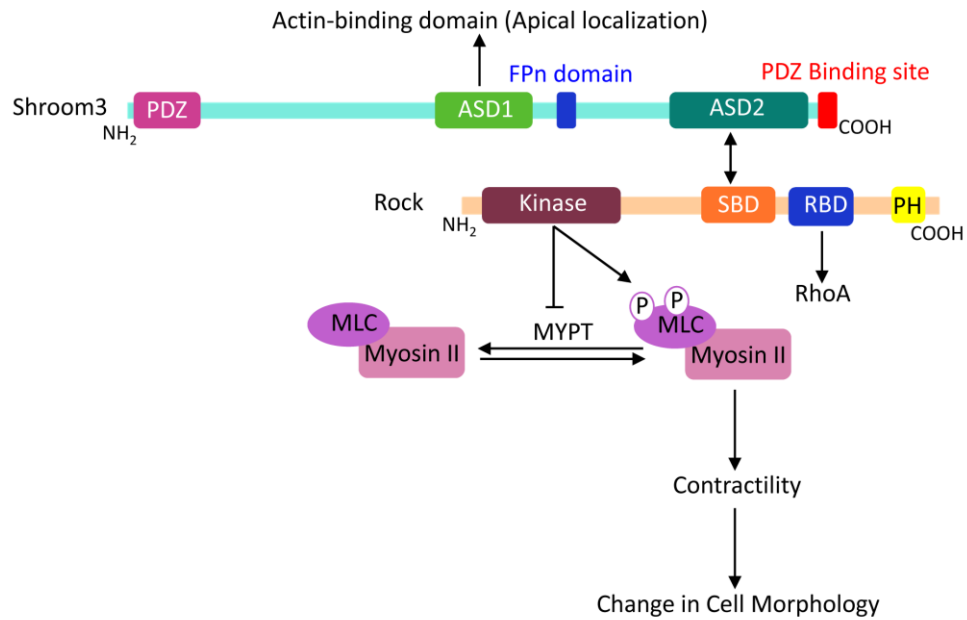
Supplementary 8. A schematic diagram of the Shroom3-Rock pathway. Shroom3 is localized to the apical junction of the cell via interaction of its centrally ASD1 domain with F-actin. ASD2 domain of Shroom3 binds directly to the SBD domain of Rock. This interaction facilities both apical localization and activity of Rock. Rock then phosphorylates MLC directly and indirectly by inhibition of myosin phosphatase, which results in the activation of myosin II and actomyosin contraction required for cellular morphogenesis. (SBD- Shroom-binding domain, RBD- RhoA-binding domain, MLC-myosin light chain, MYPT- myosin phosphatase).

1.6 RhoA/Rock Signaling

RhoA/Rock signaling is crucial in several cellular processes including cytoskeletal dynamics, cell migration, cell polarity, and cell proliferation (Riento and Ridley, 2003). Rho-associated coiled-coil kinase (Rock), belongs to the family of Serine/Threonine kinases, is a molecular switch that act downstream of the small GTPase Rho. In vertebrates, Rock is encoded by two different genes, *Rock1* and *Rock2*. Rock1 and Rock2 share an overall 65% sequence identity with 92% identity in the kinase domain (Yoneda et al., 2005). Rock consists of an N-terminal catalytic domain, central coiled-coil-forming, and a C-terminal domain (Dawes-Hoang et al., 2005). The most conserved domain between Rock1 and Rock2 is the N-terminal kinase domain. In a study conducted by Nishimura and Takeichi, amino acids 698-957 in the central coiled-coil region of both Rock1 and Rock2 physically interact with the ASD2 domain of Shroom3 (Nishimura and Takeichi, 2008). This region was called Shroom-binding domain (SBD) of Rock. Immediately following the SBD is the Rho binding domain (RBD), within the coiled-coil region, which physically interacts with RhoA-GTP and becomes activated. Therefore, the SBD and RBD within the Rocks are located in close proximity; Shroom and RhoA-GTP can interact with Rocks simultaneously without competing with each other (Plageman et al., 2011). Shroom3 recruits Rocks to the apical junction of cells (Nishimura and Takeichi, 2008).

Rock activates non-muscle myosin II directly through phosphorylation of the myosin regulatory light chain (MRLC) and indirectly by inactivation of myosin phosphatase (Supplementary 8). Once Rock becomes enriched apically, it activates myosin II locally

via phosphorylation of MRLC. As a result, a contractile actomyosin network is reorganized to form a contractile ring at the apical area of cells and subsequent apical constriction (Hildebrand, 2005, Nishimura and Takeichi, 2008). When the Shroom3-Rock interaction is disrupted, Rock and phosphorylated myosin light chains fail to accumulate apically in epithelial cells, resulting in significant inhibition of apical constriction (Nishimura and Takeichi, 2008), while ectopic expression of Shroom3 in both cultured cells and neural epithelial cells elicits apical constriction (Hildebrand, 2005, Nishimura and Takeichi, 2008).

A number of studies have highlighted important roles of RhoA/Rock signaling in renal pathophysiology (Peng et al., 2008, Kolavennu et al., 2008). Interestingly, inhibition of this pathway by Rock inhibitors has been identified to improve renal injury and proteinuria in various models of renal diseases (Kanda et al., 2003, Kolavennu et al., 2008, Peng et al., 2008). Wang et al. generated two diabetic mouse models with podocyte specific deletion of Rock1 and inducible podocyte specific knock-in of constitutively active (cA) mutant of Rock1(Wang et al., 2012). These studies showed that targeted deletion of Rock1 in diabetic mice results in the reduction of albuminuria, while elevated levels of Rock1 causes higher urinary albumin excretion and enhanced mesangial matrix expansion (Wang et al., 2012). Therefore, Rock activity promotes progression of renal diseases.

1.7 Overall Rational:

Despite the high association of *SHROOM3* variant with CKD and kidney function identified by GWAS, definitive evidence to support a role for SHROOM3 in kidney disease and function is not well established. Since Shroom3 is known to play an important role in regulating shape changes in epithelial cells, it is an excellent candidate for involvement in epithelial morphogenesis in the kidney. Several morphological changes occur during nephrogenesis and branching morphogenesis to give rise to complex structure of nephron and collecting duct system. More importantly, podocyte differentiation requires extensive actin rearrangements and changes in cell shape to acquire a complex cytoarchitecture. Maintenance of proper actin dynamics and organization in the podocytes is critical for normal development and function of the kidney glomerulus. Recent studies by Yeo *et al*. have shown that a genetic variant within the ASD1 coding region of *Shroom3* gene of FHH rat is responsible for the glomerular injury in this strain. However, the underlying molecular mechanism of how disruption of the actin-binding domain of Shroom3 in FHH rat leads to glomerular injury has not been investigated.

2. HYPOTHESIS AND OBJECTIVES

2.1 Overall Hypothesis

The overall hypothesis of this study is that *Shroom3 is important for glomerular development and disease.*

2.2 Study Objectives

1. Investigate Shroom3 expression in embryonic and adult mouse kidneys.

   Hypothesis: *Shroom3 expression is required for normal kidney development and function.*

2. Characterize the glomerular epithelial cell phenotype in *Shroom3* knockout mouse.

   Hypothesis: *Shroom3 is required for normal glomerulogenesis and podocyte morphology.*

3. Define the molecular mechanism by which Shroom3 modulates podocyte architecture.

   Hypothesis: *Shroom3 regulates actin organization in podocyte foot processes.*

3. MATERIALS AND METHODS:

Mice and PCR Genotyping:

Animal studies were performed in accordance with Canadian Council for Animal Care and McMaster institutional guidelines (Animal utilization Protocol #10-08-55). Shroom3 heterozygous mutant mice (Shroom3$^{Gt(ROSA)53Sor}$/J) were a gift from Dr. Thomas Drysdale at the University of Western Ontario. These mice contain a gene trap cassette, SAβgalCrepA originally designed by Hildebrand and Soriano. This cassette is inserted between exon 3 and 4 of *Shroom3* gene (Hildebrand and Soriano, 1999). The gene trap contains an adenovirus splice acceptor (SA) (Friedrich and Soriano, 1991), a bifunctional gene encoding a fusion between *β-galactosidase* (β-gal), *Cre recombinase* and an MC1 polyadenylation (pA) sequence (Thomas and Capecchi, 1987). Shroom3 heterozygous mice were crossed together to generate homozygous null mice. Genotyping was performed on tail DNA using the following primers. Wild-type (*WT*) alleles were detected using a forward primer, 5'-GGTGACTGAGGAGTAGAGTCC-3', and a reverse primers, 5'-GCAACCACATGGTGGGAGACAAGC-3', while mutant alleles were detected using the same forward primer, and a reverse primer 5'-GAGTTTGTGCTCAACCGCGAGC-3'. A seperate set of primers that amplify the *LacZ* transgene was used to confirm the presence of the mutant allele using a forward primer, 5'-GTTGCAGTGCACGGCAGATACACTTGCTGA-3', and a reverse primer 5'-GCCACTGGTGTGGGCCATAATTCAATTCGC-3'.

DNA was isolated by lysing mouse tails at 95°C in 50mM NaOH for 1 hour and then 0.5M Tris-HCl pH 8.0 was added into solution. The solution was mixed and centrifuged at 12,000 rpm for 3 minutes. PCR conditions for amplification of *WT* and mutant alleles were 95°C for 1 minute, 65°C for 1 minute and 72°C for 1.5 minute for 30 cycles. The expected sizes of amplicons were 1 kb for *WT* allele and 1.5 kb for mutant allele. PCR conditions for amplification of LacZ gene were 94°C for 30 seconds, 60°C for 30 seconds and 72°C for 1 minute for 35 cycles. The expected amplicon size for the LacZ gene was 389 bp.

Micro dissection of mouse kidneys:

Noon of the day of vaginal plug was considered to be embryonic day 0.5. Mouse embryos were collected at stages E13.5, E14.5, E16.5, and E18.5. *WT* and *Shroom3*$^{Gt/+}$ mice at 3 month and 1-year of age were sacrificed under CO_2 atmosphere. Embryonic kidneys were resected under an Olympus SZ61 microscope using Dumont #5 INOX surgical forceps in cold Phosphate-buffered saline (PBS) pH 7.4. Once dissected samples were placed in 4% paraformaldehyde (PFA) for 24 hours at 4°C and then prepared for histology, IF, and β-galactosidase staining.

β-galactosidase staining:

β-galactosidase staining was performed on whole mount of excised embryonic and adult kidneys. *WT* and mutant whole kidneys were stained in parallel. Kidneys were washed in cold PBS and fixed in 4% PFA containing 100mM Hepes and 100mM NaCl. Kidneys

were washed in PBS containing 1% Triton-X (PBST) for 1 hour at room temperature. Next, kidneys were incubated in X-galactosidase stain (0.5mg/ml X-gal (Bethesda Research labs)), 400μM potassium ferrocyanide, 400μM potassium ferricyanide, and 2mM $MgCl_2$ at 37°C until staining was complete. Kidneys were washed in PBST and post fixed in 4% PFA and visualized on Olympus SZ61 microscope.

Histology:

Kidneys were fixed in 4% PFA in PBS for 24 hours at 4°C. Kidneys were processed for paraffin embedding and sectioned (4μm) and mounted onto coated slides. Paraffin embedded kidney sections were dried overnight at 37°C. For preparation for histological staining the kidney sections were deparaffinzed using three times xylene washes and rehydrated using graded ethanol washes (100%, 95%, 70%, 50%, H_2O). Tissue sections were stained using haematoxylin and eosin (Sigma, St. Louis, MO), periodic acid-Schiff, and Jone's Methamine Silver (JMS). Tissue sections then were coversliped using permanent mounting medium (Vector Labs, H-5000). Our routine histology was performed by the Toronto Center for Phenogenomics. Images were captured using either an Olympus BX60 or a Nikon 90i-eclipse upright microscope.

In situ **hybridization:**

In situ hybridization (ISH) was performed using the Affymetrix QuantiGene ViewRNA according to manufacturer's protocol. The ViewRNA ISH Tissue 2-Plex Assay, which provides robust simultaneous *in situ* detection of any two target mRNAs within the tissue

section, was used to visualize *Shroom3* and *Wt-1* RNAs within the kidney sections. This assay is based on 4 distinct steps: (1) Sample preparation to allow unmasking of RNA and probe accessibility. (2) Hybridization of specific probe set to the target RNA. TYPE 1 and TYPE 6 probe sets were generated to generate red and blue signals, respectively. (3) Signal amplification via a series of sequential hybridization steps. (4) Visualization by addition of Fast blue substrate to generate blue signal for TYPE 6 label probe and Fast red substrate to produce red signal for TYPE 1 label probe. Paraffin embedded kidney sections were deparaffinzed in xylene and washed twice in 100% ethanol. After 20 minutes air drying, sections were transferred to preheated pretreatment solution and incubated at 95°C for 10 minutes. Sections were washed with dH_2O, incubated with protease solution at 40°C for 15 minutes, washed in PBS, and fixed in 4% PFA at room temperature for 5 minutes. Kidney sections were washed in PBS and incubated with *Shroom3* TYPE 1 and *Wt-1* TYPE 6 probes at 40°C for 2 hours. Affymetrix Panomics designed these probes for detection of *Shroom3* and *Wt-1* mRNAs by ViewRNA assay. TYPE 1 and TYPE 6 probes generate red and blue signals, respectively. Sections were washed in wash buffer (provided by the Affymetrix company) and stored in storage buffer overnight at room temperature. Kidney sections were incubated with preamplifier solution at 40°C for 25 minutes and washed with wash buffer. Sections were incubated with amplifier at 40°C for 15 minutes, washed with wash buffer, and then incubated with the first alkaline phosphatase-conjugated label probe 6-AP at 40°C for 15 minutes. Sections were washed in wash buffer followed by incubation with Fast Blue Substrate to visualize *Wt-1* RNA (provided by the Affymetrix company) in the dark at room

27

temperature for 30 minutes, washed in wash buffer. Prior to proceeding with the second label probe hybridization, the residual Label probe 6-AP activity was inactivated to prevent producing red signal by residual Label probe 6-AP during subsequent step. Thus, sections were incubated with ViewRNA AP Stop QT buffer at room temperature for 30 minutes and washed with PBS. Next, kidney sections were incubated with the second alkaline phosphatase-conjugated Label Probe 1-AP at 40°C for 15 minutes. Sections were washed with wash buffer and incubated in Fast Red Substrate (provided by the Affymetrix company) to visualize *Shroom3* RNA at 40°C for 30 minutes. Sections were washed in PBS, air-dried and coversliped using Fluoromount (Sigma, F4680). Kidneys were viewed and photographed on a Nikon 90i-eclipse upright microscope.

Immunofluorescence:

Paraffin embedded kidney sections were deparaffinzed using xylene washes and rehydrated using graded ethanol washes. Kidney sections were subjected to antigen retrieval in a pressure cooker at 95-100°C for 5 minutes in 10mM sodium citrate solution pH 6.0. Sections were washed in PBS, a hydrophobic barrier (Vector Labs, H-4000) drown to outline the tissue and rewashed in PBS. The sections were then incubated in blocking buffer (DAKO, X0909) for 1 hour at room temperature. Kidney sections were incubated with primary antibodies to Wt-1 (Santa-Cruz, 1:200), nephrin (R&D, 1:200 dilution), synaptopodin (Santa-Cruz, 1:200), Podocin (Sigma, 1:200), Six2 (Proteintech Group, 1:200), Pax2 (Covance, 1:200), actin (Abcam, 1:1000), and non-muscle myosin IIA (Abcam 1:200) overnight at 4°C. Kidney sections were then washed in PBS and

28

incubated with Alexa Fluor 488 or 568-conjugated secondary antibodies (Invitrogen, 1:1000) for 1 hour at room temperature. Kidney sections were washed in PBS and stained with Dapi (Sigma, D9542; 1:1000 dilution) for 5 minutes and coversliped using Fluoromount (Sigma, F4680). All images were captured using a Nikon 90i-eclipse fluorescence microscope. Confocal images were captured by Zeiss LSM510 confocal microscopy (Oberkochen, Germany).

Immunohistochemistry:

Paraffin embedded kidney sections were deparaffinzed and rehydrated using graded ethanol washes. Kidney sections were subjected to antigen retrieval in pressure cooker at 95-100°C for 5 minutes in 10mM sodium citrate solution pH 6.0. Sections were washed in PBS, a hydrophobic barrier (Vector Labs, H-4000) drown to outline the tissue and rewashed in PBS. Endogenous peroxidase activity was quenched using 3% H_2O_2 for 10 minutes at room temperature. Kidney sections were blocked in 5% horse serum in PBS for 1 hour at room temperature followed by blocking endogenous biotin binding activity using a biotin/avidin blocking kit (Vector Labs, SP-2001). Kidney sections were incubated with Shroom3 antibody (Santa Cruz, 1:250), p-MLC (Abcam, 1:200), Rock1 (Abcam, 1:250), and Wt-1 (Santa Cruz, 1:200) for 1 hour at 37°C. In order to examine Rock1 and p-MLC localization in the podocytes, immunohistochemistry were performed on 4 μm serial sections from *WT* and mutant mice using antibody against Wt-1 (podocyte nuclear marker). Kidney sections were washed three times with PBS and incubated in biotinylated secondary antibodies (Vector labs, B-9500) for 1 hour at room temperature.

Sections were washed in PBS and incubated with Vectastain elite ABC reagent for 30 minutes at room temperature (Vector Labs, PK7100). Kidney sections were washed with PBS and incubated in peroxidase substrate solution DAB (Vector Labs, SK4100) to develop desired stain intensity and slides were mounted using permanent mounting medium (Vector Labs, H-5000). Images were captured using either an Olympus BX60 or a Nikon 90i-eclipse upright microscope.

Whole-mount immunofluorescence:

Kidneys from *WT* and *Shroom3$^{Gt/Gt}$* at E13.5 and E16.5 were flattened on 0.4μm transwell filters (Falcon) for 8 hours at 37°C in DMEM. Then, kidneys were fixed in 100% methanol at -20°C. Kidneys were washed with PBS three times and incubated in a blocking buffer containing 10% normal goat serum for 2 hours. Then, kidneys were incubated with Cytokeratin antibody (Sigma; 1:200) at 37°C for 2 hours. Kidneys were washed in PBS and incubated with 1:200 goat anti-mouse Alexafluor 568 antibody (Invitrogen) for 2 hours at 37°C. The ureteric bud branching pattern and numbers were viewed and photographed on a Nikon 90i-eclise inverted microscope.

TUNEL assay:

Terminal deoxynucleotidyl transferase-mediated dUTP nick-end labeling TUNEL assay was performed (Promega). Paraffin embedded kidney sections were deparaffinzed in xylene, dehydrated using graded ethanol washes followed by immersing slides in 85% NaCl and PBS for 5 minutes. Kidney sections were fixed in 4% PFA for 5 minutes and

washed in PBS. To permeabilize tissue, sections were treated with 20µg/ml Proteinase K solution for 10 minutes at room temperature and washed in PBS. Sections were refixed in 4% PFA for 5 minutes and washed in PBS. Kidney sections were incubated with equilibration buffer at room temperature for 5 minutes followed by incubation in rTdT reaction mix at 37°C for 1 hour. To terminate the reaction, slides were immersed in SSC solution at room temperature for 15 minutes and washed in PBS. To block the endogenous peroxidase, sections were treated with 0.3% H_2O_2 for 3 minutes and washed in PBS. Kidney sections were incubated with Streptavidin HRP solution at room temperature for 30 minutes, washed in PBS. Colour reaction was visualized using DAB (Vector Labs, SK4100) followed by counterstaining with haematoxylin and washed in H_2O, slides were mounted using permanent mounting medium (Vector Labs, H-5000). TUNEL assay was performed by Lily Morikawa from the Toronto Center for Phenogenomics. Images were captured using an Olympus BX60 microscope.

Glomerular Number Estimating:

To estimate the glomerular number in *WT, Shroom3$^{Gt/+}$*, and *Shroom3$^{Gt/Gt}$* kidneys, the kidneys were isolated at E18.5 and were paraffin embedded and sectioned at 5-µm thickness. Every tenth section was collected throughout the entire kidney and stained with haematoxylin and eosin (Sigma, St. Louis, MO), and images were taken at 10X magnification. The number of glomeruli was counted from each image and an average was calculated from 5 different *WT*, 6 different *Shroom3$^{Gt/+}$*, and 5 different *Shroom3$^{Gt/Gt}$* mice. The glomerular counting experiment was performed by Alexandra Sull From Dr.

Drysdale's Lab at the University of Western Ontario. Data was analyzed using one-way ANOVA with a Kruskal-Wallis test.

Analysis of mouse urine:

To collect urine from $Shroom3^{Gt/+}$ and WT mice at 3 month and 1-year old, mouse were grabbed by the loos skin over the neck and turned over. By pressing the bladder, 200- 500 µl urine were collected in a 1.5 ml eppendrof tube. Proteinuria was qualitatively analyzed by running equal volumes of urine samples on 10% sodium dodecyl sulfate (SDS) gels followed by Coomassie Brilliant Blue staining. Protein concentration in urine was measured using the Bradford Assay (microtiter scale) (Bio-Rad) (Perez de Lema et al., 2001). Urine creatinine was measured in duplicate for each sample using Creatinine Assay Kit (Sigma-Aldrich, MAK080). Finally, urinary protein excretion was normalized to urinary creatinine defined as protein/creatinine ratio. Protein content for each sample was divided by creatinine content for the same sample. Spot urine samples were analyzed for $Shroom3^{Gt/+}$ (n=5) and WT littermates (n=5). The data was analyzed using 2-tailed Student's t test using GraphPad Prism 6 software. A probability of less than 0.05 was considered to indicate statistical significance. Values are given as mean +/- SEM.

Immunogold labeling:

Whole WT embryonic kidney at E18.5 and cortical region of WT adult kidney at 1-year-old were prepared for immunogold labeling at the Health Science Centre at McMaster University. Kidney tissues were fixed with 4% paraformaldehyde in 0.1M sodium-

cacodylate buffer and dehydrated using graded ethanol washes and embedded in LR-white resin. Ultrathin sections were cut and mounted on nickel grids. The grids were antigen retrieved in 10mM sodium citrate solution (pH 6.0) for 2 minutes at 95°C in a PCR machine. The grids were then immersed in filtered PBS (pH 7.4) and blocked in 5% horse serum in filtered PBS (Sigma Aldrich) for 1 hour. The grids were incubated with anti-Shroom3 antibody (Santa Cruz, CA, 1:30) at 37°C for 1 hour. Next, the grids were washed with filtered PBS four times followed by incubation with 12nm donkey anti-goat gold (Jackson Immuno Research; 1:50). The grids were washed with filtered PBS three times followed by rinsing with ddH$_2$O. The grids were air dried and counterstained with 0.5% uranyl acetate and 0.5% lead citrate, and examined using a JEOL 1200 EM TEMSCAN. Tissue for immunogold labeling was prepared by Marcia Reid from EM Facility.

Electron Microscopy:

The Electron Microscopy Facility in the Health Science Centre at McMaster University performed the tissue preparation for TEM and SEM. For TEM, whole embryonic kidneys from *WT* and *Shroom3$^{Gt/Gt}$* at E18.5 were fixed with 2.5% glutaraldehyde in 0.1M sodium-cacodylate buffer (provided by EM Facility). For adult kidneys, the *WT* and *Shroom3$^{Gt/+}$* kidneys at 1-year-old were resected. Then, the kidney cortex was separated from the medulla under an Olympus SZ61 microscope using Dumont #5 INOX surgical forceps in cold PBS and minced to 2mm cubes, and further fixed in 2.5% glutaraldehyde in 0.1M sodium-cacodylate buffer. Kidney tissue was postfixed with 1% osmium

teroxide, dehydrated using graded ethanol washes and embedded in epoxy resin. Ultrathin sections were cut and stained with uranyl acetate Images were viewed using JEOL JEM 1200 EM TEMSCAN (Tokyo, Japan). Images were captured using an AMT 4 megapixel digital camera. For SEM, embryonic and adult kidney tissues were fixed in 2.5% glutaraldehyde in 0.1M sodium-cacodylate buffer, and post-fixed in osmium tetroxide, dehydrated through a series of graded ethanols, and coated with gold-palladium. The gold-impregnated kidney samples were examined under Tescan Vega II LSU scanning electron microscope (Tescan USA, PA). Tissue for immunogold labeling was prepared by Marcia Reid from EM Facility.

4. RESULTS:

4.1   Shroom3 is expressed in embryonic and adult mouse kidneys

There was no data defining the spatial and temporal expression pattern of Shroom3 in the kidney. To begin to understand the function of Shroom3 in kidney development and disease, we need to understand the Shroom3 expression pattern. We utilized the $Shroom3^{Gt(ROSA)53Sor}$/J mice, which contains a gene trap β-galactosidase reporter under the control of the endogenous *Shroom3* promoter (Figure 1) (Hildebrand and Soriano, 1999), to perform initial analysis of the Shroom3 expression pattern in the kidney. The kidneys were resected from *Shroom3* mutant ($Shroom3^{Gt/Gt}$) and heterozygous ($Shroom3^{Gt/+}$) mice, and I performed X-gal staining, which would demonstrate the endogenous gene expression. Initial analysis of whole mount LacZ demonstrated *LacZ* expression in a pattern consistent with the medullary collecting ducts and renal papilla (Figure 2). Furthermore, expression was also in a spotted appearance in the cortex of the kidney consistent with the glomeruli (Figure 2).
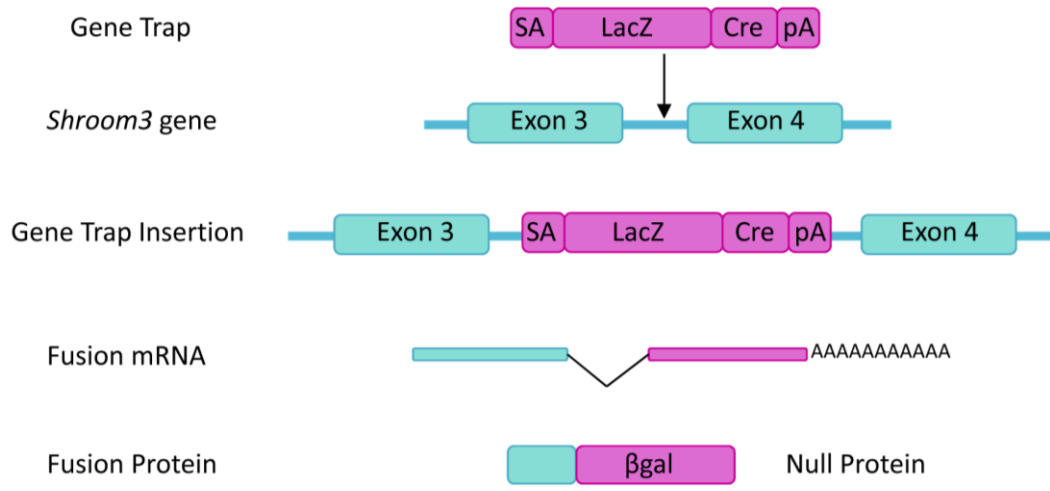
Figure 1. Schematic of Shroom3 gene trap. The gene trap is inserted between exon 3 and 4 of *Shroom3* gene. The gene trap contains an adenovirus splice acceptor (SA), a LacZ gene encoding *β-galactosidase*, *Cre recombinese,* and a poly-adenylation (pA) sequence (Hildebrand and Soriano, 1999).
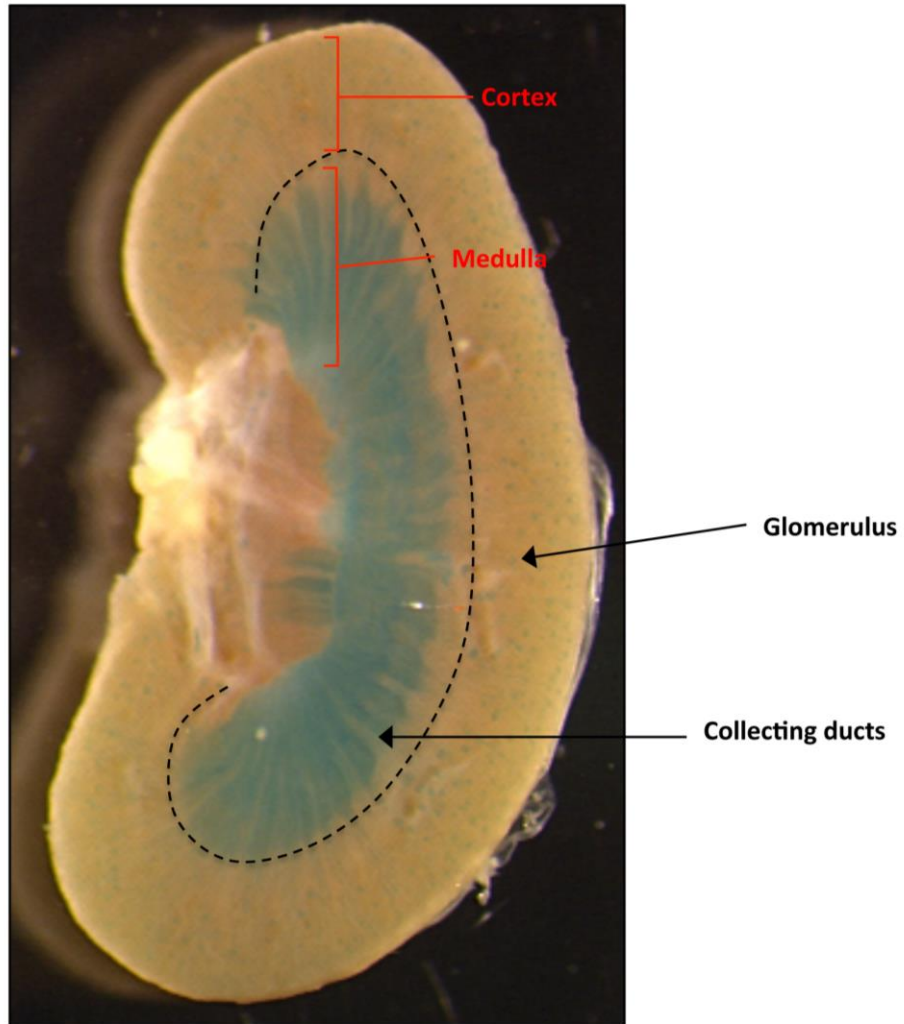
Figure 2. Whole mount X-gal staining of Shroom3 mutant kidney reveals strong LacZ expression. *LacZ* activity is observed in the cortical region of the kidney in the pattern consistent with the glomerulus. Collecting ducts in the medullary region and papilla exhibit robust *lacZ* activity.

To examine the developmental expression pattern at a cellular level, the X-gal stained whole mount kidneys were embedded in paraffin and sectioned at 4 μm. The X-gal staining showed a distinct expression pattern throughout kidney development. At E14.5, strong *LacZ* activity was observed in the condensing mesenchyme and the developing podocyte layer of the S-shaped body (Figure 3A, A'). I also observed a weak *LacZ* signal in the medullary collecting duct of *Shroom3* mutant mice at E14.5 (Figure 3A"). E18.5 embryonic kidney demonstrated marked *LacZ* reporter activity in the condensing mesenchyme and glomerulus (Figure 3B). *LacZ* activity in the glomerulus was in a pattern consistent with the podocytes and the partial epithelium of the Bowman's capsule (Figure 3B'). Moreover, E18.5 kidney exhibited robust *LacZ* activity in the collecting ducts (Figure 3B"). In addition, post-natal mice demonstrated strong *LacZ* reporter activity in the glomerulus in a pattern consistent with the podocytes and modest expression levels in the parietal epithelial cells (Figure 3C, C'). Robust *LacZ* reporter activity was also observed in the papillary collecting duct cells of *Shroom3*$^{Gt/+}$ adult mice (Figure 3D). The *LacZ* activity in the metanephric mesenchyme, the glomeruli, and the collecting ducts suggest that Shroom3 is important in both nephrogenesis and branching morphogenesis.
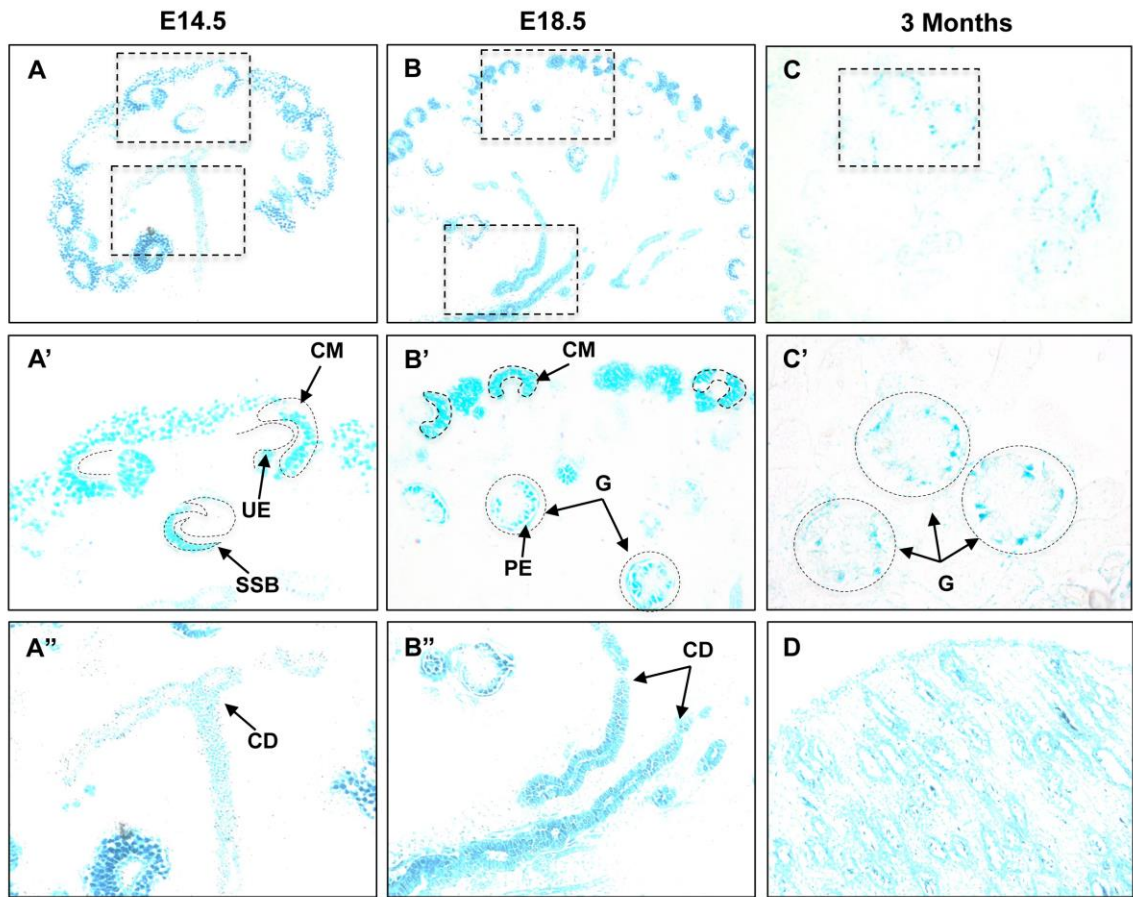
Figure 3. Shroom3 mutants exhibit LacZ reporter activity in the developing and mature Kidneys. *(*A-D) X-gal staining of E14.5, E18.5 and 3-month kidney sections demonstrating *LacZ* expression. (A'–D' are high magnification of panels A-D, respectively). (A) At E14.5, *LacZ* is expressed in the condensing mesenchyme, S-shaped body, and collecting ducts. (A', A") Higher magnification of regions represented by dotted boxes in Panel A demonstrates *LacZ* activity in the condensing mesenchyme, proximal regions of the developing S-shaped body, and the collecting ducts. (B) At E18.5, in addition to expression in the condensing mesenchyme and the collecting ducts, *LacZ* expression localizes to the glomeruli. (B') *LacZ* activity is observed in the glomerulus in the pattern consistent with the podocytes and the parietal epithelium of the Bowman's capsule. (B") Collecting ducts and renal papilla demonstrate marked *LacZ* expression at E18.5. (C, C') In 3-month adult kidneys, *LacZ* activity is observed in the glomerulus and at lower level to the parietal epithelial cells. (D) Robust *LacZ* activity is observed in the renal papilla of adult kidney. (SSB- S-shaped body, UE- ureteric epithelium, CM- condensing mesenchyme, PE-parietal epithelium, CD- Collecting duct).

39

Since *LacZ* reporter activity may not accurately represent the complete expression pattern of Shroom3, as these mice are mutants, I also performed immunohistochemistry using an antibody specific to the C-terminus of the Shroom3 protein on *WT* kidney sections. Immunohistochemistry of E14.5 *WT* kidney demonstrated Shroom3 expression in the S-shaped body, glomerulus, and collecting duct system (Figure 4A). Higher power images of a glomerulus demonstrated Shroom3 expression in the outermost layer, which is consistent with the podocytes (Figure 4B). In the collecting duct cells of E14.5 *WT* kidney, cytoplasmic localization of Shroom3 was observed (Figure 4C). At E18.5, Shroom3 was markedly expressed in the collecting duct system and glomerulus and at lower levels in the condensing mesenchymal cells (Figure 4D). High power image from E18.5 kidney demonstrated strong cytoplasmic brown staining in the outermost layer of glomerulus consistent with the podocytes (Figure 4E). I also observed Shroom3 localization in the cytoplasm of collecting duct cells (Figure 4F). In addition to the *WT* embryonic kidneys, I also performed immunohistochemistry on *WT* adult kidney and demonstrated cytoplasmic Shroom3 localization in the outermost layer of the glomerulus, consistent with the podocytes, parietal epithelium, and papillary collecting duct cells (Figure 4G, H). Shroom3 was localized in the cell membrane of the collecting duct cells (Figure 4H).

Next, I performed *in situ* hybridization (ISH) using the Affymetrix ISH to analyze *Shroom3* mRNA expression on *WT* embryonic and adult kidneys. *Shroom3* mRNA, represented by the red dots, was expressed in the condensing mesenchyme in the outer marginal zone of the kidney, glomerulus, and collecting ducts (Figure 5A-C). These

studies confirmed *LacZ* and Shroom3 protein expression patterns in the developing and adult kidneys. Expression of *Shroom3* in the condensing mesenchyme, developing and mature glomeruli, and the collecting ducts suggests it may play an important role during kidney development. Based on the function of Shroom3 in the neuroepithelial cells, I speculated it might induce cell shape changes required for distinct stages of nephrogenesis and branching morphogenesis.
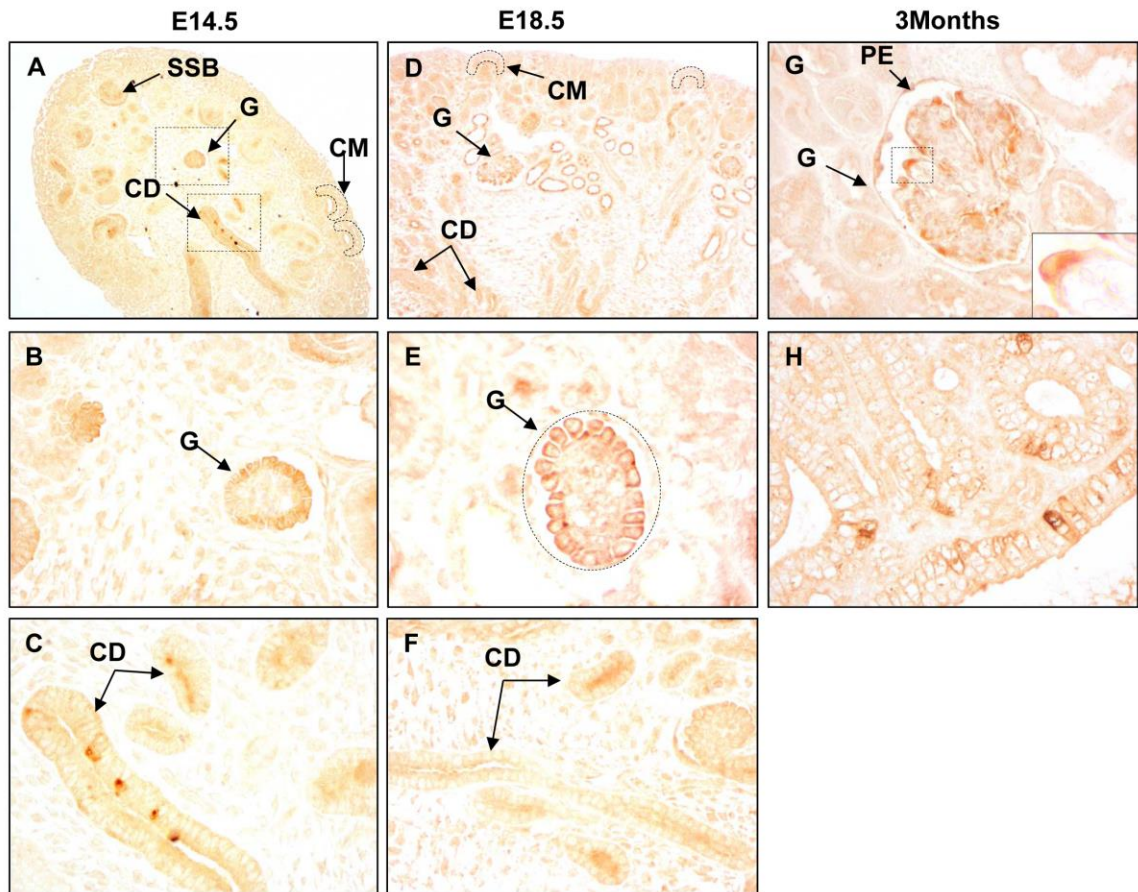
Figure 4. Spatial and temporal expression of Shroom3 protein in the developing and mature Kidneys. *(*A-H) Analysis of Shroom3 expression using immunohistochemistry in E14.5, E18.5, and 3-month kidneys. (A) At E14.5, *WT* kidney tissue demonstrates shroom3 expression in the condensing mesenchyme, S-shaped body, glomerulus, and collecting duct system. (B, C) Higher magnification images from boxed region in panel A show cytoplasmic localization of Shroom3 protein in the outermost layer of glomerulus and collecting duct cells. (D) Low power image from E18.5 *WT* kidney exhibits Shroom3 expression in the condensing mesenchyme, glomerulus, and collecting duct system. (E, F) Cytoplasmic shroom3 localization was detected in high power images from the glomerulus and collecting duct cells at E18.5. (G, H) Shroom3 expression was detected by immunohistochemistry using Shroom3 antibody in *WT* kidney at 3-months old. Shroom3 expression pattern in the glomerulus is consistent with the podocytes (inset). Cytoplasmic shroom3 expression is observed in the cells of papillary collecting duct. (SSB-S-shaped body, CM- condensing mesenchyme, CD-collecting duct, G-glomerulus, PE- parietal epithelium).
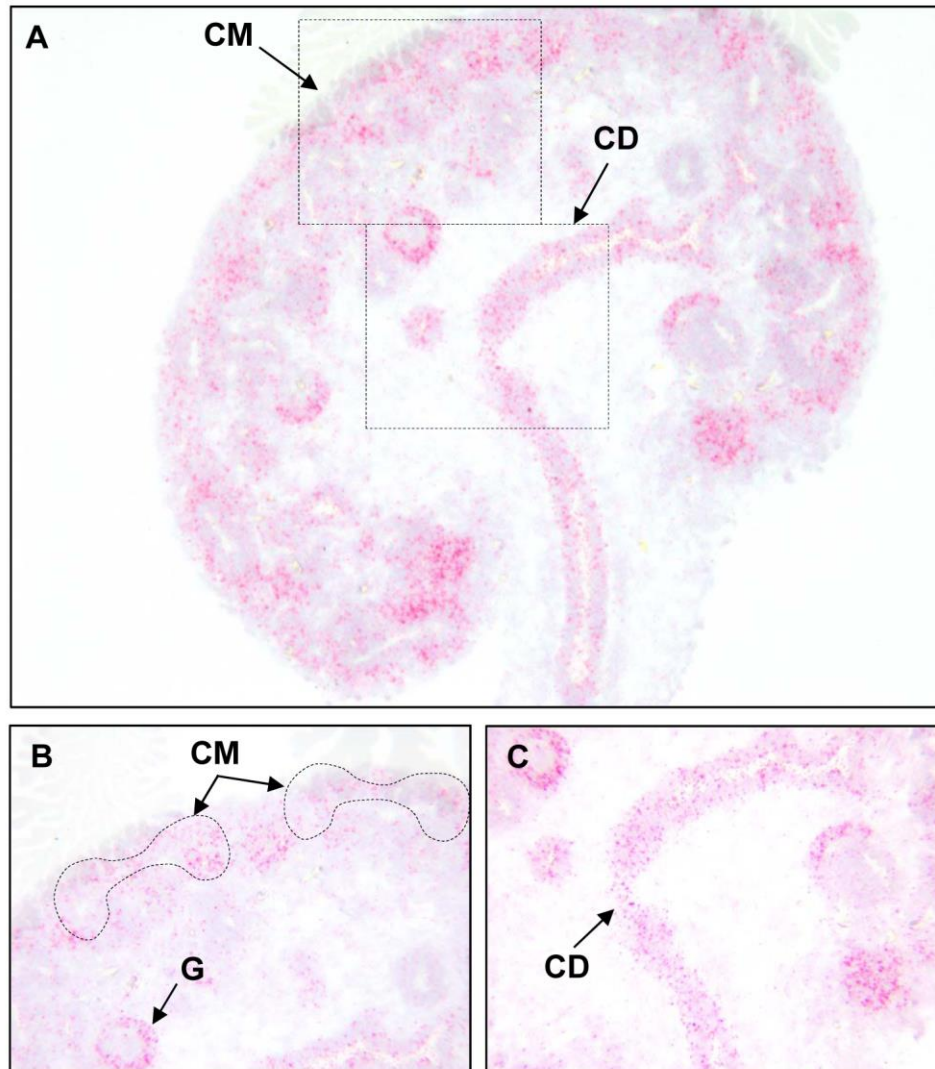
Figure 5. Shroom3 mRNA is expressed in the developing and adult kidneys. (A-C) In situ hybridization for *Shroom3* mRNA in E14.5 *WT* kidney. (A) Shroom3 mRNA, represented by red dots, is expressed in the condensing mesenchyme, developing and mature glomeruli, and collecting ducts. (B) Higher magnification of the boxed region from panel A demonstrates *Shroom3* mRNA in the condensing mesenchyme and glomerulus. (C) Higher magnification of the boxed region from panel A shows presence of *Shroom3* mRNA in the collecting ducts. (CM- condensing mesenchyme, CD-collecting duct, G-glomerulus).

Based on this expression pattern, there are numerous potential research questions for Shroom3 function and role in the kidney. I focused on the glomerular role because 1) Shroom3 expression analysis was most promising in the podocyte, 2) the podocyte contains a network of actin filaments, and 3) rearrangement of the podocyte actin cytoskeleton and damage to its complex cytoarchitecture serves as a common denominator in numerous kidney diseases. Therefore, I further defined the expression of Shroom3 within the glomerulus to determine the specific cells that express it. To do this, I performed ISH using the Affymetrix two-plex ISH, which allows the analysis of two different mRNA targets on the same tissue sample. I labeled *Wt-1* mRNA, a podocyte marker, and *Shroom3* mRNA on *WT* embryonic and adult kidneys. As expected *Wt-1* mRNA was expressed in the condensing mesenchyme and podocytes during nephrogenesis and was represented by the blue dots (Figure 6A, A', B, and B'). In the same tissue, expression of *Shroom3* mRNA, represented by the red dots, overlapped the expression of *Wt-1* demonstrating that *Shroom3* was expressed in the condensing mesenchyme, developing and more mature podocyte layer at E14.5 and E18.5 (Figure 6A, A', B, and B'). Higher magnification of boxed regions in figure 6A and B demonstrated *Shroom3* mRNA expression, which overlapped with *Wt-1* mRNA in the podocyte layer of S-shaped body and mature glomerulus (Figure 6A", B"; insets represent *Shroom3* and *Wt-1* mRNAs in a single podocyte). *Shroom3* mRNA was also expressed in the podocytes of adult kidneys and demonstrated overlapping with *WT-1* mRNA (Figure 5C, inset). This result demonstrates that Shroom3 is expressed in the podocyte lineage and maintained in adult podocytes. This finding, combined with the fact that the actin

44

cytoskeleton determines the complex structure of the podocyte, suggests that Shroom3 might play an important role in the regulation of actin dynamics and podocyte morphology.
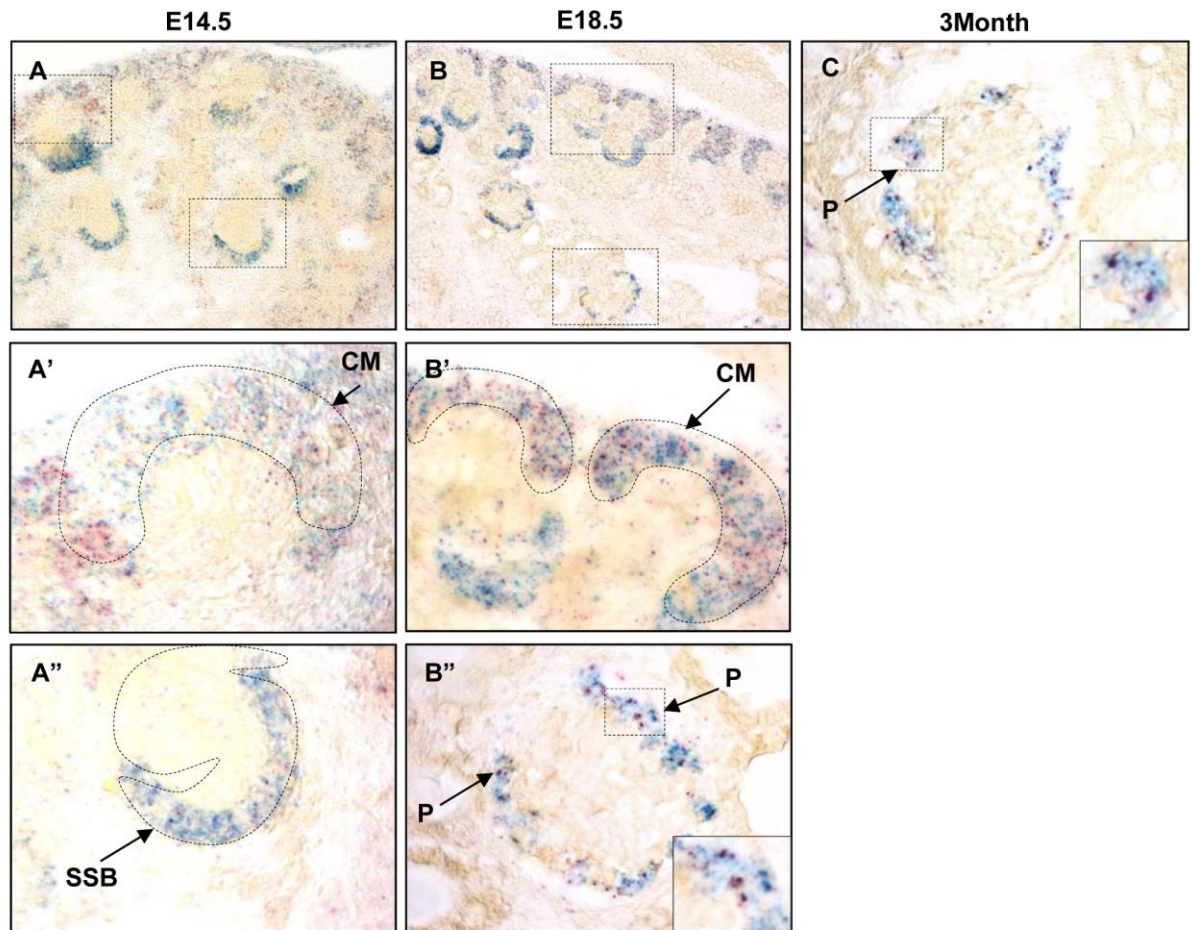
Figure 6. Shroom3 mRNA is expressed in the developing and mature podocytes. (A-C)
Double-in situ hybridization labeling of *Shroom3* and *Wt-1* mRNA demonstrates
expression of *Shroom3* in the developing and mature podocytes. Red and blue dots
represent *Shroom3* and *Wt-1* mRNA, respectively. (A) At E14.5, *Shroom3* mRNA is
expressed in the condensing mesenchyme and podocyte layer of the developing
glomerulus. (A') Higher magnification of represented box in panel A demonstrates
Shroom3 mRNA expression and overlapping with *Wt-1* mRNA in the condensing
mesenchymal cells. (A'') Higher magnification of represented box in panel A shows
overlapping of *Shroom3* and *Wt-1* mRNA. (B) Expression and overlapping of *Shroom3*
and *Wt-1* mRNA are observed in the condensing mesenchyme and podocytes of the
mature glomerulus at E18.5. (B') Higher magnification of boxed region in panel B
demonstrates *Shroom3* mRNA expression in the condensing mesenchyme. (B'') Higher
magnification of one glomerulus exhibits expression and overlapping of *Shroom3* and *Wt-
1* mRNA in the podocytes. Insets represent higher magnification of the dotted box. (C)
Shroom3 mRNA expression in the podocytes persists into the adulthood. Insets represent
higher magnification of the dotted box. (SSB- S-shaped body, CM- condensing
mesenchyme, P- podocytes).

For the first time, we have shown the spatial and temporal expression pattern of Shroom3 in the podocyte. I also explored its precise subcellular distribution in the podocytes by performing immunogold labeling and electron microscopy using Shroom3 antibody on ultrathin sections of *WT* kidneys. Immunogold electron microscopy technique is a superior method for detecting and localizing proteins in sub- and supra-cellular compartments. Transmission electron micrographs of immunogold stained E18.5 kidney demonstrated gold particles in both the podocyte cell body and secondary and tertiary foot processes (Figure 7A). 60,000X magnification of the boxed region in figure 7A demonstrates the small round distinctive gold particles (12nm), which represent labeling of Shroom3 protein in the apical plasma membrane of secondary and tertiary foot processes (Figure 7A'; inset). In the adult kidney, a similar pattern of Shroom3 localization was observed (Figure 7B). Higher magnification of the region represented by a black box in figure 7B exhibits gold particles for Shroom3 localized in the apical membrane of secondary and tertiary foot processes (Figure 7B'; inset). These results demonstrate, for the first time, the precise subcellular localization of Shroom3 in the podocyte foot processes of mammalian kidney. Since the foot processes contain actin filaments, this expression analysis suggests that Shroom3 might play a role in the regulation and formation of the foot processes actin cytoskeleton, which is consistent with Shroom3 function.
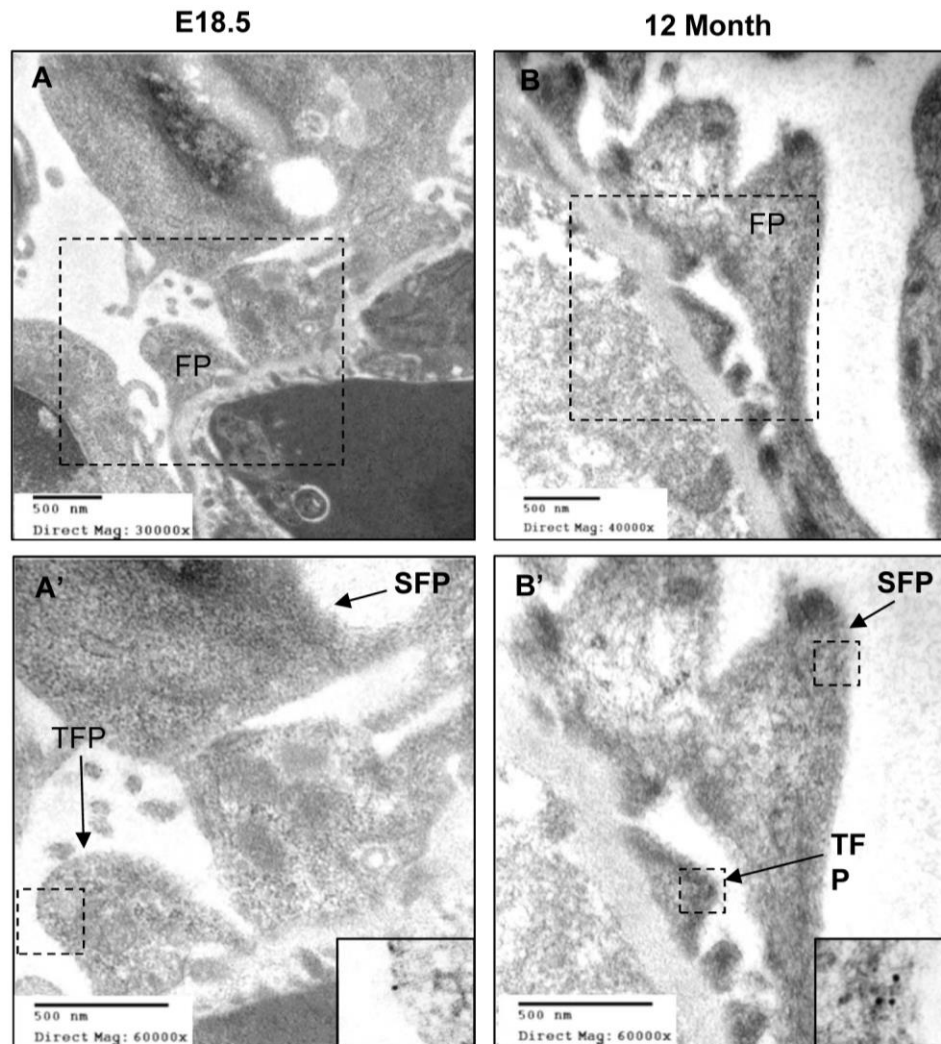
Figure 7. Shroom3 localizes in the podocyte cytoplasm and foot processes. (A)
Immunogold labeling for Shroom3 demonstrates its localization in the podocyte
cytoskeleton at E18.5. (A') Higher magnification of panel A shows the presence of gold
particles in the apical plasma membrane of podocyte cell body and foot processes. (B) In
the adult mouse, gold particles labeling Shroom3 are observed in both podocyte cell body
and foot processes. (B') Higher magnification of secondary and tertiary foot processes
demonstrates localization of gold particles representing Shroom3 in the apical membrane
of foot processes. Insets in panel A' and B' represent higher magnification of dotted
boxes. (FP- foot process, SFP- secondary foot process, TFP- tertiary foot process).

48

4.2 Reduce Kidney Size in *Shroom3$^{Gt/Gt}$* mice

In order to understand the role of Shroom3 in the kidney, we utilized and crossed *Shroom3* heterozygous mice to generate mutants. To identify *Shroom3$^{Gt/Gt}$*, *Shroom3$^{Gt/+}$*, and *WT* embryos, I performed PCR using primers that detected the mutant and *WT* allele (Figure 8A, B). The PCR amplification of the mutant and *WT* allele generated a 1.5 Kb and 1 Kb amplicons, respectively. Presence of the mutant allele in *Shroom3$^{Gt/Gt}$* and *Shroom3$^{Gt/+}$* embryos was further confirmed by amplifying the *LacZ* inserted allele (389 bp) (Figure 8C).

In order to begin our investigation, we analyzed the gross anatomy of mutant kidneys. Gross anatomical analysis of E13.5 and E14.5 mice revealed that *Shroom3* mutant and *WT* kidneys were similar in shape and size. However, *Shroom3$^{Gt/Gt}$* kidneys at E16.5 and E18.5 were visually smaller compared to the *WT* kidney, which was confirmed by histology (Figure 9A). Examination of the kidney length (superior pole to inferior pole) on the histology sections from E16.5 and E18.5 mice revealed significant reduction in the length of *Shroom3$^{Gt/Gt}$* kidneys when compared to the *WT* littermates (Figure 9B). No significant changes in the length of *Shroom3* heterozygous kidney were observed (Figure 9B).

Since branching morphogenesis and nephron number are fundamental to establishing the kidney size (Nigam and Shah, 2009), we sought to determine whether abnormal branching morphogenesis or nephron formation contributed to the small size of *Shroom3$^{Gt/Gt}$* kidneys. Thus, I analyzed branching morphogenesis by performing whole-mount immunofluorescence using an anti-cytokeratin antibody to mark ureteric buds and

collecting ducts in the *WT* and *Shroom3$^{Gt/Gt}$* kidneys at E13.5. Normal ureteric bud branching pattern and branches number were observed in *Shroom3$^{Gt/Gt}$* kidneys when compared to *WT* kidneys (Figure 10A, B). To establish whether branching morphogenesis remained intact over-time, I also analyzed branching morphogenesis at E16.5. High magnification view of *Shroom3$^{Gt/Gt}$* kidney surface revealed regular shape and organization of branching ureteric bud tips compared to *WT* kidney (Figure 10C, D). Therefore, these results demonstrated that Shroom3 deficiency did not disrupt the branching morphogenesis during kidney development.
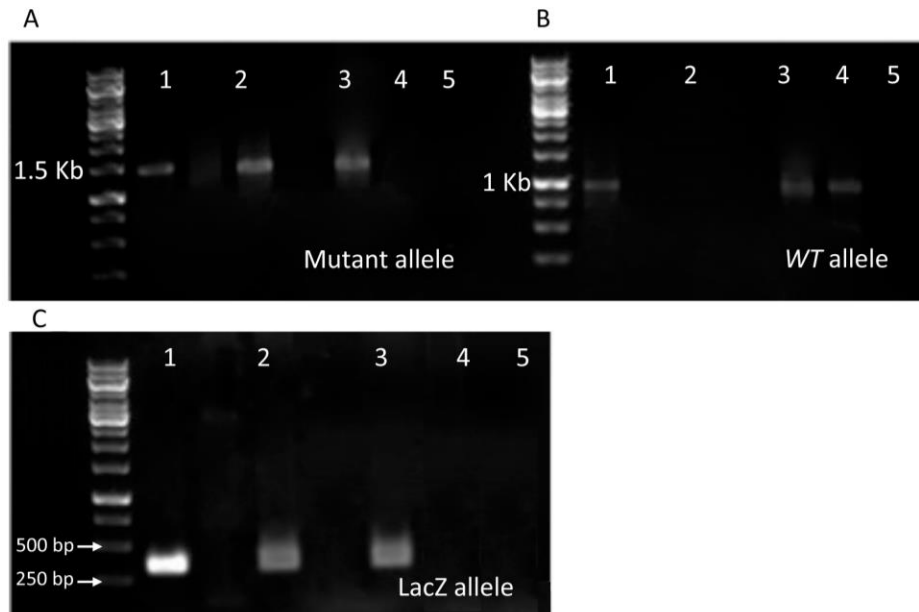
Figure 8. PCR genotyping of WT, Shroom3^{Gt/+} and Shroom3^{Gt/Gt}mice. (A, B, C)
Genotyping of embryos using primers specific the mutant, *WT*, and *LacZ* inserted allele.
(A) Primers amplify the mutant allele (1.5 Kb). (B) Primers amplify the *WT* allele (1 Kb).
(C) Primers amplify the *LacZ* allele (398 bp). Genotypes for following embryos:
Shroom3^{Gt/Gt} (lane 2), *Shroom3^{Gt/+}*(lane 3), and *WT* (lane 4). A negative control was used
to establish that there was no contamination in the PCR reaction.
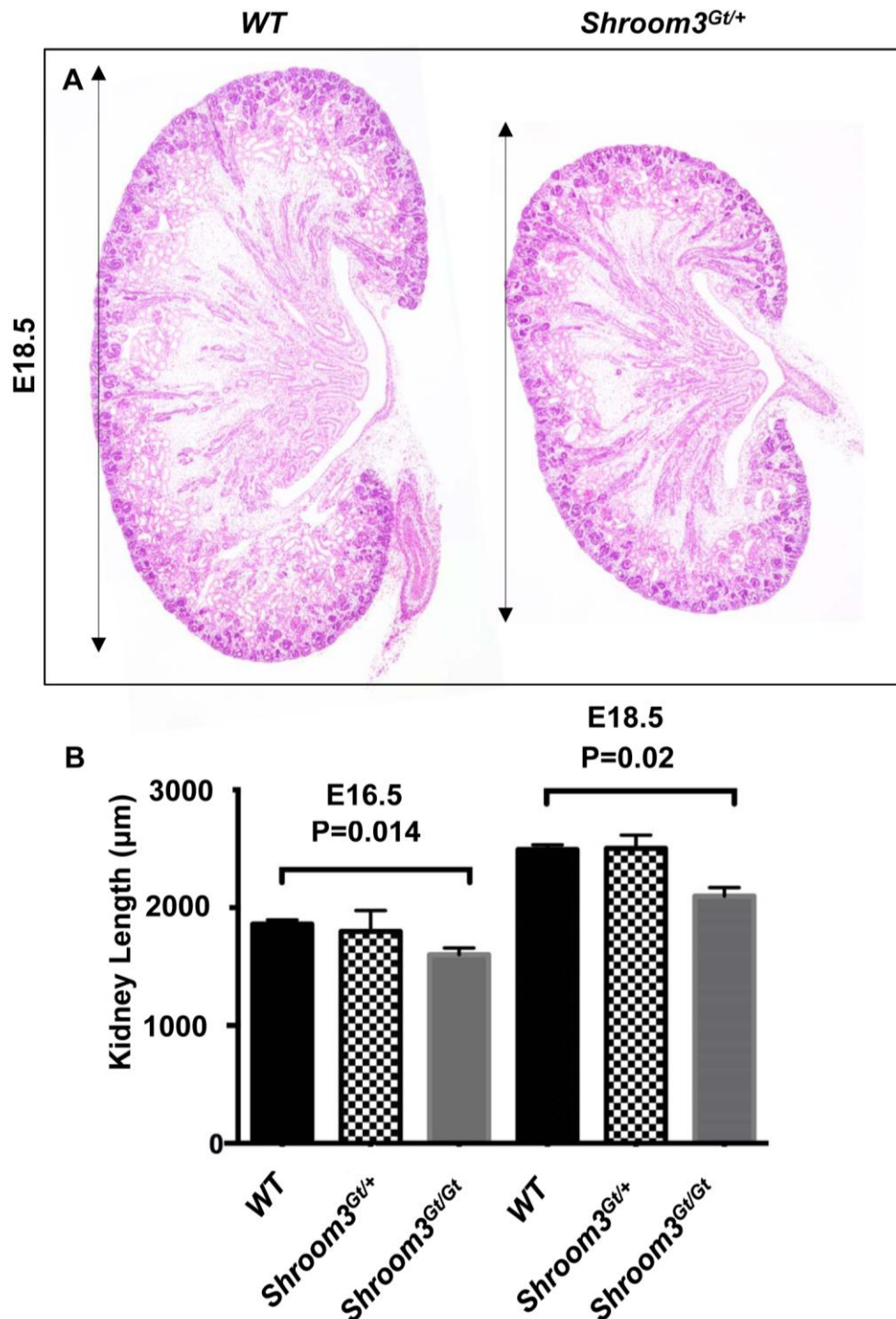
Figure 9. Shroom3^{Gt/Gt} mice display small kidney phenotype. (A) Histological analysis of kidneys at E18.5 demonstrates *Shroom3^{Gt/Gt}* kidneys are smaller than *WT* kidney (n=3). (B) Kidney length in *Shroom3* homozygous mutant mice is significantly reduced in comparison to *WT* littermates. While, *Shroom3* heterozygous mutant mice display normal kidney length.
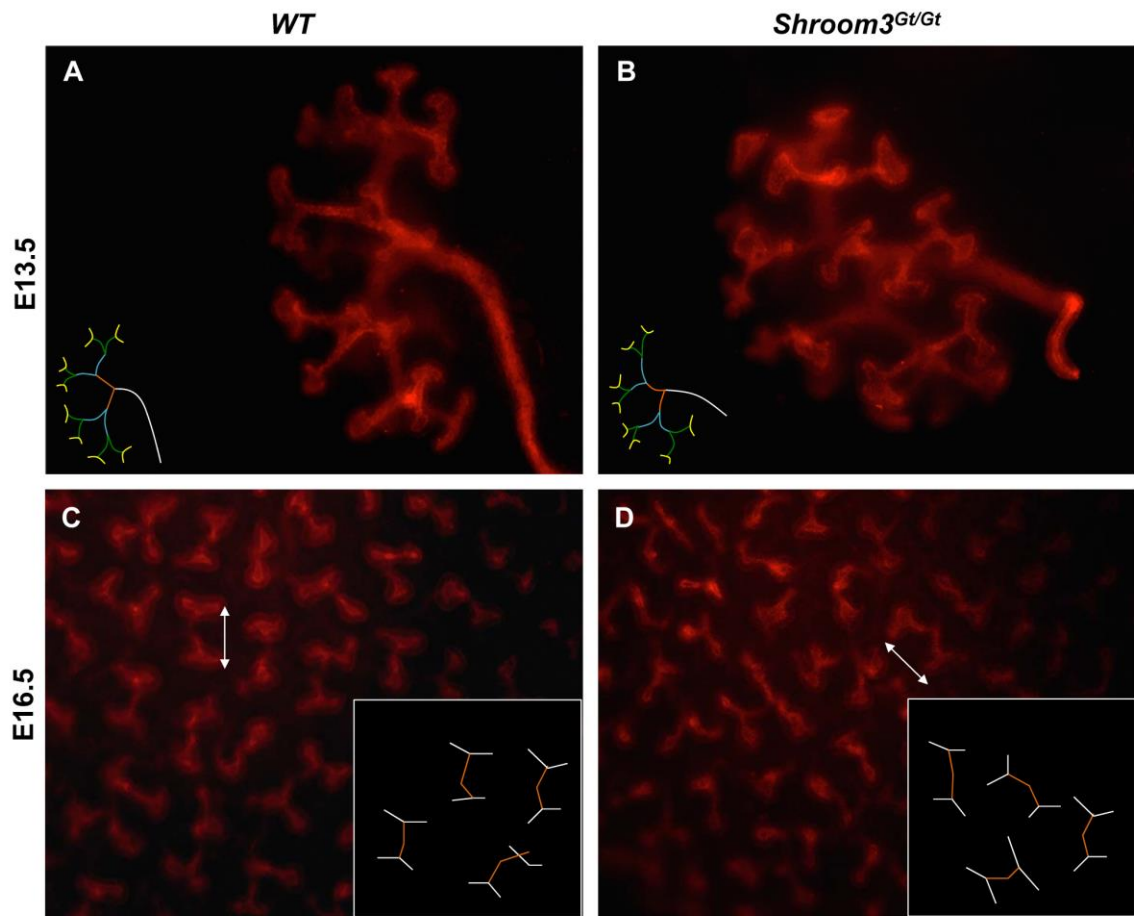
Figure 10. Shroom3^{Gt/Gt} mice demonstrate normal branching morphogenesis. (A-D)
Whole mount immunofluorescence using anti-cytokeratin antibody demonstrate normal
pattern of branching morphogenesis in *Shroom3^{Gt/Gt}* kidneys. (A, B) At E13.5, the
number and pattern of ureteric branches in *Shroom3^{Gt/Gt}* kidneys are similar to *WT*
kidneys (n=3). (C, D) Regular pattern of ureteric bud branching is observed in
Shroom3^{Gt/Gt} kidneys at E16.5 when compared to *WT* kidneys (n=3).

Although the pattern of branching morphogenesis remained intact in the mutant kidneys, the smaller kidney phenotype might be due to a defect in longitudinal elongation of collecting ducts, where Shroom3 is highly expressed. Since Shroom3 plays a role in inducing cell shape changes and cell elongation, I suspected that the collecting duct cells in *Shroom3$^{Gt/Gt}$* kidneys failed to alter their shape and cause elongation of collecting tubules. Therefore, I measured the height and width of collecting duct cells in three different papillary, medullary, and cortically regions under light microscope in *WT*, *Shroom3$^{Gt/+}$*, and *Shroom3$^{Gt/Gt}$* kidneys at E18.5 (Figure 11A). A comparison of cell width measurement revealed no changes between *WT*, *Shroom3$^{Gt/+}$* and *Shroom3$^{Gt/Gt}$*, while cell height of medullary and papillary collecting ducts were significantly increased in *Shroom3$^{Gt/Gt}$* kidneys when compared to *WT* kidneys (Figure 11B). Increase in the cell height of collecting ducts without changes in the cell width caused thickening and shortening of collecting tubules. Taken together, these analyses suggest that Shroom3 might play a role in the elongation of collecting tubules. Since the focus of this project was on the developmental and functional role of Shroom3 on the podocyte and glomerulus, we did not further assess the effect of Shroom3 in the elongation of collecting ducts.
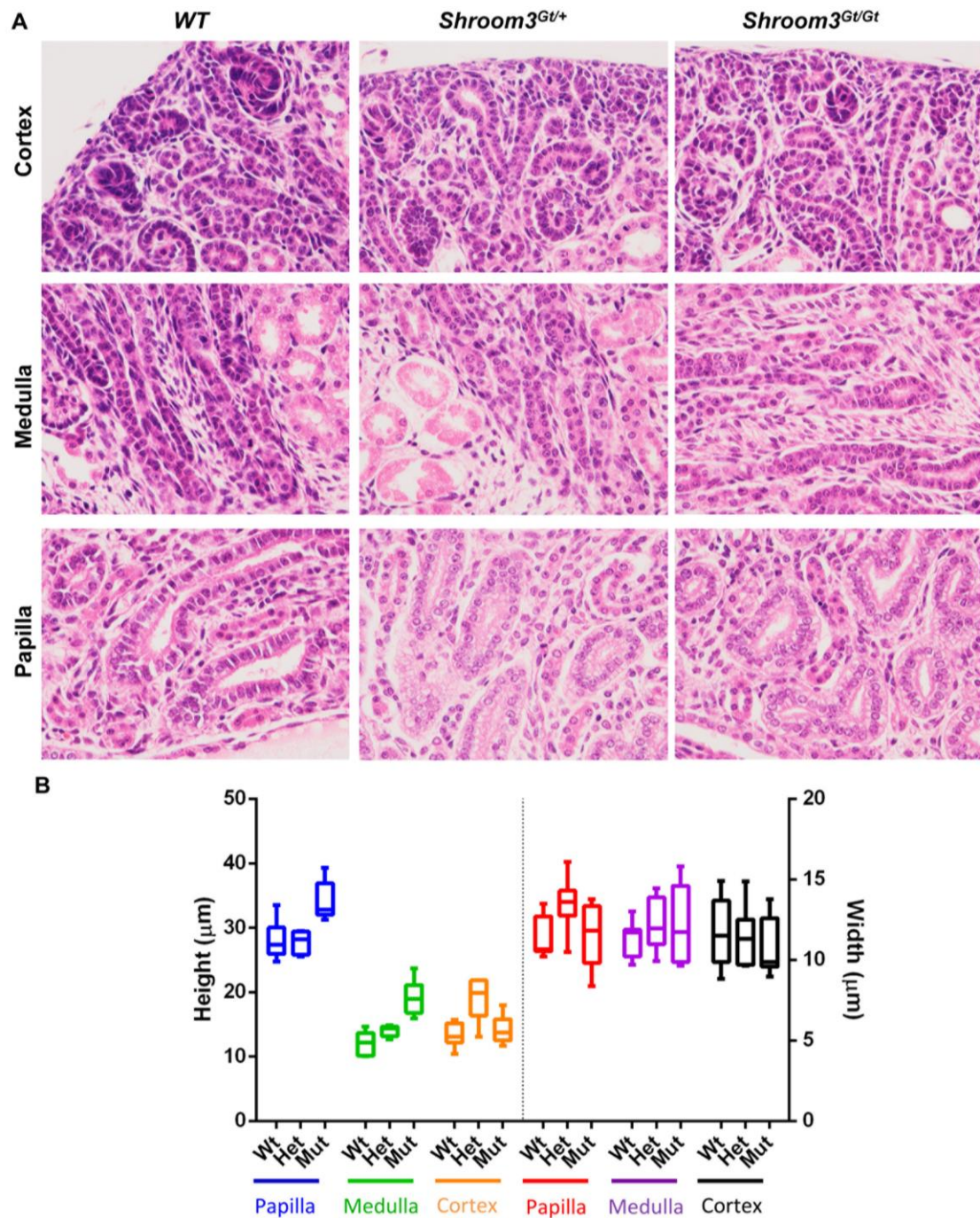
Figure 11. Thickening and shortening of collecting tubules cause Shroom3^{Gt/Gt} kidneys become smaller. (A) Histological analyses of cortically, medullary, and papillary regions of CDs from *WT*, *Shroom3^{Gt/+}*, and *Shroom3^{Gt/Gt}* kidneys at E18.5. (B) Measuring the cell height and width of CDs in *WT*, *Shroom3^{Gt/+}*, and *Shroom3^{Gt/Gt}* kidneys demonstrate cell width remain unchanged between distinct regions and different genotypes. While *Shroom3^{Gt/Gt}* kidneys demonstrate cell height of papillary and medullary CDs increase when compared to *WT* kidneys.

Next, to investigate if the smaller kidney phenotype in *Shroom3* mutants was due to a defect in nephron formation, I analyzed the condensing mesenchymal cells, which give rise to the nephron. I first used an antibody against Six2, a marker of the mesenchymal progenitor population. Although Shroom3 was expressed in the condensing mesenchymal cells, *Shroom3* mutant kidneys demonstrated similar expression pattern of Six2 positive cells compared to *WT* kidneys (Figure 12A-C). Therefore, normal expression of Six2 suggests that the nephron progenitors remained intact in *Shroom3* mutant kidneys. I next analyzed Pax2, a marker for the condensed mesenchyme and early differentiating epithelial structures including renal vesicle, comma- and S-shaped bodies. Normal nephrogenesis and organization of the condensing mesenchymal cells around the ureteric bud tips were observed in *Shroom3$^{Gt/+}$* and *Shroom3$^{Gt/Gt}$* kidneys when compared to *WT* kidney (Figure 12D-F). These analyses indicate that the absence of Shroom3 did not seem to affect the organization of condensing mesenchymal cells and initial nephron formation.
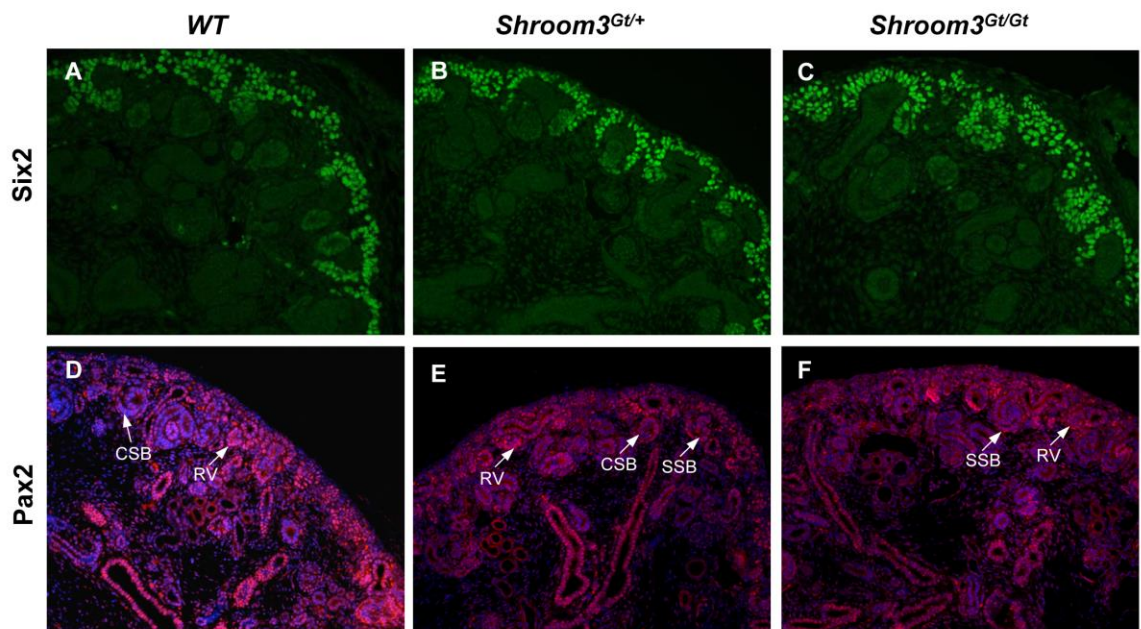
Figure 12. Nephron progenitors and nephron formation remain intact in Shroom3$^{Gt/Gt}$.
(A-C) Analysis of the Six2 cell population in *WT*, *Shroom3$^{Gt/+}$*, and *Shroom3$^{Gt/Gt}$*
demonstrates similar pattern of Six2 expression. (D-F) Analysis of the mesenchymal cell
population and early nephron structures using anti-Pax2 antibody reveals regular
distribution of the mesenchymal cells around the ureteric bud tips and formation of renal
vesicle, comma- and S-shaped bodies in *Shroom3* mutants. (RV- Renal vesicle, CSB-
Comma shaped body, SSB-S-shaped body).

4.3 *Shroom3* mutant kidneys demonstrate abnormal glomerulogenesis

Considering the highly restricted pattern of Shroom3 expression in the podocytes within the glomerulus and its critical role in cell shape changes in epithelial cells, I analyzed the histology of developing glomeruli in embryonic kidneys. In E13.5 *WT* kidneys, normal comma-, S-shaped bodies, and developing glomeruli were observed in the renal cortex (Figure 13A). In *Shroom3* heterozygote and mutant mice at E13.5, a few normal looking glomeruli were observed, however there were several glomeruli that appeared like globs of eosin positive, collapsed, and degenerating glomeruli with distinct Bowman's capsule (Figure 13B-C; arrows and insets). In addition, other glomeruli demonstrated a glomerular atrophy and a dilation of the Bowman's space (Figure 13B, C' asterisks). These glomeruli were observed in both heterozygous and homozygous mutants. At later stages of development, E14.5 and E18.5, I rarely observed the degenerating collapsed glomeruli; however, numerous glomeruli with dilated Bowman's spaces were observed in *Shroom3*$^{Gt/+}$ and *Shroom3*$^{Gt/Gt}$ kidneys (Figure 13D-I, asterisk). These abnormalities were rarely found in *WT* kidneys at any developmental age (Figure 13A, D, and G).
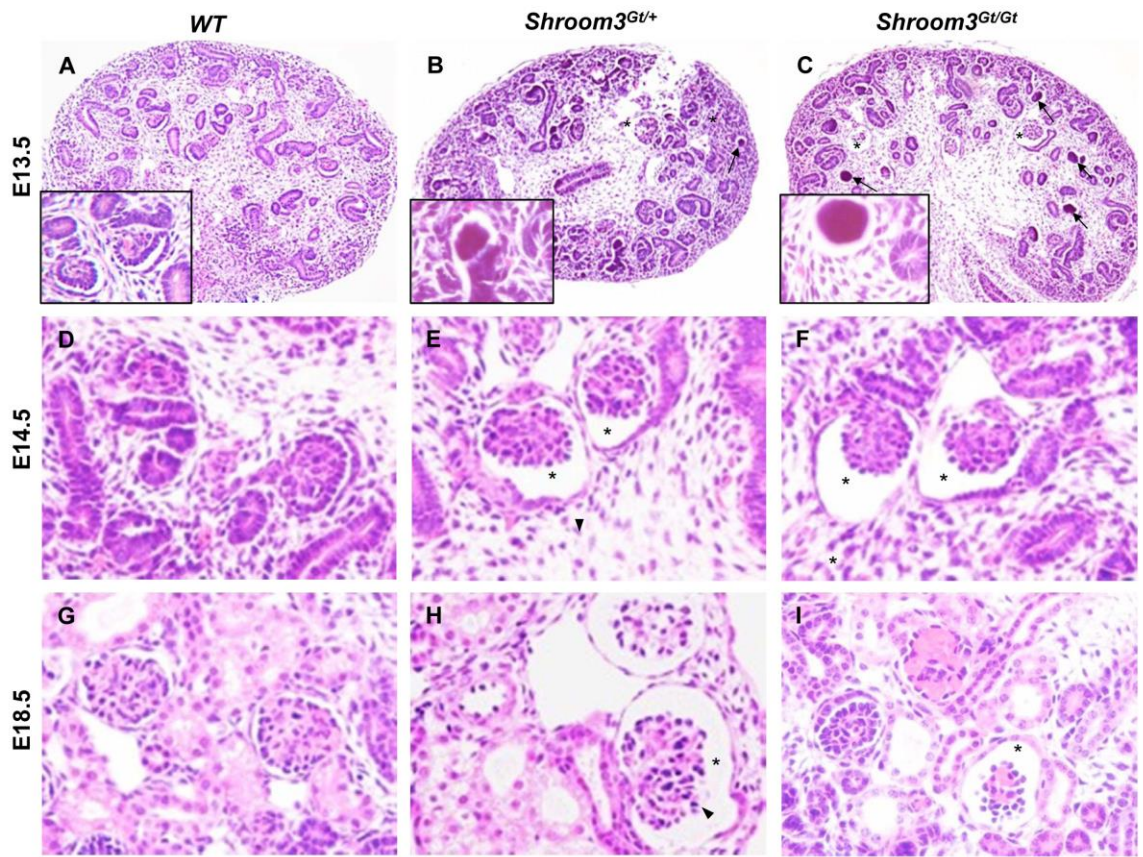
Figure 13. Abnormal glomerulogenesis in developing Shroom3 mutant kidneys (A-I)
Histological analyses of E13.5, E14.5 and E18.5 *WT* and *Shroom3* mutant kidneys
sections using Hematoxylin & Eosin staining. (A-C) At E13.5 *Shroom3$^{Gt/+}$* and
Shroom3$^{Gt/Gt}$ kidneys demonstrate collapsing degenerating glomeruli and cystic dilation
of the Bowman's space. Insets represent high magnification of abnormal glomeruli. These
abnormalities were not observed in *WT* kidneys. (D-I) At E14.5 and E18.5, *Shroom3$^{Gt/+}$*
and *Shroom3$^{Gt/Gt}$* kidneys exhibit cystic glomeruli with dilation of the Bowman's capsule
(*) when compared to *WT* kidneys.

To better understand the glomerular abnormalities, I performed an ultrastructure analysis of glomeruli from *WT*, *Shroom3$^{Gt/+}$*, and *Shroom3$^{Gt/Gt}$* mice at E18.5. A low power TEM image of a *WT* glomerulus demonstrated a portion of Bowman's capsule in which the podocytes are tightly packed and covered the capillary, and the partial epithelial cells surrounded the urinary space (Figure 14A). Higher magnification of the boxed region in Figure 14A demonstrates the glomerular filtration barrier with normal foot processes and slit diaphragm in *WT* glomerulus at E18.5 (Figure 14A'). In contrast to *WT* glomeruli, *Shroom3$^{Gt/Gt}$* glomeruli exhibited increased urinary space and podocytes were less densely packed (Figure 14B). On a higher magnification, segments of the podocyte foot processes demonstrated effacement and loss of the integrity of slit diaphragm in *Shroom3$^{Gt/Gt}$* podocytes (Figure 14B').

We next analyzed scanning electron micrograph of *WT* and *Shroom3$^{Gt/Gt}$* glomeruli to get a better perspective of the morphology and cytoarchitecture of the podocytes. The SEM image of the *WT* glomerulus demonstrated the surface architecture of the podocytes were tightly packed and uniformly covered the glomerular capillaries at E18.5 (Figure 14C). In contrast to *WT* glomerulus, *Shroom3$^{Gt/Gt}$* SEM analysis at the same developmental stage revealed that the cell bodies of podocytes were more rounded than normal (Figure 14D). We also observed increased spacing between the podocytes *Shroom3$^{Gt/Gt}$* glomeruli, which resulted in a less compacted appearance of podocytes (Figure 14D). Therefore, the loss of Shroom3 results in morphological defects in the podocytes of *Shroom3$^{Gt/Gt}$* mice. Considering that defects in glomerular formation may affect glomerular number (Komhoff et al., 2000), we suspected that the abnormal glomeruli

observed at E13.5 were degenerating and thus leading to reductions in glomerular number. Therefore, we estimated the number of glomeruli at E18.5 by performing serial sectioning of the whole kidney and counting the glomeruli of every 10th section to avoid counting the same glomeruli twice. This analysis demonstrated that the average estimated glomerular number in *WT* mice was about 1350 glomeruli per kidney (n=5), which is consistent with previous report (Arsenault et al., 2014). In contrast, *Shroom3$^{Gt/+}$* mice demonstrated 1100 glomeruli per kidney (n=7) and *Shroom3$^{Gt/Gt}$* mice showed 800 glomeruli per kidney (n=5). Quantitation of estimated glomerular number in E18.5 kidneys of these mice demonstrated that 1.2 and 1.51 fold reduction in the glomerular number of *Shroom3$^{Gt/+}$* and *Shroom3$^{Gt/Gt}$* mice, respectively, compared to their *WT* littermates (Figure 14E). These data demonstrate that reducing the Shroom3 levels results in a dose dependent reduction in the number of glomeruli. Taken together, these results suggest that abnormal glomerulogenesis in *Shroom3* mutants, causes dysmorphic glomeruli that might undergo degeneration resulting in reduced glomerular number.
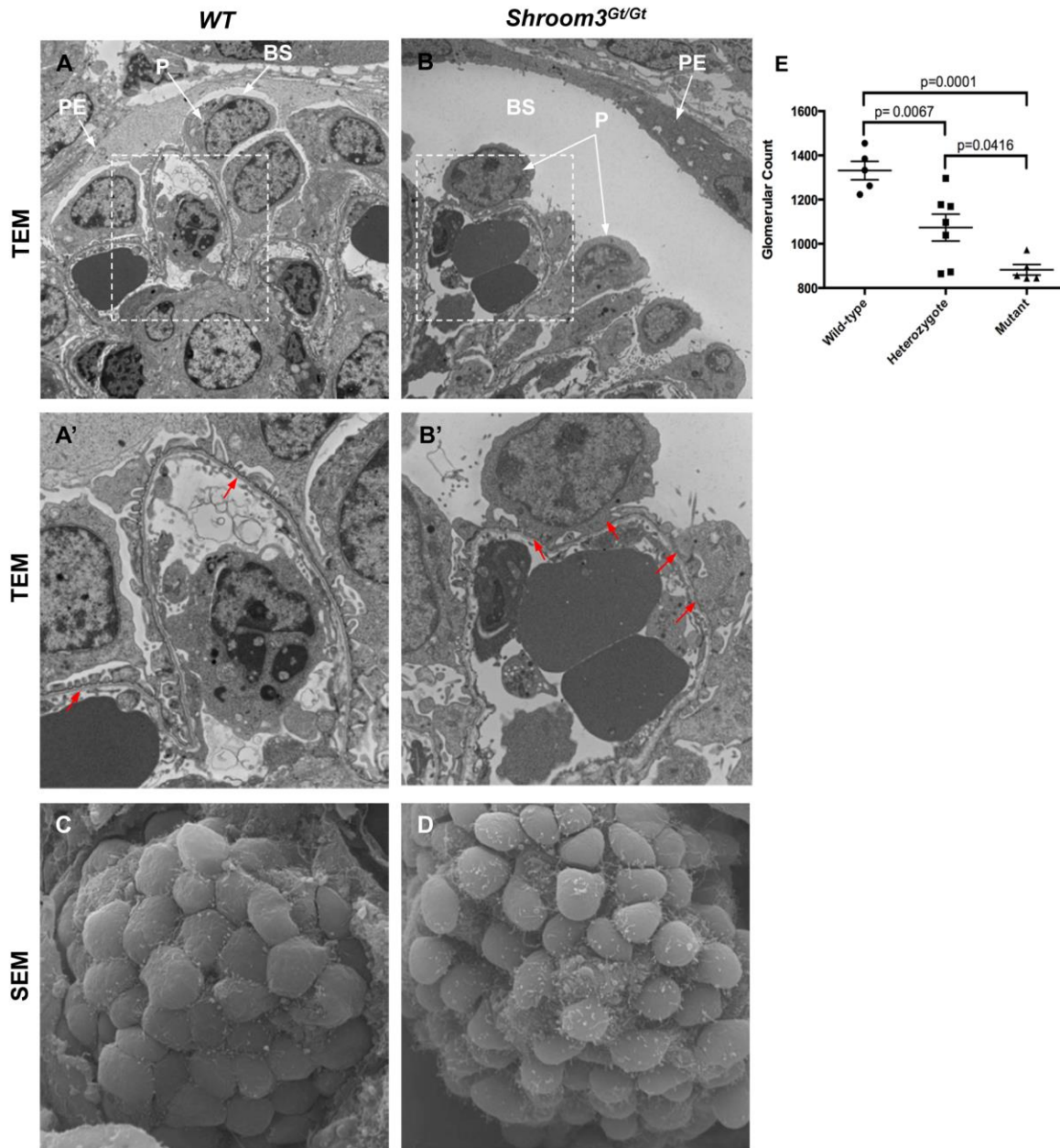
Figure 14. Ultra-structural analysis of the WT and Shroom3$^{Gt/Gt}$ glomeruli demonstrates altered podocyte morphology. (A, B) TEM of *Shroom3$^{Gt/Gt}$* glomeruli exhibits dilatation of Bowman's capsule and abnormal podocyte cell bodies. (A', B') Higher magnification of regions represented by white boxes in A and B demonstrate focal foot processes effacement in *Shroom3$^{Gt/Gt}$* glomeruli (red arrows). (C, D) Low power SEM image of *Shroom3$^{Gt/Gt}$* glomeruli demonstrates atypical spacing between adjacent podocytes compared to wild type glomeruli. (E) Quantitative analysis of glomerular number at E18.5 reveals a 1.24 fold and 1.51 fold reduction in glomerular number in *Shroom3$^{Gt/+}$* and *Shroom3$^{Gt/Gt}$* mutant kidneys, respectively.

4.4 *Shroom3* mutants depict reduction in podocyte number

Irregular distribution of podocytes along the glomerular capillary wall of $Shroom3^{Gt/Gt}$ kidneys might be caused by abnormalities in podocyte development and an inability to maintain the abnormal podocytes. To investigate this irregular distribution of podocytes, I first performed immunofluorescence staining using an antibody specific to the podocyte nuclear marker, Wt-1. We analyzed expression, distribution, and number of Wt-1 positive cells in kidneys from *WT, Shroom3$^{Gt/+}$,* and *Shroom3$^{Gt/Gt}$* mice at E18.5. Interestingly, the nuclei exhibited a sporadic distribution in the glomeruli of *Shroom3$^{Gt/+}$* and *Shroom3$^{Gt/Gt}$*, which was rarely observed in *WT* glomeruli (Figure 15A-C). This result is consistent with the electron microscopy findings that demonstrate inability of podocytes to maintain a complete cover of the glomerular capillary tuft.

Moreover, the number of Wt-1 positive cells was counted in 10 randomly selected glomeruli from 3 different *WT* kidneys and demonstrated 21.7 +/- 2.7 podocytes per glomerulus. In contrast, I observed 18 +/- 2.3 and 17 +/- 2.6 Wt-1 positive cells in 10 glomeruli from *Shroom3$^{Gt/+}$* and *Shroom3$^{Gt/Gt}$* kidneys, respectively (n=3 for each genotype). This quantification of podocyte number demonstrated a significant reduction in the number of Wt-1 positive cells in *Shroom3$^{Gt/+}$* and *Shroom3$^{Gt/Gt}$* kidneys compared to their control littermates (Figure 15G).

I next examined whether the reduction in the podocyte number and its abnormal distribution were due to apoptosis. Since DNA fragmentation is a hallmark of apoptosis, I utilized a TUNEL analysis, which demonstrated brown TUNEL positive cells in the developing podocyte cell layer and parietal epithelial cells of the Bowman's capsule in

Shroom3$^{Gt/+}$ and *Shroom3$^{Gt/Gt}$* kidneys (Figure 15D-F). I speculated that abnormalities in the Bowman's capsule cells might cause the dilated cystic phenotype in the glomeruli of *Shroom3* mutant kidneys. I next quantified TUNEL positive cells and demonstrated significant increase of 1.77 and 2.05 fold in apoptotic cells of *Shroom3$^{Gt/+}$* and *Shroom3$^{Gt/Gt}$* glomeruli, respectively, compared to *WT* glomeruli (Figure 15H).
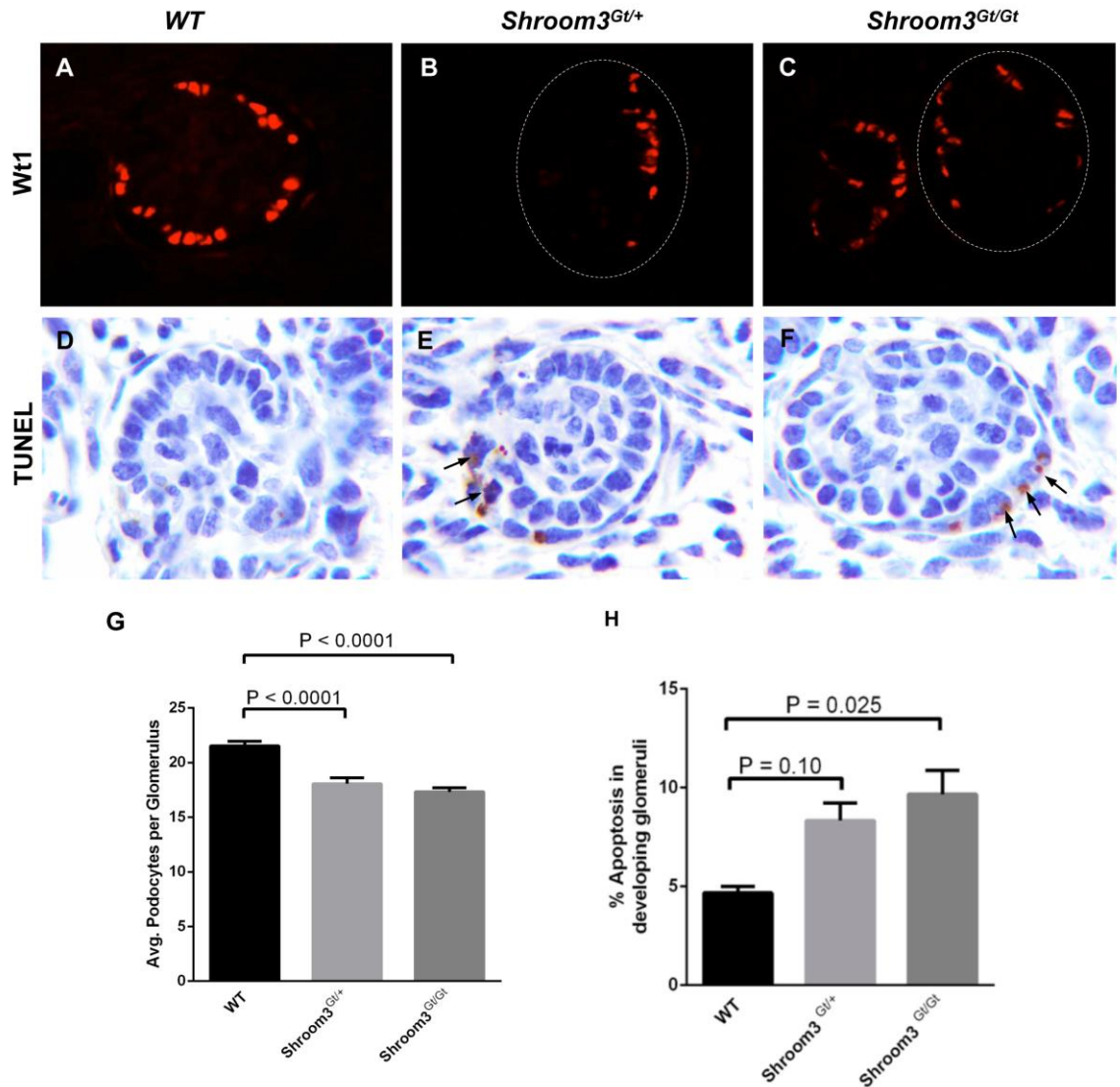
Figure 15. Shroom3 mutants depict sporadic distribution of Wt-1 positive cells and apoptosis in the developing glomeruli. (A-C) Wt-1 positive podocytes are distributed sporadically, forming a discontinuous cell layer on the outer aspect of the *Shroom3*^{Gt/+} and *Shroom3*^{Gt/Gt} mutant glomeruli as compared to control littermates (Dotted line represents glomeruli). (D-F) *Shroom3*^{Gt/+} and *Shroom3*^{Gt/Gt} mutants reveal increased levels of TUNEL-positive cells specific in the developing glomeruli (black arrows). (G) Quantitative analysis of Wt-1 positive nuclei reveals a significant reduction in podocyte cell number in *Shroom3*^{Gt/+} (1.2 fold decrease) and *Shroom3*^{Gt/Gt} (1.2 fold decrease) mutant glomeruli compared to controls. (H) Quantification of TUNEL analysis demonstrates increased podocyte apoptosis in *Shroom3*^{Gt/+} (1.77 fold increase, p=0.1, not significant) and *Shroom3*^{Gt/Gt} (2.05 fold increase, p=0.025) when compared to control littermates.

4.5 The interdigitating foot processes architecture is disrupted in *Shroom3* mutants

The foot processes of podocytes contain an actin-based cytoskeleton, which maintains the complex cytoarchitecture of the podocytes. Furthermore, regulation of the actin cytoskeleton is crucial for the structure and movement of foot processes. At the basal membrane of the foot processes, the actin cytoskeleton is connected to the GBM via integral membrane proteins, and disturbances of this connection can lead to podocyte loss (Kretzler, 2002). Therefore, the actin cytoskeleton is essential for podocyte structure and function and its disruptions can cause podocyte loss (Kretzler, 2002, Lasagni et al., 2013). To evaluate the cytoarchitecture of *Shroom3*$^{Gt/Gt}$ podocytes, we utilized SEM to image the podocyte morphology and foot processes organization in *WT* and *Shroom3*$^{Gt/Gt}$ kidneys at E18.5. We observed that podocyte cell bodies were flattened in the *WT* kidney to cover most of the capillary tuft surface, leaving less capillary membrane in direct contact with the urinary space. In contrast, podocyte cell bodies of *Shroom3*$^{Gt/Gt}$ kidneys were more swollen, leaving some regions of GBM denuded (Figure 16A, B). A close analysis of the foot processes showed they were disorganized with less interdigitation than that observed in the control glomeruli (Figure 16A, B). In addition, the tertiary foot processes appeared to be loosely adhered to the underlying GBM and disorganized. Similar changes were seen in the transmission electron micrographs of *Shroom3*$^{Gt/Gt}$ glomeruli, demonstrating a large distance between podocyte cell body and the GBM, when compared to *WT* littermates (Figure 16C, D). In addition, analysis of *WT* glomeruli by TEM revealed that the foot processes from adjacent podocytes were regularly interdigitated and covered the

glomerular capillary. In contrast, TEM image of *Shroom3$^{Gt/Gt}$* glomeruli demonstrated segmental foot processes effacement (Figure 16D; red arrowhead). Combined these results suggest a role for Shroom3 in the development and/or maintenance of podocyte foot process architecture.
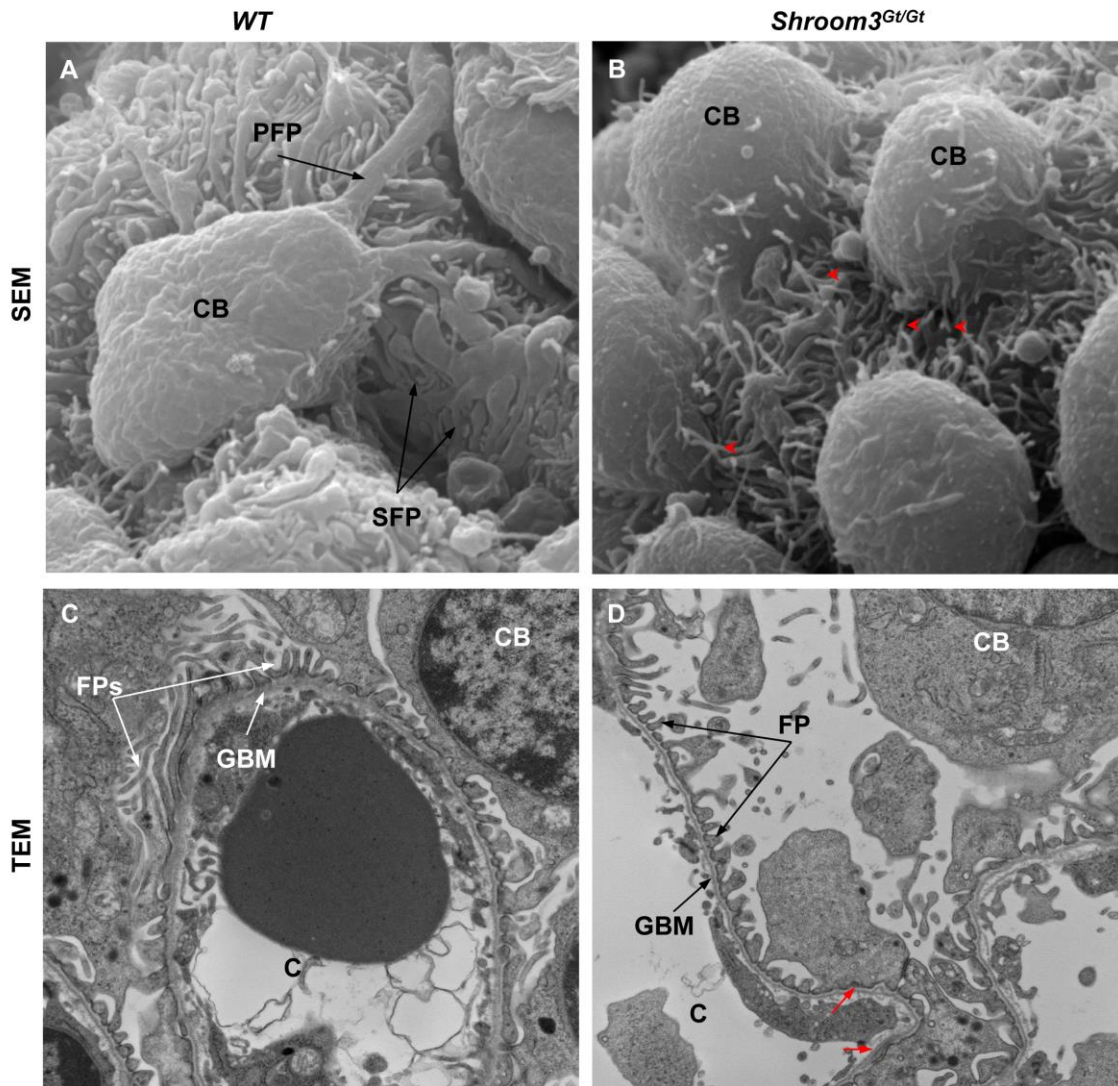
Figure 16. Shroom3 mutants demonstrate disorganized interdigitating foot processes.
(A, B) Scanning electron micrograph shows disorganized podocyte foot processes with poor interdigitation (red arrowheads) and swelling of the podocyte cell bodies in *Shroom3*^{Gt/Gt} mice compared to wild type control, original magnification 20,000X. (C, D) Transmission electron micrograph showing segmental foot processes effacement in *Shroom3*^{Gt/Gt} compared to control littermates (red arrows), and large distance between podocyte cell body and the GBM, original magnification 15,000X. (CB-cell body, PFP-primary foot process, SFP-secondary foot process, C-capillary, GBM-glomerular basement membrane).

4.6 *Shroom3* mutants exhibit alterations in essential podocyte proteins

Considering the alterations in the podocyte and podocyte foot processes architecture, I suspected abnormalities in the expression of key podocyte associated proteins. Nephrin is a transmembrane protein that is localized to the slit diaphragm between adjacent podocytes to form the filtration barrier and restrict the passage of protein into the ultrafiltrate. The extracellular domains of nephrin from neighboring podocytes interact with each other and form the slit diaphragm backbone (Khoshnoodi et al., 2003). Nephrin, via its intracellular domain, is indirectly connected to the actin cytoskeleton of foot processes. Mutations in the Nephrin gene lead to the disruption of slit diaphragm, rearrangement of foot processes actin cytoskeleton, and foot processes effacement (Kestila et al., 1998). Since nephrin is crucial for the maintenance of foot processes and podocyte integrity, I analyzed the expression and distribution of nephrin in *Shroom3* mutant kidneys at E18.5. In the *WT* kidney, nephrin is regularly distributed along the GBM in a linear-like pattern (Figure 17A). In contrast to *WT*, nephrin was expressed in a more diffused pattern in *Shroom3*$^{Gt/+}$ and *Shroom3*$^{Gt/Gt}$ mice, which suggests impairment of slit diaphragm integrity (Figure 17B, C). Podocin is a membrane protein that localizes in the podocyte slit diaphragm and interacts with both nephrin and the cytoskeleton of foot processes. Reduced expression of podocin has been reported in many glomerular diseases. Therefore, I analyzed the expression of podocin in *Shroom3* mutant kidneys. In *WT* kidneys, podocin staining revealed a linear pattern along the GBM, corresponding to its localization in the slit diaphragm (Figure 17D). Although podocin expression in *Shroom3*$^{Gt/+}$ mice was not significantly altered compared to *WT* at E18.5 (Figure 17E), its

expression in *Shroom3*$^{Gt/Gt}$ mice was markedly reduced and appeared in an irregular continuous thin linear layer (Figure 17F; arrowheads). Therefore, it can be concluded that reduction in expression of podocin and nephrin may be associated with the effacement phenotype and loss of slit diaphragm in *Shroom3* mutant mice.
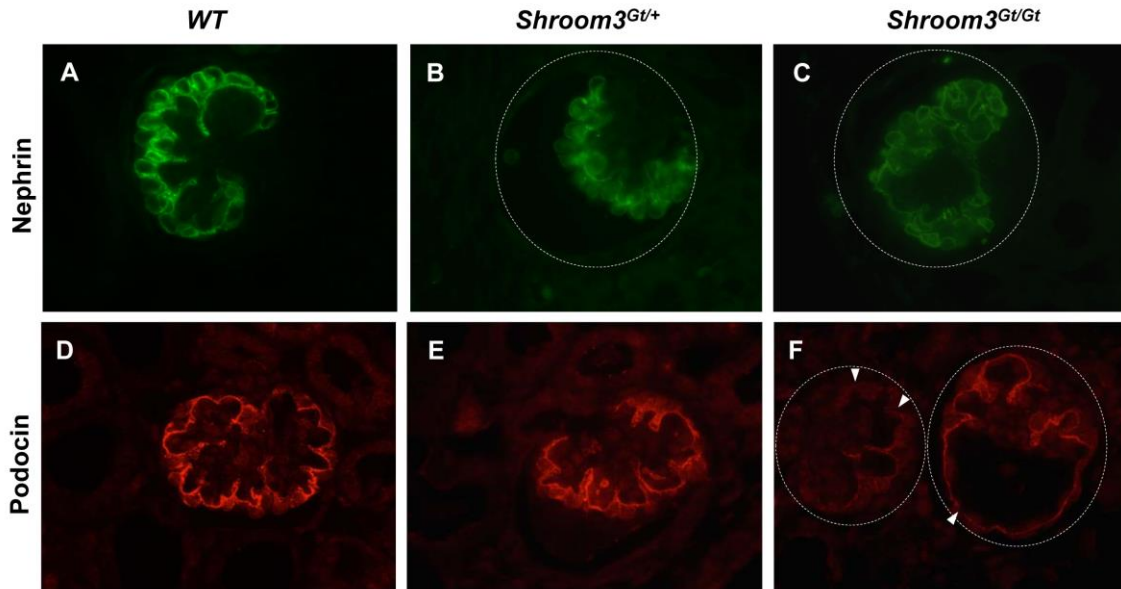
Figure 17. Shroom3 mutants exhibit alterations in essential podocyte proteins. (A-I) Immunofluorescence images of podocyte specific proteins in embryonic *WT* and *Shroom3* mutants. (A-C) In contrast to *WT*, nephrin protein expression in *Shroom3$^{Gt/+}$* and *Shroom3$^{Gt/Gt}$* mutant glomeruli shows a more diffuse expression pattern than control littermates. (D-F) Podocin expression in *Shroom3$^{Gt/+}$* glomeruli is similar to *WT*. In contrast, *Shroom3$^{Gt/Gt}$* glomeruli show marked alterations in the podocin expression pattern with a marked thinning in the podocyte layer. (Glomerulus has been marked with dotted lines in panels B, C, and F).

4.7 Shroom3 is required for Rock1 localization and function in the podocytes

Based on the known function of Shroom3 and the essential role of the actin cytoskeleton in the podocyte, we investigated if actin-associated proteins in podocytes were altered in absence of Shroom3. Synaptopodin is an actin-associated protein that expresses in the differentiated podocyte foot processes. Synaptopodin contributes to the complex cytoskeleton of the mature podocytes by inducing actin filament bundling (Mundel and Shankland, 2002, Yanagida-Asanuma et al., 2007). Since synaptopodin is crucial for the integrity of foot processes architecture, I analyzed the expression and distribution of synaptopodin in *WT* and *Shroom3* mutant kidneys at E18.5. In the *WT* kidneys at E18.5, synaptopodin was localized around the glomerular capillary, corresponding to its localization in the foot processes (Figure 18A). Although *Shroom3$^{Gt/+}$* glomeruli showed similar intensity of immunostaining for synaptopodin as *WT*, synaptopodin was absent in some regions of the glomeruli (Figure 18B; arrowheads). In *Shroom3$^{Gt/Gt}$* kidneys, we observed that a regular expression pattern of synaptopodin was absent in some regions of the mutant glomeruli (Figure 18C; arrowheads). This result suggests that irregular distribution of synaptopodin may be associated with ultrastructure of podocyte and poor foot process organization in the mutant kidneys.
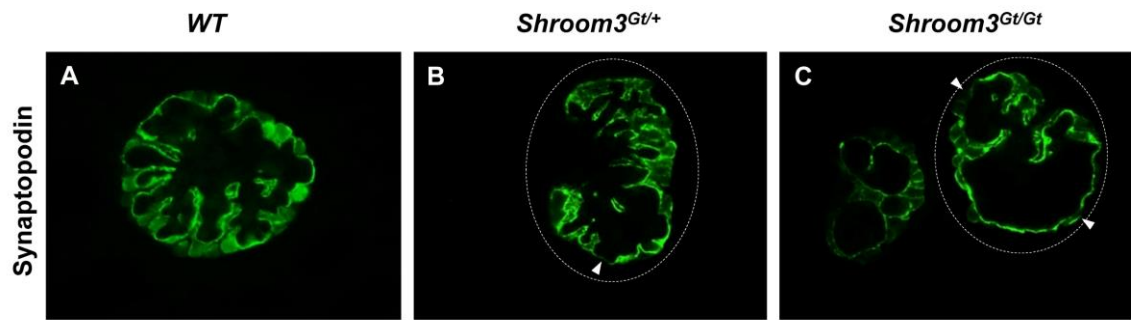
Figure 18. Shroom3 mutants exhibit irregular distribution of actin-associated proteins.
(A-C) Compared to *WT*, synaptopodin demonstrates an irregular expression pattern in
Shroom3^{Gt/+} and *Shroom3^{Gt/Gt}* mutant glomeruli (white arrowheads).

Recent in vitro studies have shown that Shroom3 contributes to the organization of actin stress fiber (McGreevy et al., 2015). Based on the fact that the major cytoskeleton of foot processes consists actin filaments, I sought to determine whether actin distribution was altered in the podocytes of $Shroom3^{Gt/Gt}$ mice. I therefore examined the distribution of actin in the podocytes of WT and $Shroom3^{Gt/Gt}$ kidneys at E18.5 by performing serial sectioning and immunostaining using anti-actin and Wt-1 antibodies. Actin distributions were visualized by confocal microscopy. In WT podocytes expressing Shroom3, actin was found along the apical margin of the podocyte cell bodies (Figure 19A, A'). While, in $Shroom3^{Gt/Gt}$ podocytes actin distribution was profoundly altered from a dense linear organization to a fine dotted pattern (Figure 19B, B'). Schematic drawing of the podocyte actin cytoskeleton demonstrates the dense linear pattern of actin along the apical membrane of the podocyte cell body is disrupted in the $Shroom3^{Gt/Gt}$ glomeruli (Figure 19C).
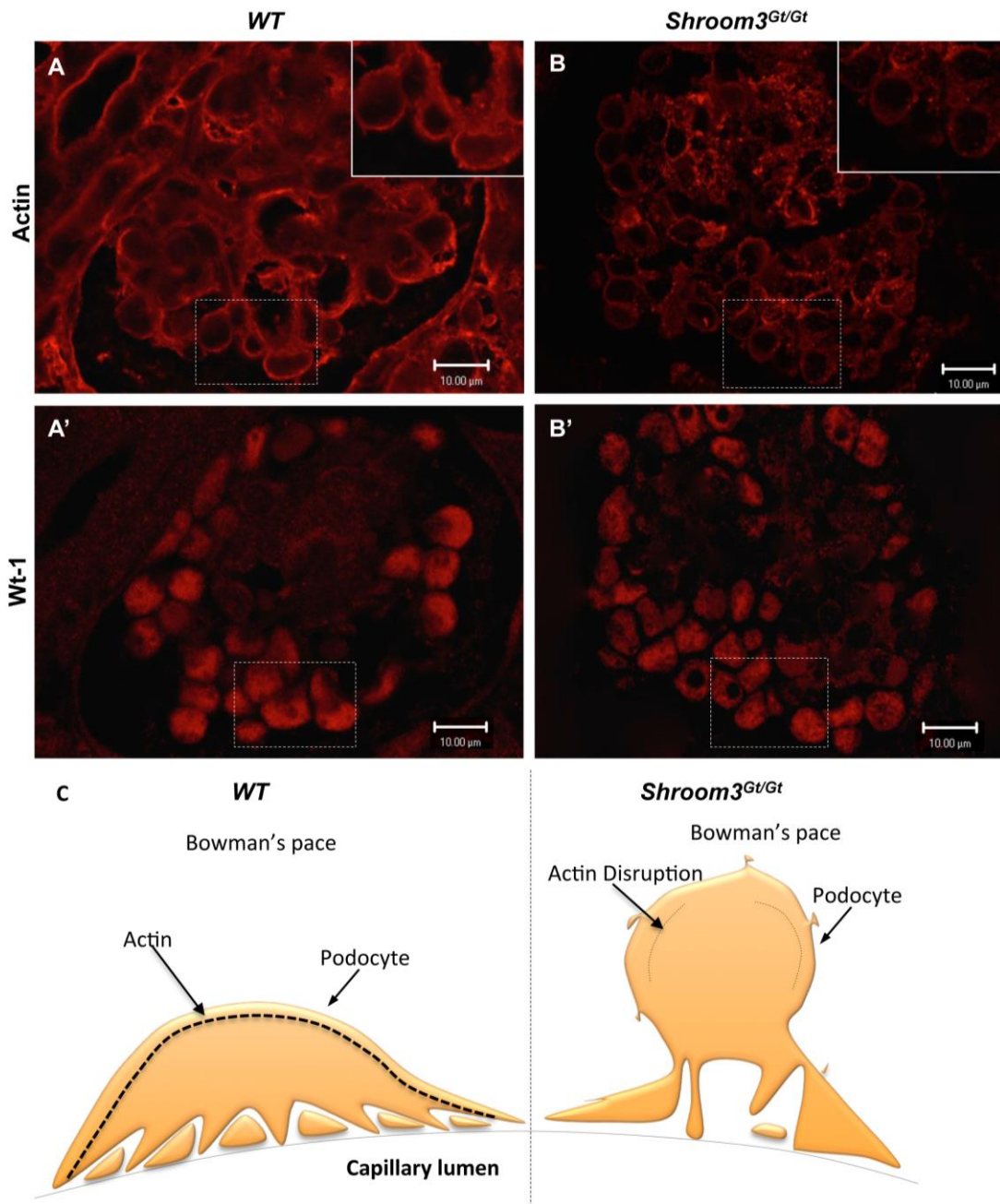
Figure 19. Actin organization is disrupted in Shroom3 mutant podocytes. (A, A', B, B')
Serial sections of *WT* and *Shroom3*$^{Gt/Gt}$ kidneys at E18.5 were incubated with anti-actin
and Wt-1 antibodies. (A) A linear pattern of actin distribution is observed in the plasma
membrane of *WT* podocytes. (B) The linear pattern of actin distribution is changed into a
patchy dot-like pattern in *Shroom3*$^{Gt/Gt}$ podocytes. Insets represent high magnification of
doted boxes. (C) A diagram shows actin distribution in the *WT* and *Shroom3*$^{Gt/Gt}$
podocytes. In the *WT*, actin is localized in the apical membrane of podocytes. However,
actin was virtually absent in the apical side of *Shroom3* mutant podocyte.

75

The actin cytoskeleton of foot processes determines the structural maintenance of the glomerular filtration barrier and slit diaphragm (Mundel and Shankland, 2002). Shroom3 function in neuroepithelial cells is dependent on its capability to bind both F-actin and Rho kinase (Rock) (Hildebrand, 2005). Direct binding of Shroom3 to the F-actin results in Shroom3 localization to the apical aspect of neuroepithelial cells. Shroom3 then recruits Rock to the apical area of the cell, resulting in the localized activation of myosin II via phosphorylation of myosin light chain. This further results in a contractile ring in the apical area of the cells and subsequent apical constriction (Hildebrand, 2005, Nishimura and Takeichi, 2008). Based on the fact that podocytes are epithelial cells with the complex architecture that express Shroom3, I hypothesized that Shroom3, through interaction with Rock, regulates the actomyosin network and the structure of podocyte foot processes. Therefore, I investigated the Shroom3/Rock/myosin pathway in the podocytes.

In order to examine whether Rock1 was mislocalized in the podocytes of *Shroom3* mutants, I performed immunohistochemistry on serial sections using Rock1 and Wt-1 antibodies. In the *WT* kidney at E18.5, Rock1 was prominent along the apical surface of the podocytes and area connected to the glomerular basement membrane (Figure 20A; inset). In contrast, *Shroom3$^{Gt/Gt}$* mice demonstrated mislocalization of Rock1 from the apical membrane of the podocyte to being more prominently in the cytoplasm (Figure 20B, inset). To confirm that Rock1 mislocalization was exclusive to the podocytes, I performed immunohistochemistry on serial sections using the podocyte marker Wt-1. This demonstrated the mislocalization of Rock1 in Wt-1 positive cells (Figure 20A', B';

boxed regions). These results are consistent with that observed in neuroepithelial cells, which showed that Shroom3-Rock binding is important in the apical localization of Rock1.

Since Rock1 was mislocalized in *Shroom3* mutant podocytes, I next aimed to determine if this mislocalization results in inactivation of the Rock target, myosin light chain (MLC) of myosin II. Therefore, I performed immunohistochemistry on serial sections of kidneys from E18.5 *WT* and *Shroom3$^{Gt/Gt}$* mice using antibodies for phosphorylated MLC (pMLC). In the *WT* podocytes, pMLC was localized primarily to the cytoplasm of cell body and apical membrane (Figure 20C). In contrast, *Shroom3$^{Gt/Gt}$* kidneys revealed a significant reduction in pMLC in the apical membrane of the podocytes (Figure 20D). To confirm that these changes were specific to the podocytes, I performed immunohistochemistry on serial sections using podocyte marker, Wt-1. Reduction in pMLC was found in Wt-1 positive cells of *Shroom3$^{Gt/Gt}$* kidneys when compared to *WT* (Figure 20C', D'; boxed region). Therefore, in absence of Shroom3, Rock1 failed to phosphorylate MLC in the apical region of the podocytes. These results were consistent with previous reports, demonstrating that Shroom3 is required for both apical localization and activation of Rock1. These alterations resulted in decreased actomyosin contractility and morphological changes to the actin cytoskeleton in the apical membrane of podocytes. These results indicate a key regulatory role of Shroom3 in proper actin organization of the podocytes through interactions with Rock.
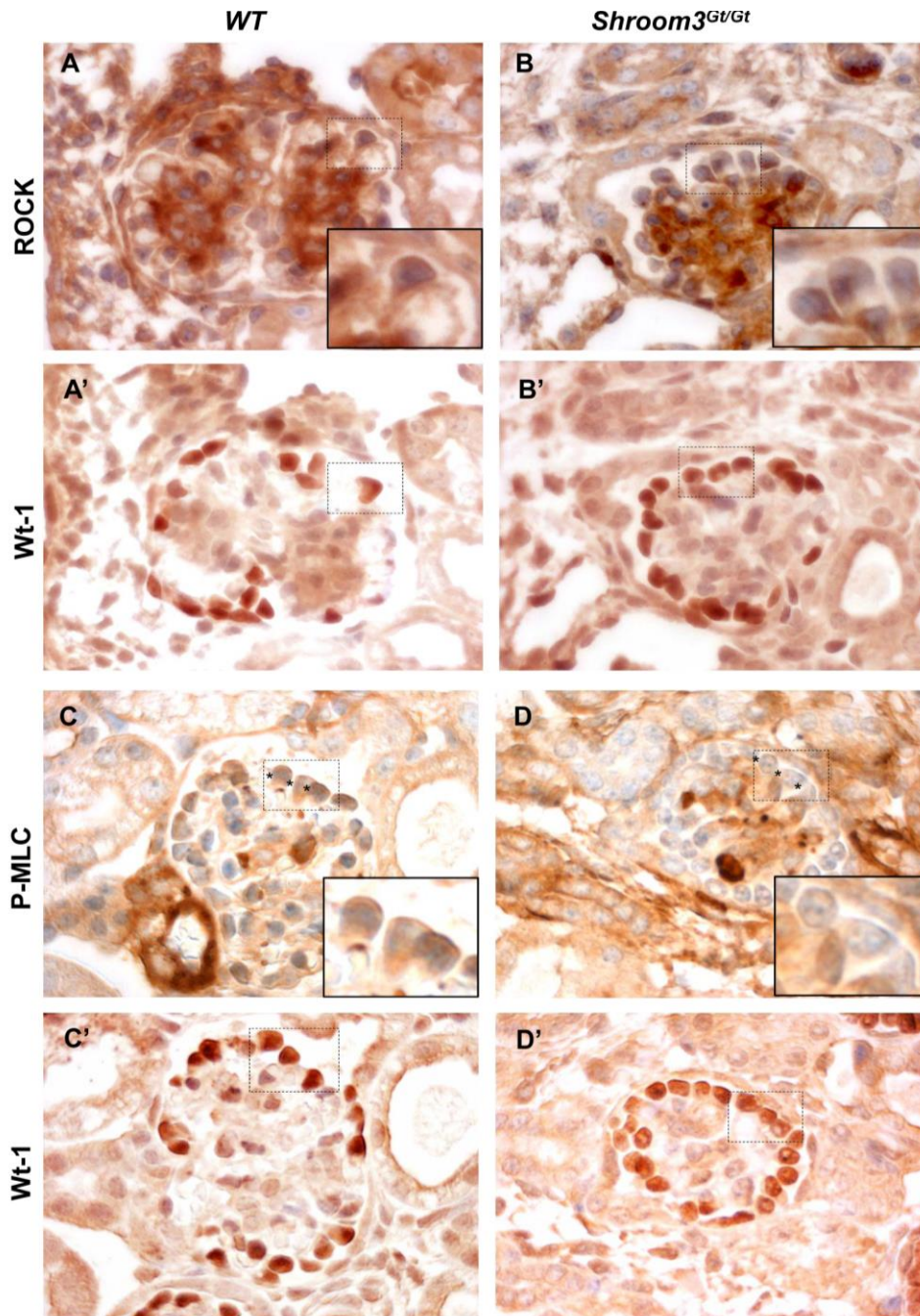
Figure 20. Shroom3 is required for Rock1 localization and function. (A, A', B, B') Serial sections of *WT* and *Shroom3*$^{Gt/Gt}$ kidneys at E18.5 were incubated with Rock1 and Wt-1 antibodies. (A) The linear pattern of Rock1 localization was observed in the apical membrane of podocytes. (B) *Shroom3*$^{Gt/Gt}$ mice demonstrate mislocalization of Rcok1 from the apical membrane to the cytoplasm of the podocytes. (C, C', D, D') Serial sections of *WT* and *Shroom3*$^{Gt/Gt}$ kidneys at E18.5 were incubated with pMLC and Wt-1 antibodies. (C) pMLC is localized primarily in the apical membrane of the *WT* podocytes. (D) *Shroom3*$^{Gt/Gt}$ mice exhibit reduced level of pMLC in both the cytoplasm and apical membrane of the podocytes. Insets represent high magnification of doted boxes.

78

4.8 Adult *Shroom3* heterozygote mice exhibit glomerular disease

I suspected that the alterations in podocyte morphology and reduced glomerular number will cause glomerular lesions that may progress to adult onset glomerular and renal disease. Since *Shroom3$^{Gt/Gt}$* mice die at birth due to neural tube defects (Hildebrand and Soriano, 1999), we analyzed kidneys from *Shroom3$^{Gt/+}$* and *WT* littermates. I initially analyzed kidney tissue from *Shroom3$^{Gt/+}$* and *WT* mice at 3-months postnatal. Histological analysis of H&E stained kidney tissue demonstrated no obvious changes in tissue morphology and glomerular structure when compared to *WT* kidneys (Figure 21A, B). I next used periodic acid–Schiff (PAS) and Jones' methenamine silver (JMS) staining to highlight matrix collagen deposition. No overt glomerular pathologies in *Shroom3$^{Gt/+}$* kidneys were observed when compared to *WT* littermates (Figure 21C-F). Furthermore, the analysis of *Shroom3$^{Gt/+}$* mice demonstrated no evidence of proteinuria in 3-month old mice as assessed by dipstick and SDS-PAGE (n=5).

Considering kidney disease can often be progressive, I suspected that there might be changes at later stages. Therefore, I analyzed kidney tissue from 1-year old *WT* and *Shroom3$^{Gt/+}$* mice. H&E staining of *WT* kidneys revealed normal glomerular architecture (Figure 22A). However, some glomeruli in *Shroom3$^{Gt/+}$* kidneys exhibited the adhesion of the podocytes to the parietal epithelial cells of the Bowman's capsule (Figure 22A, B; blue arrows). This phenotype was never observed in the control mice. Next, I analyzed the presence of sclerosis in the glomeruli by performing PAS and JMS staining. These analyses revealed mild increased matrix deposition and a thickening of the Bowman's capsule in most of the glomeruli in the *Shroom3$^{Gt/+}$* kidneys when compared to *WT*

(Figure 22C-F; black arrows and arrowheads). These abnormalities were barely observed in *WT* kidneys. Histological analyses suggest that *Shroom3*$^{Gt/+}$ mice developed mild segmental glomerulosclerosis by 1-year of age.
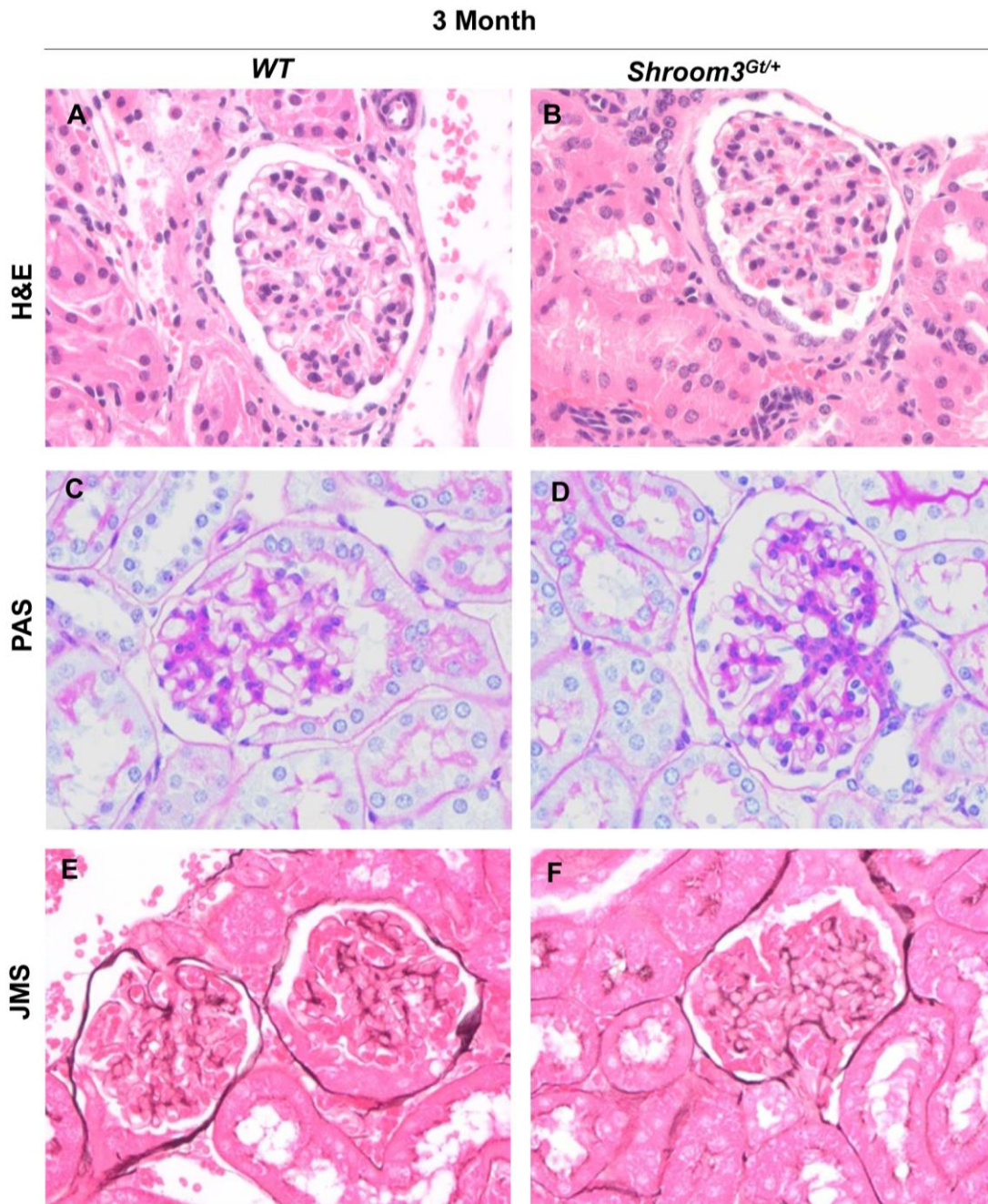
3 Month

Figure 21. Shroom3 mutant mice exhibit normal glomerular structure by 3-month age. (A-F) Histopathological characterization of kidneys from 3-month old *WT* and *Shroom3* mutant mice. (A, B) H&E staining of at 3 months kidneys demonstrates no overt pathological changes in *Shroom3$^{Gt/+}$* kidneys when compared to *WT*. (C-F) PAS and JMS staining of *Shroom3$^{Gt/+}$* kidney sections reveal no overt pathological changes when compared to *WT*. (H&E- Heamatoxylin & Eosin, PAS- Periodic-acid-Schiff, JMS-Jone's Methamine Silver).
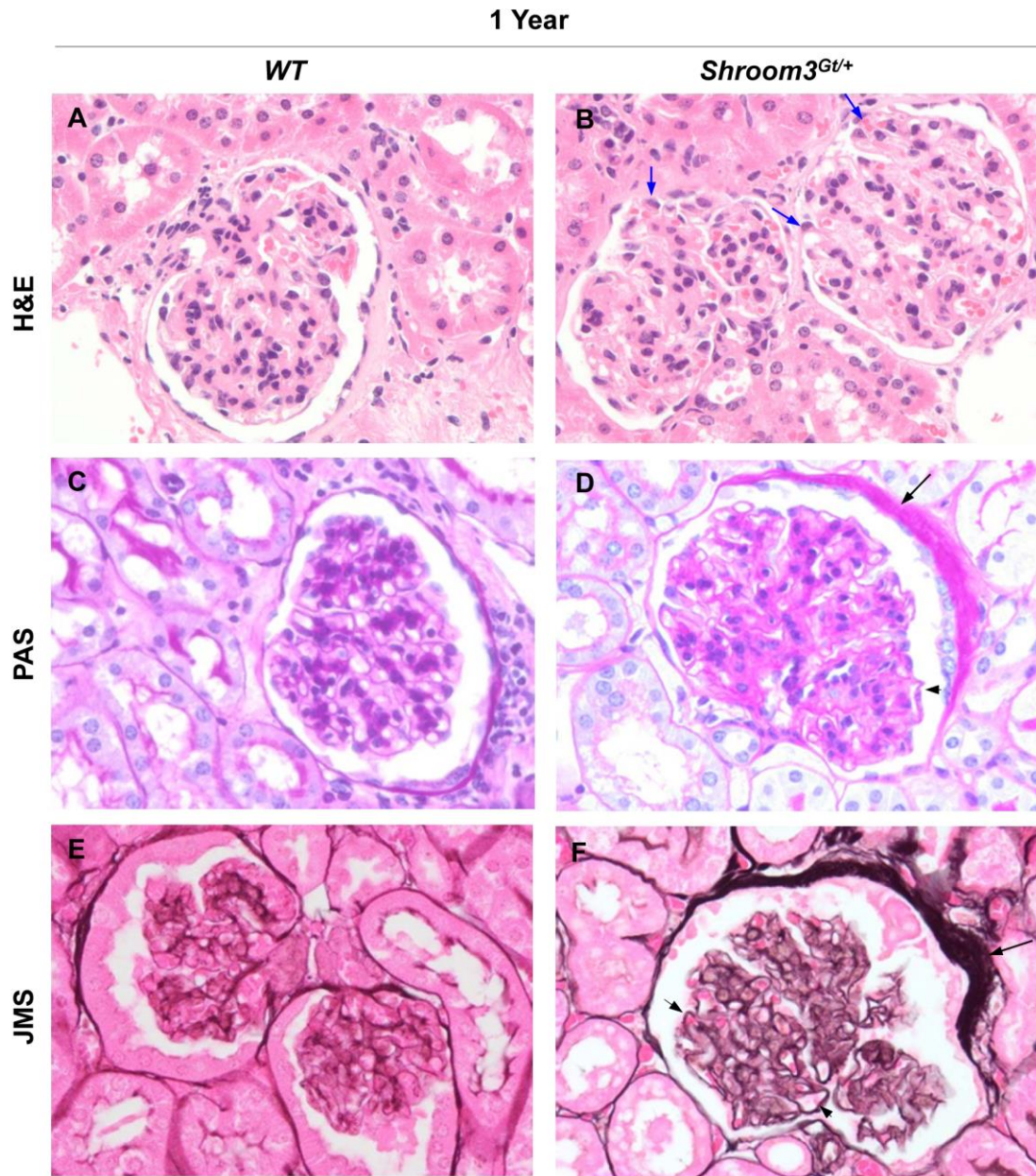
Figure 22. One-year-old Shroom3 mutant mice exhibit glomerular disease (A-F)
Histopathological characterization of kidneys from 1-year old *WT* and *Shroom3* mutant
mice. (A, B) H&E staining of *Shroom3*$^{Gt/+}$ kidneys at 1-year demonstrates glomeruli with
podocyte adhesion to the Bowman's capsule. (C-F) At 1-year, PAS and JMS staining
demonstrate a mild increased matrix deposition (black arrowhead), and a thickening of
the Bowman's capsule (black arrow) in *Shroom3*$^{Gt/+}$ mutants when compared to *WT*.
(H&E- Heamatoxylin & Eosin, PAS- Periodic-acid-Schiff, JMS-Jone's Methamine
Silver).

To further determine the ultrastructure characteristics of the glomerulus, both SEM and TEM were performed on 1-year old $Shroom3^{Gt/+}$ and WT kidneys. We analyzed two different $Shroom3^{Gt/+}$ mice by SEM and in each case we observed the overall glomerular architecture remained intact. However, effacement of foot processes was seen in numerous regions of the glomeruli of both $Shroom3^{Gt/+}$ kidneys (Figure 23B). In the WT, I also observed foot processes effacement, but not nearly to the extent of that observed in $Shroom3^{Gt/+}$ kidneys. I next performed transmission electron microscopy using three different $Shroom3^{Gt/+}$ and WT kidneys at 1-year. Electron micrograph of WT glomeruli exhibited healthy podocytes with well-formed foot processes (Figure 23C). At high magnification, we observed normal foot process interdigitation connected by the slid diaphragm in the WT glomeruli (Figure 23E). However, analysis of the glomerular ultrastructure of $Shroom3^{Gt/+}$ glomeruli revealed podocyte hypertrophy (Figure 23D; black arrows). In addition, at higher magnification $Shroom3^{Gt/+}$ glomeruli showed several regions with foot processes effacement and loss of the slit diaphragm (Figure 23F; red arrows). GBM did not appear to change in $Shroom3^{Gt/+}$ glomeruli when compared to WT littermates (Figure 23E, F).
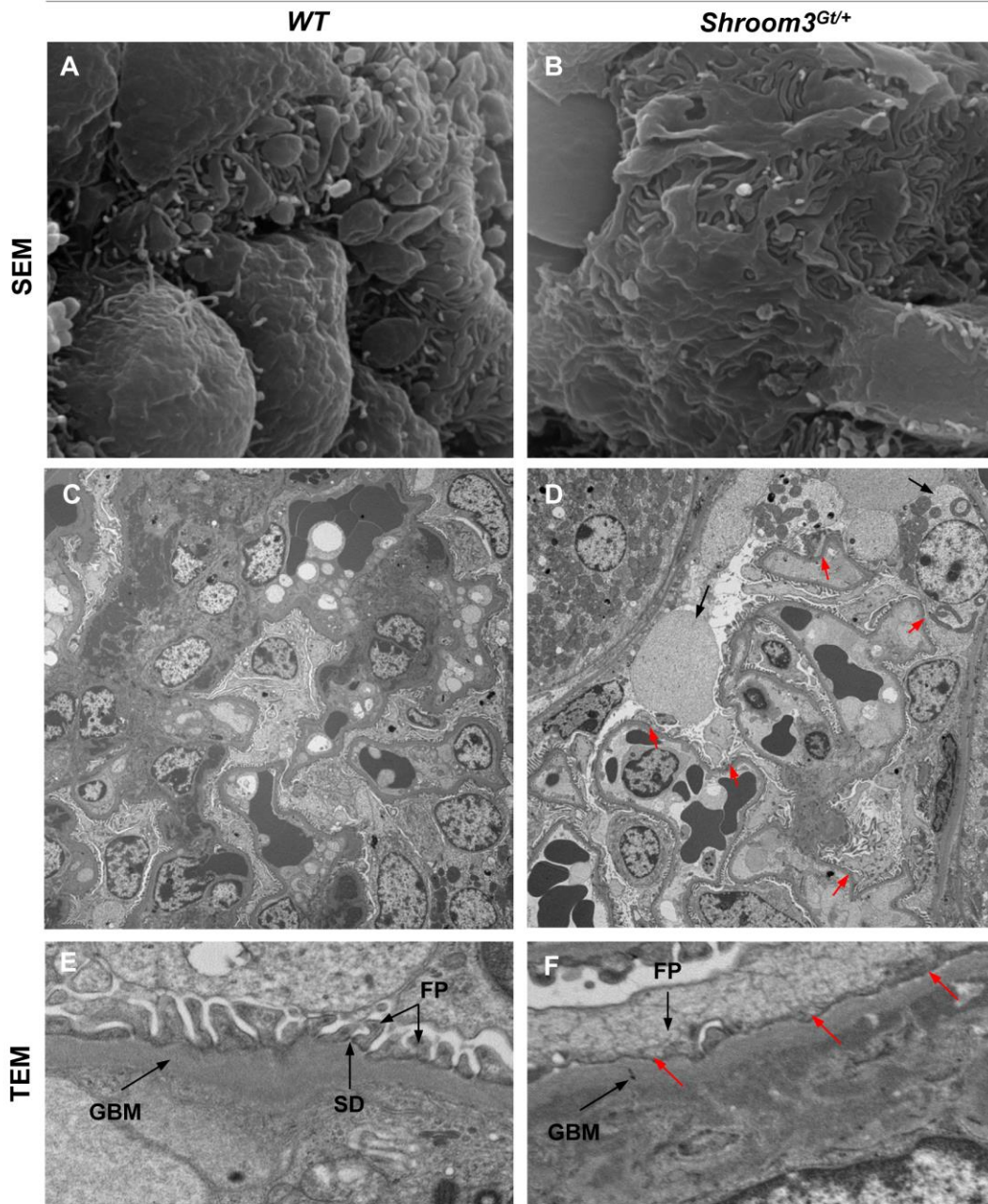
Figure 23. Adult Shroom3 mutant mice exhibit podocyte damage with foot processes effacement. (A, B) Scanning electron micrograph of *Shroom3*^{G/+} glomeruli demonstrates segmental foot processes effacement compared to wild type littermates. (C, D) Transmission electron micrograph of *Shroom3*^{Gt/+} glomeruli from 1-year old mice exhibits podocyte hypertrophy (black arrows) with numerous foot processes effacement (red arrows). (E, F) At higher magnification, *Shroom3* heterozygote kidneys demonstrate foot processes effacement and loss of slit diaphragm in some regions of the glomeruli (red arrows). (GBM-glomerular basement membrane, FP-foot process, SD- slit diaphragm).

Podocyte foot processes effacement and slit diaphragm loss results in the breakdown of filtration barrier and protein leakage (Shi et al., 2008, Deegens et al., 2008). Presence of high molecular weight protein like albumin in the urine is an indicator of glomerular and podocyte damage. As effacement with alterations in the slit diaphragm was observed in *Shroom3*$^{Gt/+}$ kidneys at 1-year, I suspected this phenotype would cause proteinuria. Thus, I collected urine from three *WT* and three *Shroom3*$^{Gt/+}$ mice. 1-year-old *Shroom3*$^{Gt/+}$ mice demonstrated abnormally dark and brownish urine that was never observed in urine from *WT* mice. I next performed urine analysis on 1-year *Shroom3*$^{Gt/+}$ and *WT* mice by taking 10μl of urine, and running it on a SDS-PAGE gel followed by Coomassie staining to visualize the protein in the urine. As shown in figure 24A, SDS-PAGE analysis revealed that an ~70 kDa band in all urine samples from *Shroom3*$^{Gt/+}$ mice, demonstrating the presence of albumin in the urine. In addition, to albumin band, I observed low-molecular weight protein ~40 kDa in the urine of one *Shroom3*$^{Gt/+}$ mouse. Since proteins greater than 40 kDa are normally prevented from filtering into the urinary ultrafiltrate through the glomerular filtration barrier, excretion of low molecular weight proteins indicates tubular damage.

I also quantitated the urinary protein by Bradford assay and normalized with urinary creatinine, since increases in the urinary protein can be due to changes in urine concentration. First, I qualitatively measured the level of urinary protein in triplicate for each urine sample (n=5; *WT* and *Shroom3*$^{Gt/+}$) by Bradford assay, the protein content in the urine sample was calculated using a standard curve. I then measured urinary creatinine using a colorimetric assay in triplicate for each sample and calculated

concentration of creatinine in the sample. Finally, urinary protein excretion was normalized to urinary creatinine by dividing the urinary protein content for each sample by creatinine content for the same sample, defined as protein/creatinine ratio. The ratio was 2.12 fold higher in *Shroom3*$^{Gt/+}$ than in *WT* mice (Figure 24B). These histopathlogical and urine analyses demonstrate that mice with *Shroom3* haploinsufficiency developed glomerular changes by at least at 1-year old, which was associated by the presence of protein in the urine.
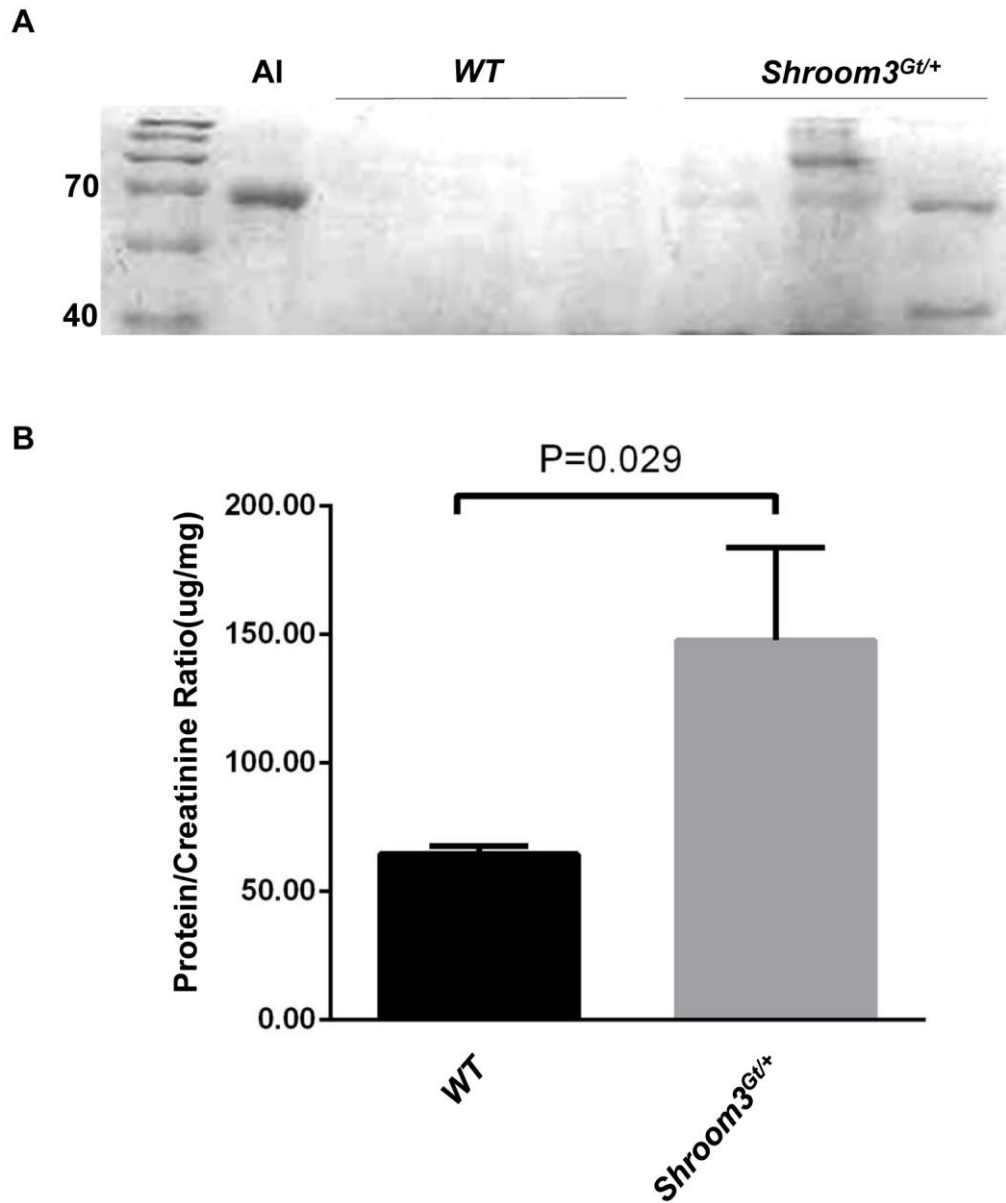
Figure 24. Adult Shroom3^{Gt/+} developed proteinuria. (A) Coomassie stained SDS-PAGE gel of urine demonstrates proteinuria in 1-year old Shroom3$^{Gt/+}$ mice. A 70kDa Albumin (Al) band is shown in lane 2. This demonstrates the presence of albumin and lower molecular weight proteins in the urine of *Shroom3$^{Gt/+}$* mice. (B) Quantitation of urinary protein to creatinine ratio from 5 1-year old *WT* and *Shroom3$^{Gt/+}$* mice demonstrate a significant increase in the urinary protein (P=0.029).

5. DISCUSSION

5.1 Overall Findings

GWAS studies have identified numerous genes with genetic variants that are associated with CKD and abnormal renal function. The *SHROOM3* locus was identified with the second highest risk association linked to CKD, behind the *UMOD* locus (Kottgen et al., 2009). While GWAS studies have linked the *SHROOM3* gene to CKD, it is not clear if SHROOM3 has a role in kidney disease and function. Therefore in this study, we aimed to determine if this candidate gene plays a role in the kidney. For the first time, I demonstrated that Shroom3 is expressed in the kidney in a unique spatial and temporal pattern during kidney development and in the adult kidney. In addition, my analysis of *Shroom3* mutant mice identified marked glomerular abnormalities. My research demonstrated that Shroom3 is required for the development and/or maintenance of complex podocyte cytoarchitecture via the modulation of the actin distribution in a Rock/myosin II dependent manner. Finally, the developmental abnormalities observed during kidney development manifest in postnatal kidney disease with associated proteinuria. Taken together, these studies demonstrate that Shroom3 is important in the kidney and further support the GWAS studies.

5.2 Shroom3 in the Kidney

GWAS studies, using estimated glomerular filtration rate, have identified SNPs in several loci that strongly associated with kidney disease and function (Kottgen et al., 2009, Boger et al., 2011b). Other studies have confirmed that genes associated with CKD, detected by GWAS studies, have a functional role in the development of kidney disease. For example, GWAS studies associated uromodulin (*UMOD*) with kidney disease (Kottgen et al., 2009, Boger et al., 2011b). Generation of *Umod* mutant mouse lines has demonstrated that uromodulin deficiency leads to the onset and progression of renal dysfunction (Kemter et al., 2013). Numerous GWAS studies reported that the intronic *SHROOM3* variant, rs17319721, is significantly associated with CKD and kidney function (Kottgen et al., 2009, Boger et al., 2011b). The minor allele (A) of this SNP in the *SHROOM3* gene was shown to have a significant association with a lower glomerular filtration rate estimated by serum creatinine (Kottgen et al., 2009, Boger et al., 2011b). In a GWAS study conducted by Boger et al., the same SNP in *SHROOM3* was the second highest ranking SNP for albuminuria (Boger et al., 2011a, Ellis et al., 2012). Although GWAS have successfully identified that *SHROOM3* is associated with kidney disease and function, there were large gaps in the functional role of SHROOM3 in the kidney, since these studies did not offer any direct evidence about the molecular mechanism involved in the pathogenesis of kidney disease. The majority of identified SNPs in GWAS are located in the non-transcriptional regions including the intronic SNP in *SHROOM3*. It is possible that these regions have a regulatory role and their dysregulation may result in the disease phenotype.

Two recent publications have identified a role for Shroom3 in the kidney (Menon et al., 2015, Yeo et al., 2015). Menon *et al*. focused on chronic allograft nephropathy (CAN) in a cohort of renal allograft recipients. They demonstrated that the *SHROOM3* gene containing the risk allele, rs17319721, in the donor kidney is correlated with an increased *SHROOM3* expression in the allograft at 3 months and a higher risk of CAN at 12 months after transplantation (Menon et al., 2015). They investigated the underlying mechanism of elevated *SHROOM3* transcript levels in the allograft, and revealed that the risk allele of *SHROOM3* contains a TCF7L2-dependent enhancer element, which is responsible for enhancing *SHROOM3* transcription. In *vitro* studies on renal tubular cells have shown that TGF-β1, known as a key driver of renal fibrosis (Lan, 2011), regulates *SHROOM3* expression in a Wnt/β-catenin/TCF7L2-dependent manner. In turn, the risk allele of *SHROOM3* facilitates canonical TGF-β1 signaling and expression of the profibrotic gene, which subsequently promotes renal fibrosis (Menon et al., 2015). They also demonstrated that *SHROOM3* overexpression in renal epithelial cell line cause changes in cytoskeletal reorganization and increased actin bundling. Thus, they showed that the risk variant of the *SHROOM3* gene could affect the success of kidney transplants. Although these studies introduced *SHROOM3* as a predictor of fibrosis in CAN, they did not highlight a role for SHROOM3 in non-transplant CKD.

A second study demonstrated that genetic variants in *Shroom3* gene were correlated with kidney disease in the Fawn-Hooded Hypertensive (FHH) rat (Yeo et al., 2015). They demonstrated that the replacement of the *Shroom3* gene from the FHH rat with the wild type *Shroom3* gene improved the glomerular function. In this study, it has been shown

that a variant in the *Shroom3* gene of the FHH rat was responsible for the disruption of actin-binding function of Shroom3 and likely contributed to the glomerular filtration defects in the FHH rat (Yeo et al., 2015). They generated podocyte-specific disruption of *shroom3* in zebrafish and demonstrated podocyte foot processes effacement with defects in glomerular filtration barrier. While these studies highlight an important role for Shroom3 in the kidney, it was not clear which cell types within the kidney express Shroom3. Furthermore, the developmental role of Shroom3 in the mammalian metanephric kidney remained to be investigated. More importantly, the role of Shroom3 in podocytes and whether Shroom3 regulates podocyte cytoskeletons through the same mechanisms observed in other epithelial cell types have not been investigated.

5.3   Shroom3 Expression in the Kidney

Knowing which cell populations within the kidney express Shroom3 leads to a better understanding of its role and function in the kidney. In a study conducted by Lee et al., *Shroom3* transcripts were detected in the pronephric kidney of the Xenopus embryo (Lee et al., 2009). Yeo et al. demonstrated expression of *shroom3* in the zebrafish pronephric glomerulus and tubules using ISH (Yeo et al., 2015). However, there was no information on its expression in the mammalian kidney. Recently, microarray analyses on the podocytes isolated from mouse glomerulus provided a complete atlas of gene expression in the podocyte that demonstrated *Shroom3* expression (Brunskill et al., 2011).

Despite these studies, the spatial and temporal expression pattern of Shroom3 in the mammalian kidney was not defined. Since the mutant mice have a gene trap containing

the *LacZ* gene reporter under the control of *Shroom3* promoter, I used X-gal staining to show endogenous gene expression. I observed *LacZ* expression in the condensing mesenchyme, developing and mature glomerulus, parietal epithelium of Bowman's capsule, and collecting ducts throughout kidney development. We did not observe expression in the proximal and distal convoluted tubules of the nephron. However, since *Shroom3* mutants are transgenic mice containing *LacZ* insertion and they have a kidney phenotype, there is possibility that the *LacZ* activity might not accurately report the endogenous *Shroom3* expression. My analysis of immunohistochemistry demonstrated similar expression pattern as that observed in *LacZ* in the condensing mesenchyme, glomerulus, and collecting duct cells. Furthermore, Shroom3 localization was also detected in the parietal epithelial cells of Bowman's capsule by immunohistochemistry. Although the expression pattern of Shroom3 in the glomerulus was consistent with the podocytes, I was unable to confirm it by co-localization with a podocyte marker because available Shroom3 antibodies did not work for immunofluorescence. Thus, the expression of Shroom3 in the podocyte was confirmed at mRNA level by performing 2-plex in situ hybridization. This novel assay enabled us to visualize any two gene combinations in complex tissue architecture. Using two sets of probes specific to *Shroom3* and *Wt-1* mRNA, I demonstrated that *Shroom3* mRNA was expressed in the podocyte throughout kidney development and in the adult kidney, suggesting a role for Shroom3 in the podocyte. I was not able to show any expression in the tubular portions of the nephron. Previous studies have suggested SHROOM3 expression in the proximal tubule of human kidney but not in any other segment of the nephron including the podocyte (Menon et al.,

2015). These findings are in contrast to the expression pattern defined in our study. The difference between these two studies may be due to species differences. However, since the brown staining was observed only in the proximal tubules, neither in the podocytes nor Bowman's capsule cells, I believe this might be a false positive staining. Close inspection of their data reveals antibody accumulation and/or substrate reaction at the proximal tubule brush border.

5.4   Shroom3 Function in the Kidney

Our expression analyses in the kidney raised an important question: what is the necessity of Shroom3? It is well defined that the Shroom3 protein is required for inducing cell shape changes during epithelial morphogenesis in the neural, gut, and lens epithelium (Hildebrand and Soriano, 1999, Chung et al., 2010, Plageman et al., 2011). Thus, in case of renal epithelial cells that undergo several morphogenesis processes during kidney development, (Kuure et al., 2000), Shroom3 may play a similar role. During embryonic development and postnatal growth of the kidney, the collecting ducts decrease in diameter and elongate by two cellular mechanisms of oriented cell division and convergent extension (Costantini, 2012). Defective convergent extension results in smaller kidney with shortened collecting tubules (Lienkamp et al., 2012). Of particular interest, it has been demonstrated that Shroom3 plays a role in convergent extension movement during mouse neural tube morphogenesis (McGreevy et al., 2015). Therefore, expression of Shroom3 in the epithelial cells of collecting duct is most likely to contribute to the elongation of collecting ducts as my data confirmed that *Shroom3$^{Gt/Gt}$* kidneys were

93

smaller with thickened collecting ducts.

Mesenchymal cells are nephron progenitor cells that undergo a mesenchymal-to-epithelial transition including changes in cell polarization along the apical-basal and proximal-distal axes (Saxen and Sariola, 1987, Rocque et al., 2015). Our expression analyses demonstrate that Shroom3 is expressed in the condensing mesenchyme. Since the functional role of Shroom3 is currently limited to polarized epithelial cells (Hildebrand, 2005), it would be possible that Shroom3 plays a role in the polarization of the condensing mesenchymal cells. There is another potential role for Shroom3 in the condensing mesenchymal cells. Since the metanephric mesenchymal cells are renal epithelial stem cells that undergo morphological changes (Little and McMahon, 2012), it is possible that the metanephric mesenchymal cells express Shroom3 for their subsequent shape changes and formation of the renal vesicle, comma- and S-shaped bodies. Despite the expression of Shroom3 in the condensing mesenchyme, we did not observe any evidence of abnormalities in this cell population in mutant mice. A potential explanation that may account for this normal phenotype could be that these cells do not initially undergo morphological changes. Thus, Shroom3 might be required for the subsequent cell shape changes of the condensing mesenchyme.

Podocytes undergo extensive changes in cellular morphology to acquire their characteristic architecture (Pavenstadt et al., 2003). Therefore, expression of Shroom3 in the podocytes suggests that Shroom3 may act as a potent inducer of podocyte shape changes. This was confirmed by our SEM analysis that showed *Shroom3$^{Gt/Gt}$* podocytes with swelling of cell bodies and poor organization of foot processes. The complex

architecture of the podocyte is dependent upon the highly organized actin cytoskeleton. Considering Shroom3 is an actin-binding protein, identifying its precise subcellular localization in the podocyte would provide further insight into its function. In this regard, I performed immunogold labeling using Shroom3 antibody and demonstrated cytoplasmic localization of Shroom3 protein in the podocyte cell body and the apical membrane of secondary and tertiary foot processes. Therefore, Shroom3 may play a role in the regulation of actin cytoskeleton of podocyte foot processes. Taking together, expression of Shroom3 in developing and mature podocytes strongly recommends that Shroom3 is required for morphological changes during podocyte differentiation.

5.5   Abnormal Glomerulogenesis in *Shroom3* mutant mice

Our histological analyses on embryonic kidneys demonstrated that *Shroom3* mutant kidneys were reduced in size compared with *WT* kidneys, but displayed relatively intact architecture with the normal-appearing nephrogenic zone and collecting duct system. Although nephrogenesis occurred in *Shroom3* mutants, numerous glomerular abnormalities were observed as evidenced by cystic and degenerating glomeruli. During early kidney development in *Shroom3* mutant mice, superficial glomeruli located in the cortex were degenerating, whereas the glomerulocystic phenotype was only observed in the glomeruli located in the deeper cortex. As development progressed, no degenerating glomeruli were observed in *Shroom3* mutants. Since podocytes undergo several morphological changes during an early phase of normal glomerular development, I thought that the impairment of podocyte maturation might lead to the destruction of some

developing glomeruli in *Shroom3* mutants.

Reduction in the glomerular number can cause hyperfiltration in the remaining glomeruli. During embryonic development, as early as nephron formation, the glomerulus starts its function to filter the blood and passes the filtrate at around E14.5-E15.5. Therefore, one possible explanation for the presence of cystic glomeruli with dilation of Bowman's space in *Shroom3$^{Gt/Gt}$* embryonic kidneys is that there was an increased pressure in the Bowman's capsule of *Shroom3$^{Gt/Gt}$* glomeruli due to the reduced glomerular number. Although the cystic glomeruli with dilation of Bowman's space were also reported in other mouse model including nephrin-deficient mice (Done et al., 2008), the mechanism of glomerular cyst formation remains largely undefined. Parietal epithelial cells of the Bowman's capsule may play an important role in the formation of the glomerular cyst. We demonstrated that Shroom3 was strongly expressed in the parietal epithelial cells of the Bowman's capsule, and a considerable amount of apoptosis was present in these cells in the absence of Shroom3. Therefore, these observations suggest that a loss of Shroom3 resulting in the reduced number of the parietal epithelial cells, which can lead to an inability of Bowman's capsule to counteract the increased forces of filtrate and subsequently cause a dilation of Bowman's space.

5.6   Role of Shroom3 in Modulating Podocyte Morphology

5.6.1 Rock Signaling in the Podocyte

Rock is a downstream effector of Rho GTPases signaling that is a principal modulator of cytoskeletal dynamics (Riento and Ridley, 2003). Rho-Rock signaling regulates several cellular processes including cell proliferation, adhesion, motility and morphological changes (Riento and Ridley, 2003). Several studies have assessed the role of Rho-Rock signaling pathway in the podocytes. In vitro studies in the podocytes have shown that the Rock inhibitor, Y-27632, induced disassembly of actin filaments and stress fibers in the podocyte cell body also disappeared (Gao et al., 2004). Consistent with these findings, we also demonstrated reduced Rock activity and observed reduced actin in the apical margin of the podocyte cell body. Although the importance of regulation and maintenance of the podocytes actin cytoskeleton is undeniable, the precise molecular mechanism of Rock in actin cytoskeletal regulation of these cells has not been clearly studied.

5.6.2 Shroom3-Rock-Myosin Pathway in the Podocyte

There are different actin populations within the cell including stress fiber, cytoplasmic population of F-actin, and cortical actin (Dietz et al., 2006). Shroom family members exhibit distinct abilities to interact with the actin cytoskeleton. It has been shown that Shroom3 can directly interact with actin stress fibers, while other Shroom proteins bind to a different population of actin in fibroblasts (Dietz et al., 2006). Healthy podocytes

contain actin stress fibers running along their apical plasma membrane that function as rails for actin-motor proteins thereby mediating cellular contractility (Cortes et al., 2000). Therefore, based on our expression analysis showing predominant expression of Shroom3 in the podocytes, it is possible that Shroom3 regulates actin fiber contraction in these cells.

Since Rock and myosin are involved in the regulation of actin stress fiber dynamics in the podocyte, we predicted that a clear understanding of the role of Shroom3 in the Rock-myosin pathway would provide insight into actin cytoskeletal organization in the pathogenesis of podocyte injury. The function of Shroom3 has been studied in epithelial morphogenesis by inducing apical constriction and regulating the actin cytoskeleton in neural, lens, and gut epithelial cells (Nishimura and Takeichi, 2008, Plageman et al., 2011, Chung et al., 2010). In neuroepithelial cells, Shroom3 interacts with Rock and recruits it to the apical junction of cells. Then, apical localization of Rock by Shroom3 causes phosphorylation of myosin and actomyosin contraction and subsequent apical constriction of neural epithelial cells. This Shroom3-Rock interaction is essential for the regulation neuroepithelial cell arrangement (Nishimura and Takeichi, 2008). Since actin within the podocyte apical membrane is markedly reduces in $Shroom3^{Gt/Gt}$ mice, we examined the Shroom3/Rock/myosin pathway.

First, I demonstrated that Rock1 was mislocalized from the apical membrane to the cytoplasm of the podocytes of $Shroom3^{Gt/Gt}$ mice. This result was consistent with the other studies, in which Rock localization was reduced in the apical area of the neuroepithelial cells lacking Shroom3 (Nishimura and Takeichi, 2008). Since Rock can

98

phosphorylate and activate nearby myosin, its absence in the apical side of the neuroepithelial cells, lacking Shroom3, results in the reduced level of pMLC (Nishimura and Takeichi, 2008). Therefore, I expected that mislocalization of Rock in *Shroom3* mutant podocytes would result in a reduced level of phosphorylated myosin in the apical area of the podocytes. By performing immunohistochemistry using pMLC antibody, I observed a marked reduction of the phosphorylated form of Rock substrate, MLC. As a consequence, reduction in the level of pMLC would lead to a decrease in the actin-myosin contraction in the apical membrane of podocytes. We showed that actin distribution altered from a dense linear organization in the *WT* podocyte to a fine punctate pattern at the edge of *Shroom3$^{Gt/Gt}$* podocytes. Consistent with our finding, inhibition of Rock leads to disassembly of actin stress fibers in the podocyte (Gao et al., 2004). These alterations in actin cytoskeleton are associated with foot processes effacement, as observed by electron microscopy in *Shroom3* mutant kidneys. Taken together, these findings confirmed an important role for Rock signaling in podocyte cytoarchitecture. Moreover we provided the first evidence that Shroom3 is crucial for the maintenance of podocyte structure upstream of Rock-Myosin signaling.

5.7   Adult Onset of Kidney Disease in *Shroom3* mice

Alterations in the ultrastructure of the podocyte cell body and its foot processes are the histologic hallmark of glomerular disease. Damage to the ultrastructure of podocytes are closely linked to disruption of the actin cytoskeleton (Faul et al., 2007). Scanning and transmission electron microscopy of *Shroom3$^{Gt/Gt}$* glomeruli from embryonic mice

revealed abnormalities in the podocyte cell bodies, foot processes effacement and microvillus transformation. At the same time that we have been investigating the role of Shroom3 in the podocytes, Yeo et al. published an article that supports our results. They generated a podocyte-specific knockdown of *shroom3* in zebrafish and demonstrated foot processes effacement (Yeo et al., 2015). These podocyte abnormalities can lead to the impairment of the glomerular filtration barrier and adult-onset glomerular disease.

Reduction in glomerular number is another developmental defect that associates with adult-onset kidney diseases (Kett and Bertram, 2004, Luyckx et al., 2011). Defect in nephrogenesis during kidney development is one of the important causes of reduced nephron number (Douglas-Denton et al., 2006). Glomerular hypertrophy and intraglomerular hypertension develop when nephron number is reduced as a compensatory mechanism (Douglas-Denton et al., 2006). This compensatory glomerular hypertrophy may further cause progression of kidney disease (Douglas-Denton et al., 2006). Our observation of reduced glomerular number in *Shroom3*$^{Gt/+}$ and *Shroom3*$^{Gt/Gt}$ embryos suggests that Shroom3 may play a key role in the development of glomerular disease later in life. Kidneys from *Shroom3* heterozygote mice at an age of 1-year revealed a number of histopathological characteristics of focal segmental glomerulosclerosis. Both scanning and transition electron micrographs from *Shroom3*$^{Gt/+}$ adult kidneys demonstrated that normal foot process architecture was lost and affected in some but not all areas of *Shroom3* heterozygote glomeruli. Effacement of foot processes is present in most proteinuric glomerular diseases (Shi et al., 2008). We demonstrated that *Shroom3*$^{Gt/+}$ adult mice developed albuminuria. Both structural alterations in podocyte

foot processes and proteinuria are consequences of podocyte damage with *Shroom3* haploinsufficiency. Taking together, we conclude that Shroom3 is required for the formation of foot processes and maintenance of proper podocyte morphology.

The actin cytoskeleton of podocytes and foot processes allows podocytes to continuously and dynamically alter their shape to respond to changes in the glomerular capillary pressure and modulate the glomerular filtration rate (Shankland, 2006). In this process, Shroom3 may play a role in the dynamic regulation of actin fiber to facilitate changes in the podocyte and foot processes cytoarchitecture. Therefore, it would be interesting to determine if Shroom3 contributes to the dynamic changes of the podocyte actin cytoskeleton by challenging *Shroom3*$^{Gt/+}$ mice and inducing podocyte injury. This will be accomplished by treating *Shroom3*$^{Gt/+}$ mice with puromycin aminonucleoside nephrosis (PAN), which induces podocyte injury and proteinuria and leads to reversible changes in the podocyte actin cytoskeleton. These experiments will reveal if Shroom3 is necessary for actin structural changes that occur during induction and recovery from podocyte injury. It is more likely that *Shroom3*$^{Gt/+}$ PAN-treated mice show more severe phenotype than *WT* mice and display impaired or delayed recovery from PAN-induced podocyte injury. These studies will undoubtedly be helpful in gaining a better understanding of Shroom3 function in the regulation of podocyte architecture.

5.8   Model

It has been shown that Shroom3 has an ability to bind Rock. This Shroom3-Rock interaction causes recruitment of Rock to the apical membrane of podocytes. Then, apical localization of Rock triggers actomyosin contractility by phosphorylation of its downstream target, myosin light chain. Increased phosphorylation of MLC induces formation of a network of apical actin stress fibers and stabilization of actin cytoskeleton in the podocytes. Therefore, Shroom3 regulates podocyte morphology via the apical positioning of an actomyosin network. While in *Shroom3* mutant podocytes, Rock fails to localize apically resulting in reduced apical accumulation of phosphorylated myosin light chain along the apical membrane of podocytes. This leads to a decreased formation of contractile actin-myosin containing stress fibers in the apical membrane of podocytes leading to aberrant morphological changes of podocyte cell bodies and foot processes. Poor organization of foot processes results in impaired slit diaphragm filtration and albuminuria in *Shroom3* mutants.

5.9 Conclusion

Here, we present the first spatial-temporal expression analysis of Shroom3 in the metanephric kidney. Shroom3 is specifically expressed in key structures in the developing and mature kidney. Our studies of Shroom3 in the podocyte have demonstrated that Shroom3 is required for localization of actin along the apical membrane of podocytes. The developmental abnormalities manifest in *Shroom3* mutant adult mice, which have kidney disease such as segmental glomerulosclerosis and proteinuria. This suggests that potential hypomorphic human *SHROOM3* alleles could directly result in kidney disease or increased susceptibility to chronic kidney disease.
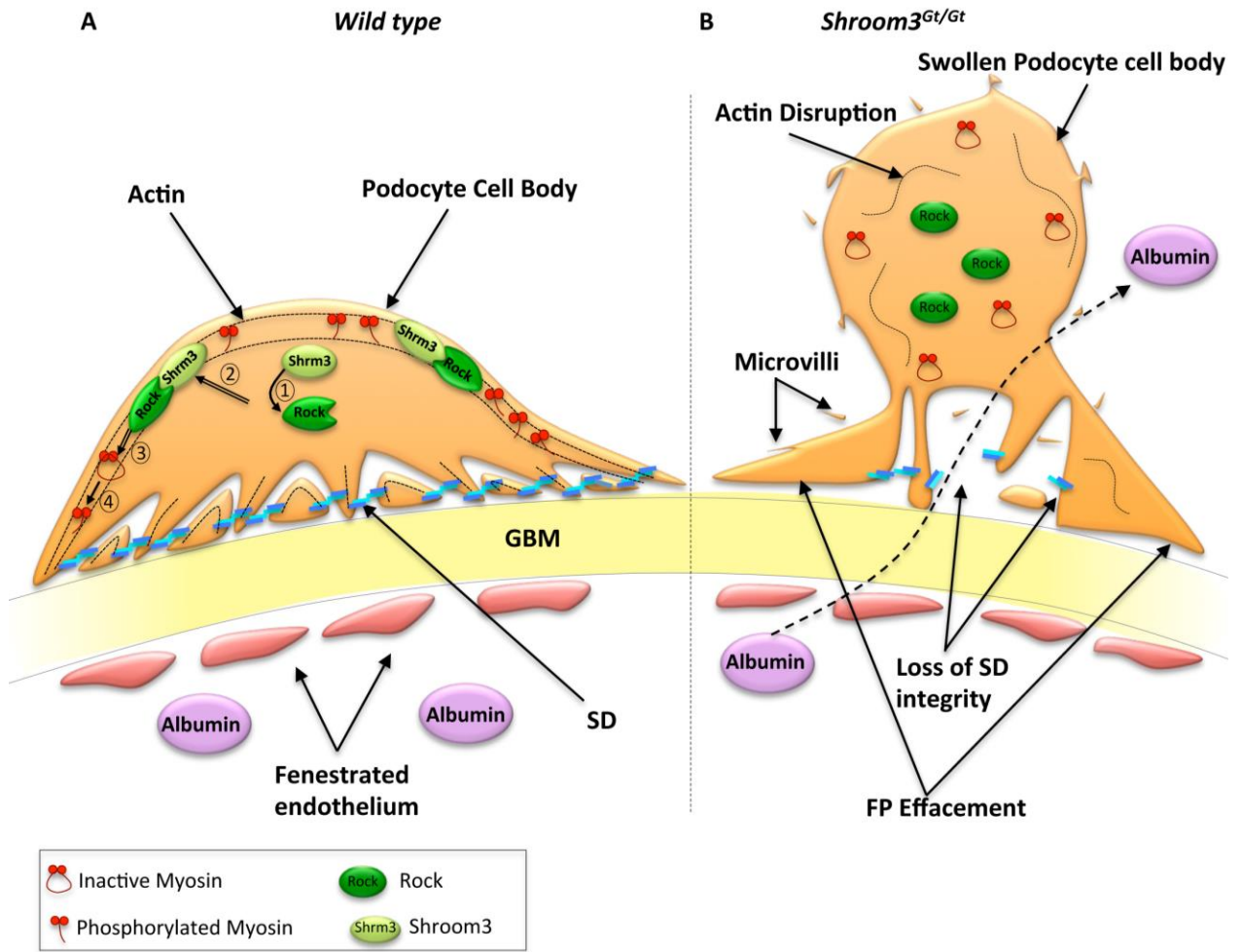
Figure 25. Model of the Shroom3-mediated the apical positioning of Rock and actomyosin network in the podocyte. This model illustrates that Shroom3 regulates podocyte morphology via Rock-Myosin pathway. (A) In the wild type podocyte, (1) Shroom3 binds and (2) recruits Rock to the apical membrane of podocyte. (3) Rock phosphorylates myosin light chain and (4) induces formation of apical actin stress fiber and contractility in the podocyte. (B) In the absence of Shroom3, Rock fails to localize in the apical side of podocyte resulting in reduced phosphorylation of MLC and contractility in the apical membrane of podocytes. These alterations cause less actin stress fiber assembly in the podocytes leading to aberrant morphological changes including swelling of cell body, foot processes effacement and impairment of slit filtration.

6. REFERENCES

ARMSTRONG, J. F., PRITCHARD-JONES, K., BICKMORE, W. A., HASTIE, N. D. & BARD, J. B. 1993. The expression of the Wilms' tumour gene, WT1, in the developing mammalian embryo. *Mech Dev,* 40**,** 85-97.

ARSENAULT, M. G., MIAO, Y., JONES, K., SIMS, D., SPEARS, J., WRIGHT, G. M. & HARTWIG, S. 2014. Estimation of total glomerular number using an integrated disector method in embryonic and postnatal kidneys. *Can J Kidney Health Dis,* 1**,** 12.

BOGER, C. A., CHEN, M. H., TIN, A., OLDEN, M., KOTTGEN, A., DE BOER, I. H., FUCHSBERGER, C., O'SEAGHDHA, C. M., PATTARO, C., TEUMER, A., LIU, C. T., GLAZER, N. L., LI, M., O'CONNELL, J. R., TANAKA, T., PERALTA, C. A., KUTALIK, Z., LUAN, J., ZHAO, J. H., HWANG, S. J., AKYLBEKOVA, E., KRAMER, H., VAN DER HARST, P., SMITH, A. V., LOHMAN, K., DE ANDRADE, M., HAYWARD, C., KOLLERITS, B., TONJES, A., ASPELUND, T., INGELSSON, E., EIRIKSDOTTIR, G., LAUNER, L. J., HARRIS, T. B., SHULDINER, A. R., MITCHELL, B. D., ARKING, D. E., FRANCESCHINI, N., BOERWINKLE, E., EGAN, J., HERNANDEZ, D., REILLY, M., TOWNSEND, R. R., LUMLEY, T., SISCOVICK, D. S., PSATY, B. M., KESTENBAUM, B., HARITUNIANS, T., BERGMANN, S., VOLLENWEIDER, P., WAEBER, G., MOOSER, V., WATERWORTH, D., JOHNSON, A. D., FLOREZ, J. C., MEIGS, J. B., LU, X., TURNER, S. T., ATKINSON, E. J., LEAK, T. S., AASAROD, K., SKORPEN, F., SYVANEN, A. C., ILLIG, T., BAUMERT, J., KOENIG, W., KRAMER, B. K., DEVUYST, O., MYCHALECKYJ, J. C., MINELLI, C., BAKKER, S. J., KEDENKO, L., PAULWEBER, B., COASSIN, S., ENDLICH, K., KROEMER, H. K., BIFFAR, R., STRACKE, S., VOLZKE, H., STUMVOLL, M., MAGI, R., CAMPBELL, H., VITART, V., HASTIE, N. D., GUDNASON, V., KARDIA, S. L., LIU, Y., POLASEK, O., CURHAN, G., KRONENBERG, F., PROKOPENKO, I., RUDAN, I., ARNLOV, J., HALLAN, S., NAVIS, G., CONSORTIUM, C. K., PARSA, A., FERRUCCI, L., CORESH, J., SHLIPAK,

M. G., et al. 2011a. CUBN is a gene locus for albuminuria. *J Am Soc Nephrol,* 22**,** 555-70.

BOGER, C. A., GORSKI, M., LI, M., HOFFMANN, M. M., HUANG, C., YANG, Q., TEUMER, A., KRANE, V., O'SEAGHDHA, C. M., KUTALIK, Z., WICHMANN, H. E., HAAK, T., BOES, E., COASSIN, S., CORESH, J., KOLLERITS, B., HAUN, M., PAULWEBER, B., KOTTGEN, A., LI, G., SHLIPAK, M. G., POWE, N., HWANG, S. J., DEHGHAN, A., RIVADENEIRA, F., UITTERLINDEN, A., HOFMAN, A., BECKMANN, J. S., KRAMER, B. K., WITTEMAN, J., BOCHUD, M., SISCOVICK, D., RETTIG, R., KRONENBERG, F., WANNER, C., THADHANI, R. I., HEID, I. M., FOX, C. S., KAO, W. H. & CONSORTIUM, C. K. 2011b. Association of eGFR-Related Loci Identified by GWAS with Incident CKD and ESRD. *PLoS Genet,* 7**,** e1002292.

BRUNSKILL, E. W., GEORGAS, K., RUMBALLE, B., LITTLE, M. H. & POTTER, S. S. 2011. Defining the molecular character of the developing and adult kidney podocyte. *PLoS One,* 6**,** e24640.

CEBRIAN, C., BORODO, K., CHARLES, N. & HERZLINGER, D. A. 2004. Morphometric index of the developing murine kidney. *Dev Dyn,* 231**,** 601-8.

CHUNG, M. I., NASCONE-YODER, N. M., GROVER, S. A., DRYSDALE, T. A. & WALLINGFORD, J. B. 2010. Direct activation of Shroom3 transcription by Pitx proteins drives epithelial morphogenesis in the developing gut. *Development,* 137**,** 1339-49.

COSTANTINI, F. 2012. Genetic controls and cellular behaviors in branching morphogenesis of the renal collecting system. *Wiley Interdiscip Rev Dev Biol,* 1**,** 693-713.

D'AGATI, V. D., FOGO, A. B., BRUIJN, J. A. & JENNETTE, J. C. 2004. Pathologic classification of focal segmental glomerulosclerosis: a working proposal. *Am J Kidney Dis,* 43**,** 368-82.

DAWES-HOANG, R. E., PARMAR, K. M., CHRISTIANSEN, A. E., PHELPS, C. B., BRAND, A. H. & WIESCHAUS, E. F. 2005. folded gastrulation, cell shape change and the control of myosin localization. *Development,* 132**,** 4165-78.

DEEGENS, J. K., STEENBERGEN, E. J., BORM, G. F. & WETZELS, J. F. 2008. Pathological variants of focal segmental glomerulosclerosis in an adult Dutch population--epidemiology and outcome. *Nephrol Dial Transplant,* 23**,** 186-92.

DEVUYST, O., KNOERS, N. V., REMUZZI, G., SCHAEFER, F., BOARD OF THE WORKING GROUP FOR INHERITED KIDNEY DISEASES OF THE EUROPEAN RENAL, A., EUROPEAN, D. & TRANSPLANT, A. 2014. Rare inherited kidney diseases: challenges, opportunities, and perspectives. *Lancet,* 383**,** 1844-59.

DIETZ, M. L., BERNACIAK, T. M., VENDETTI, F., KIELEC, J. M. & HILDEBRAND, J. D. 2006. Differential actin-dependent localization modulates the evolutionarily conserved activity of Shroom family proteins. *J Biol Chem,* 281**,** 20542-54.

DONE, S. C., TAKEMOTO, M., HE, L., SUN, Y., HULTENBY, K., BETSHOLTZ, C. & TRYGGVASON, K. 2008. Nephrin is involved in podocyte maturation but not survival during glomerular development. *Kidney Int,* 73**,** 697-704.

DOUGLAS-DENTON, R. N., MCNAMARA, B. J., HOY, W. E., HUGHSON, M. D. & BERTRAM, J. F. 2006. Does nephron number matter in the development of kidney disease? *Ethn Dis,* 16**,** S2-40-5.

DRESSLER, G. R. 2006. The cellular basis of kidney development. *Annu Rev Cell Dev Biol,* 22**,** 509-29.

ELLIS, J. W., CHEN, M. H., FOSTER, M. C., LIU, C. T., LARSON, M. G., DE BOER, I., KOTTGEN, A., PARSA, A., BOCHUD, M., BOGER, C. A., KAO, L., FOX, C. S., O'SEAGHDHA, C. M., CONSORTIUM, C. K. & CONSORTIUM, C. A. R. 2012. Validated SNPs for eGFR and their associations with albuminuria. *Hum Mol Genet,* 21**,** 3293-8.

FAUL, C., ASANUMA, K., YANAGIDA-ASANUMA, E., KIM, K. & MUNDEL, P. 2007. Actin up: regulation of podocyte structure and function by components of the actin cytoskeleton. *Trends Cell Biol,* 17**,** 428-37.

FRIEDRICH, G. & SORIANO, P. 1991. Promoter traps in embryonic stem cells: a genetic screen to identify and mutate developmental genes in mice. *Genes Dev,* 5**,** 1513-23.

GAO, S. Y., LI, C. Y., CHEN, J., PAN, L., SAITO, S., TERASHITA, T., SAITO, K., MIYAWAKI, K., SHIGEMOTO, K., MOMINOKI, K., MATSUDA, S. & KOBAYASHI, N. 2004. Rho-ROCK signal pathway regulates microtubule-based process formation of cultured podocytes--inhibition of ROCK promoted process elongation. *Nephron Exp Nephrol,* 97**,** e49-61.

HAGENS, O., BALLABIO, A., KALSCHEUER, V., KRAEHENBUHL, J. P., SCHIAFFINO, M. V., SMITH, P., STAUB, O., HILDEBRAND, J. & WALLINGFORD, J. B. 2006a. A new standard nomenclature for proteins related to Apx and Shroom. *BMC Cell Biol,* 7**,** 18.

HAGENS, O., DUBOS, A., ABIDI, F., BARBI, G., VAN ZUTVEN, L., HOELTZENBEIN, M., TOMMERUP, N., MORAINE, C., FRYNS, J. P., CHELLY, J., VAN BOKHOVEN, H., GECZ, J., DOLLFUS, H., ROPERS, H. H., SCHWARTZ, C. E., DE CASSIA STOCCO DOS SANTOS, R., KALSCHEUER, V. & HANAUER, A. 2006b. Disruptions of the novel KIAA1202 gene are associated with X-linked mental retardation. *Hum Genet,* 118**,** 578-90.

HAIGO, S. L., HILDEBRAND, J. D., HARLAND, R. M. & WALLINGFORD, J. B. 2003. Shroom induces apical constriction and is required for hingepoint formation during neural tube closure. *Curr Biol,* 13**,** 2125-37.

HARTLEBEN, B., WIDMEIER, E., WANNER, N., SCHMIDTS, M., KIM, S. T., SCHNEIDER, L., MAYER, B., KERJASCHKI, D., MINER, J. H., WALZ, G. & HUBER, T. B. 2012. Role of the polarity protein Scribble for podocyte differentiation and maintenance. *PLoS One,* 7**,** e36705.

HE, F. F., CHEN, S., SU, H., MENG, X. F. & ZHANG, C. 2013. Actin-associated Proteins in the Pathogenesis of Podocyte Injury. *Curr Genomics,* 14**,** 477-84.

HILDEBRAND, J. D. 2005. Shroom regulates epithelial cell shape via the apical positioning of an actomyosin network. *J Cell Sci,* 118**,** 5191-203.

HILDEBRAND, J. D. & SORIANO, P. 1999. Shroom, a PDZ domain-containing actin-binding protein, is required for neural tube morphogenesis in mice. *Cell,* 99**,** 485-97.

KANDA, T., WAKINO, S., HAYASHI, K., HOMMA, K., OZAWA, Y. & SARUTA, T. 2003. Effect of fasudil on Rho-kinase and nephropathy in subtotally nephrectomized spontaneously hypertensive rats. *Kidney Int,* 64**,** 2009-19.

KEMTER, E., PRUECKL, P., SKLENAK, S., RATHKOLB, B., HABERMANN, F. A., HANS, W., GAILUS-DURNER, V., FUCHS, H., HRABE DE ANGELIS, M., WOLF, E., AIGNER, B. & WANKE, R. 2013. Type of uromodulin mutation and allelic status influence onset and severity of uromodulin-associated kidney disease in mice. *Hum Mol Genet,* 22**,** 4148-63.

KESTILA, M., LENKKERI, U., MANNIKKO, M., LAMERDIN, J., MCCREADY, P., PUTAALA, H., RUOTSALAINEN, V., MORITA, T., NISSINEN, M., HERVA, R., KASHTAN, C. E., PELTONEN, L., HOLMBERG, C., OLSEN, A. & TRYGGVASON, K. 1998. Positionally cloned gene for a novel glomerular protein--nephrin--is mutated in congenital nephrotic syndrome. *Mol Cell,* 1**,** 575-82.

KETT, M. M. & BERTRAM, J. F. 2004. Nephron endowment and blood pressure: what do we really know? *Curr Hypertens Rep,* 6**,** 133-9.

KHOSHNOODI, J., SIGMUNDSSON, K., OFVERSTEDT, L. G., SKOGLUND, U., OBRINK, B., WARTIOVAARA, J. & TRYGGVASON, K. 2003. Nephrin promotes cell-cell adhesion through homophilic interactions. *Am J Pathol,* 163**,** 2337-46.

KIFFEL, J., RAHIMZADA, Y. & TRACHTMAN, H. 2011. Focal segmental glomerulosclerosis and chronic kidney disease in pediatric patients. *Adv Chronic Kidney Dis,* 18**,** 332-8.

KOLAVENNU, V., ZENG, L., PENG, H., WANG, Y. & DANESH, F. R. 2008. Targeting of RhoA/ROCK signaling ameliorates progression of diabetic nephropathy independent of glucose control. *Diabetes,* 57**,** 714-23.

KOMHOFF, M., WANG, J. L., CHENG, H. F., LANGENBACH, R., MCKANNA, J. A., HARRIS, R. C. & BREYER, M. D. 2000. Cyclooxygenase-2-selective inhibitors impair glomerulogenesis and renal cortical development. *Kidney Int,* 57**,** 414-22.

KOTTGEN, A., GLAZER, N. L., DEHGHAN, A., HWANG, S. J., KATZ, R., LI, M., YANG, Q., GUDNASON, V., LAUNER, L. J., HARRIS, T. B., SMITH, A. V., ARKING, D. E.,

ASTOR, B. C., BOERWINKLE, E., EHRET, G. B., RUCZINSKI, I., SCHARPF, R. B., CHEN, Y. D., DE BOER, I. H., HARITUNIANS, T., LUMLEY, T., SARNAK, M., SISCOVICK, D., BENJAMIN, E. J., LEVY, D., UPADHYAY, A., AULCHENKO, Y. S., HOFMAN, A., RIVADENEIRA, F., UITTERLINDEN, A. G., VAN DUIJN, C. M., CHASMAN, D. I., PARE, G., RIDKER, P. M., KAO, W. H., WITTEMAN, J. C., CORESH, J., SHLIPAK, M. G. & FOX, C. S. 2009. Multiple loci associated with indices of renal function and chronic kidney disease. *Nat Genet,* 41**,** 712-7.

KREIDBERG, J. A. 2003. Podocyte differentiation and glomerulogenesis. *J Am Soc Nephrol,* 14**,** 806-14.

KRETZLER, M. 2002. Regulation of adhesive interaction between podocytes and glomerular basement membrane. *Microsc Res Tech,* 57**,** 247-53.

KUURE, S., VUOLTEENAHO, R. & VAINIO, S. 2000. Kidney morphogenesis: cellular and molecular regulation. *Mech Dev,* 92**,** 31-45.

LAN, H. Y. 2011. Diverse roles of TGF-beta/Smads in renal fibrosis and inflammation. *Int J Biol Sci,* 7**,** 1056-67.

LASAGNI, L., LAZZERI, E., SHANKLAND, S. J., ANDERS, H. J. & ROMAGNANI, P. 2013. Podocyte mitosis - a catastrophe. *Curr Mol Med,* 13**,** 13-23.

LEE, C., LE, M. P. & WALLINGFORD, J. B. 2009. The shroom family proteins play broad roles in the morphogenesis of thickened epithelial sheets. *Dev Dyn,* 238**,** 1480-91.

LIENKAMP, S. S., LIU, K., KARNER, C. M., CARROLL, T. J., RONNEBERGER, O., WALLINGFORD, J. B. & WALZ, G. 2012. Vertebrate kidney tubules elongate using a planar cell polarity-dependent, rosette-based mechanism of convergent extension. *Nat Genet,* 44**,** 1382-7.

LITTLE, M. H. & MCMAHON, A. P. 2012. Mammalian kidney development: principles, progress, and projections. *Cold Spring Harb Perspect Biol,* 4.

LUYCKX, V. A., SHUKHA, K. & BRENNER, B. M. 2011. Low nephron number and its clinical consequences. *Rambam Maimonides Med J,* 2**,** e0061.

MCGREEVY, E. M., VIJAYRAGHAVAN, D., DAVIDSON, L. A. & HILDEBRAND, J. D. 2015. Shroom3 functions downstream of planar cell polarity to regulate myosin II distribution and cellular organization during neural tube closure. *Biol Open,* 4**,** 186-96.

MENON, M. C., CHUANG, P. Y., LI, Z., WEI, C., ZHANG, W., LUAN, Y., YI, Z., XIONG, H., WOYTOVICH, C., GREENE, I., OVERBEY, J., ROSALES, I., BAGIELLA, E., CHEN, R., MA, M., LI, L., DING, W., DJAMALI, A., SAMINEGO, M., O'CONNELL, P. J., GALLON, L., COLVIN, R., SCHROPPEL, B., HE, J. C. & MURPHY, B. 2015. Intronic locus determines SHROOM3 expression and potentiates renal allograft fibrosis. *J Clin Invest,* 125**,** 208-21.

MOHAN, S., RIZALDY, R., DAS, D., BAUER, R. J., HEROUX, A., TRAKSELIS, M. A., HILDEBRAND, J. D. & VANDEMARK, A. P. 2012. Structure of Shroom domain 2 reveals a three-segmented coiled-coil required for dimerization, Rock binding, and apical constriction. *Mol Biol Cell,* 23**,** 2131-42.

MUNDEL, P. & SHANKLAND, S. J. 2002. Podocyte biology and response to injury. *J Am Soc Nephrol,* 13**,** 3005-15.

NIGAM, S. K. & SHAH, M. M. 2009. How does the ureteric bud branch? *J Am Soc Nephrol,* 20**,** 1465-9.

NISHIMURA, T. & TAKEICHI, M. 2008. Shroom3-mediated recruitment of Rho kinases to the apical cell junctions regulates epithelial and neuroepithelial planar remodeling. *Development,* 135**,** 1493-502.

PARSA, A., KAO, W. H., XIE, D., ASTOR, B. C., LI, M., HSU, C. Y., FELDMAN, H. I., PAREKH, R. S., KUSEK, J. W., GREENE, T. H., FINK, J. C., ANDERSON, A. H., CHOI, M. J., WRIGHT, J. T., JR., LASH, J. P., FREEDMAN, B. I., OJO, A., WINKLER, C. A., RAJ, D. S., KOPP, J. B., HE, J., JENSVOLD, N. G., TAO, K., LIPKOWITZ, M. S., APPEL, L. J., INVESTIGATORS, A. S. & INVESTIGATORS, C. S. 2013. APOL1 risk variants, race, and progression of chronic kidney disease. *N Engl J Med,* 369**,** 2183-96.

PAVENSTADT, H., KRIZ, W. & KRETZLER, M. 2003. Cell biology of the glomerular podocyte. *Physiol Rev,* 83**,** 253-307.

PENG, F., WU, D., GAO, B., INGRAM, A. J., ZHANG, B., CHORNEYKO, K., MCKENZIE, R. & KREPINSKY, J. C. 2008. RhoA/Rho-kinase contribute to the pathogenesis of diabetic renal disease. *Diabetes,* 57**,** 1683-92.

PEREZ DE LEMA, G., MAIER, H., NIETO, E., VIELHAUER, V., LUCKOW, B., MAMPASO, F. & SCHLONDORFF, D. 2001. Chemokine expression precedes inflammatory cell infiltration and chemokine receptor and cytokine expression during the initiation of murine lupus nephritis. *J Am Soc Nephrol,* 12**,** 1369-82.

PLAGEMAN, T. F., JR., CHAUHAN, B. K., YANG, C., JAUDON, F., SHANG, X., ZHENG, Y., LOU, M., DEBANT, A., HILDEBRAND, J. D. & LANG, R. A. 2011. A Trio-RhoA-Shroom3 pathway is required for apical constriction and epithelial invagination. *Development,* 138**,** 5177-88.

PLAGEMAN, T. F., JR., CHUNG, M. I., LOU, M., SMITH, A. N., HILDEBRAND, J. D., WALLINGFORD, J. B. & LANG, R. A. 2010. Pax6-dependent Shroom3 expression regulates apical constriction during lens placode invagination. *Development,* 137**,** 405-15.

PRICE, P. M., HIRSCHHORN, K. & SAFIRSTEIN, R. L. 2010. Chronic kidney disease and GWAS: "the proper study of mankind is man". *Cell Metab,* 11**,** 451-2.

RIENTO, K. & RIDLEY, A. J. 2003. Rocks: multifunctional kinases in cell behaviour. *Nat Rev Mol Cell Biol,* 4**,** 446-56.

ROCQUE, B. L., BABAYEVA, S., LI, J., LEUNG, V., NEZVITSKY, L., CYBULSKY, A. V., GROS, P. & TORBAN, E. 2015. Deficiency of the planar cell polarity protein vangl2 in podocytes affects glomerular morphogenesis and increases susceptibility to injury. *J Am Soc Nephrol,* 26**,** 576-86.

SAXEN, L. & SARIOLA, H. 1987. Early organogenesis of the kidney. *Pediatr Nephrol,* 1**,** 385-92.

SCHIAFFINO, M. V., BASSI, M. T., RUGARLI, E. I., RENIERI, A., GALLI, L. & BALLABIO, A. 1995. Cloning of a human homologue of the Xenopus laevis APX gene from the ocular albinism type 1 critical region. *Hum Mol Genet,* 4**,** 373-82.

SCHWARTZ, G. J., MUNOZ, A., SCHNEIDER, M. F., MAK, R. H., KASKEL, F., WARADY, B. A. & FURTH, S. L. 2009. New equations to estimate GFR in children with CKD. *J Am Soc Nephrol,* 20**,** 629-37.

SEVILLA-PEREZ, J., KONIGSHOFF, M., KWAPISZEWSKA, G., AMARIE, O. V., SEEGER, W., WEISSMANN, N., SCHERMULY, R. T., MORTY, R. E. & EICKELBERG, O. 2008. Shroom expression is attenuated in pulmonary arterial hypertension. *Eur Respir J,* 32**,** 871-80.

SHANKLAND, S. J. 2006. The podocyte's response to injury: role in proteinuria and glomerulosclerosis. *Kidney Int,* 69**,** 2131-47.

SHI, S., YU, L., CHIU, C., SUN, Y., CHEN, J., KHITROV, G., MERKENSCHLAGER, M., HOLZMAN, L. B., ZHANG, W., MUNDEL, P. & BOTTINGER, E. P. 2008. Podocyte-selective deletion of dicer induces proteinuria and glomerulosclerosis. *J Am Soc Nephrol,* 19**,** 2159-69.

SHONO, A., TSUKAGUCHI, H., YAOITA, E., NAMETA, M., KURIHARA, H., QIN, X. S., YAMAMOTO, T. & DOI, T. 2007. Podocin participates in the assembly of tight junctions between foot processes in nephrotic podocytes. *J Am Soc Nephrol,* 18**,** 2525-33.

STAUB, O., VERREY, F., KLEYMAN, T. R., BENOS, D. J., ROSSIER, B. C. & KRAEHENBUHL, J. P. 1992. Primary structure of an apical protein from Xenopus laevis that participates in amiloride-sensitive sodium channel activity. *J Cell Biol,* 119**,** 1497-506.

STEAD, E. A., JR., MYERS, J. D., SCHEINBIERG, P., CARGILL, W. H., HICKAM, J. B. & LEVITAN, B. A. 1950. Studies of cardiac output and of blood flow and metabolism of splanchnic area, brain, and kidney. *Trans Assoc Am Physicians,* 63**,** 241-5.

TARIQ, M., BELMONT, J. W., LALANI, S., SMOLAREK, T. & WARE, S. M. 2011. SHROOM3 is a novel candidate for heterotaxy identified by whole exome sequencing. *Genome Biol,* 12**,** R91.

THOMAS, K. R. & CAPECCHI, M. R. 1987. Site-directed mutagenesis by gene targeting in mouse embryo-derived stem cells. *Cell,* 51**,** 503-12.

UHLENHAUT, N. H. & TREIER, M. 2008. Transcriptional regulators in kidney disease: gatekeepers of renal homeostasis. *Trends Genet,* 24**,** 361-71.

WANG, W., WANG, Y., LONG, J., WANG, J., HAUDEK, S. B., OVERBEEK, P., CHANG, B. H., SCHUMACKER, P. T. & DANESH, F. R. 2012. Mitochondrial fission triggered by hyperglycemia is mediated by ROCK1 activation in podocytes and endothelial cells. *Cell Metab,* 15**,** 186-200.

YANAGIDA-ASANUMA, E., ASANUMA, K., KIM, K., DONNELLY, M., YOUNG CHOI, H., HYUNG CHANG, J., SUETSUGU, S., TOMINO, Y., TAKENAWA, T., FAUL, C. & MUNDEL, P. 2007. Synaptopodin protects against proteinuria by disrupting Cdc42:IRSp53:Mena signaling complexes in kidney podocytes. *Am J Pathol,* 171**,** 415-27.

YEO, N. C., O'MEARA, C. C., BONOMO, J. A., VETH, K. N., TOMAR, R., FLISTER, M. J., DRUMMOND, I. A., BOWDEN, D. W., FREEDMAN, B. I., LAZAR, J., LINK, B. A. & JACOB, H. J. 2015. Shroom3 contributes to the maintenance of the glomerular filtration barrier integrity. *Genome Res,* 25**,** 57-65.

YONEDA, A., MULTHAUPT, H. A. & COUCHMAN, J. R. 2005. The Rho kinases I and II regulate different aspects of myosin II activity. *J Cell Biol,* 170**,** 443-53.